Stable Covalent pH-Sensitive Metallophthalocyanines Thin Monolayer Films for Selective Detection of Neurotransmitters

A thesis submitted in fulfilment of the requirements for the degree of

Doctor of Philosophy

By

Idowu, Abosede Omowumi Atinuke

DEDICATION

To my mentors

Prof. Ifeolu Kehinde Adewumi

(A great gift to the family in love and kindness)

And

Late Prof. Rowland Olaitan Seweje

(who passed on before the completion of this programme)

And to the memory of my parent

Late Chief Abraham Adewumi and Late Chief Comfort Adewumi

ACKNOWLEDGEMENTS

The Lord is my strength and shield; I trust Him with all my heart. He helps me, and my heart is filled with joy. (Psalm 28:7, 105:1). THANK YOU, GOD, I AM GRATEFUL.

My sincere gratitude and appreciation go to my Supervisor, Prof. Philani Nkosinathi Mashazi, for his guidance, supervision and constructive criticisms that have helped me throughout the years of my programme. Your help and contributions to my work and life are highly appreciated.

I appreciate the help of Prof. Sam Khene for his assistance. My heartfelt thanks go to Dr. Wale Osifeko and Dr Saibu for their supports to me in Rhodes University. I also enjoyed cooperation of Dr. David Oluwole, Bukola Oguntade, Daniel Mwanza, Nnaji Ihaemeka, Tayo Adeniyi, Dupe Ojo, Martins Ogunmolasuyi and everyone in F3, F5, S22 Laboratories and staff of Chemistry Department, Rhodes University.

My appreciation to everyone in my office at the Adeniran Ogunsanya College of Education, Ijanikin, Lagos, Nigeria, for their cooperation and supports throughout the duration of this program. The Council Members, the Management, the Provosts, TERTFund Desk Officer (Dr Oladipupo Awofisayo), Deans, Staff of School of Science, HOD and everyone in Chemistry Department. *E Seun mi o (Yor.)*

My gratitude also goes to my siblings, Engr-Prof. Ifeolu and Prof. Adejoke Adewumi, Prof. Olaitan (Late) & Dr Taiwo Seweje, Pastor Olaleye and Deaconess Lola Olokoshe, Pastor Tayo and Deaconess Bisi Olowe, Mr Ademola and Mrs Oluyemisi Banjo, and all my Junior ones, thanks all for being there for me.

My profound gratitude also is extended to the Board of Tertiary Education Trust fund (TETFUND) Nigeria, for sponsoring this programme.

ABSTRACT

The global challenge in solving the problem of neurodegenerative diseases (NDDs) that affect neurons in the human brain is to date unresolved. The statistical population of the affected people increases each year. Neurons are prone to damage or death as a result of an imbalanced level of released neurotransmitters (NTs). These imbalances affect the proper functioning of the brain and body. Early detection of the imbalances of NTs could suppress or correct the symptoms of NDDs. The detection has been the focus of researchers employing different techniques for both *in-vivo* and *in-vitro* detection of NTs. The research is based on electrochemical technique due to its fast response with adequate qualitative and quantitative results. The electrochemical methods are easy to handle, and the working electrode in the system can be modified for a specific purpose. The materials used in this work were the first-row transition metals octacarboxyphenoxy phthalocyanines complexes. The complexes were immobilized onto gold electrode surfaces and used as electrocatalysts for the detection of NTs. The immobilization method used to modify gold electrode was highly stable throughout the analyses in this study. The complexes improved the efficiency of the gold electrodes towards the detection of the NTs and suppressed the presence of ascorbic acid as a strong interference. The focus of this research is to solve the problem of interference faced during the detection of NTs. The thin film of octacarboxyphenoxy metallophthalocyanines was immobilized onto the gold electrode. The complexes, due to their catalytic activity, detected dopamine, epinephrine, serotonin and norepinephrine accurately. The range of detection of prominent chemicals associated with NTs was done using electroanalytical methods. Due to the pH sensitive functional groups (COOH), the thin monolayer phthalocyanine films suppressed ascorbic acid interference. The electrochemical analysis of neurotransmitters gave excellent limit of detection at μM range for all studied NTs. The results obtained with the modified electrode are proof of good electrocatalytic abilities of the complexes synthesized. This study recommends the use of the methods in this work for development of electrodes for NTs detection in human serum and tissue samples.

Table of Contents

List of Abbreviations

AuE	Gold electrode
Au-PA	Gold electrode-phenylamino
CA	Chronoamperometry
CoOcPhOPc	Cobalt octacarboxyphenoxy phthalocyanine complex
CV	Cyclic voltammetry
DA	Dopamine
DBN	1,5–Diazabicyclo [4.3.0] non-5-ene
DBU	1,8–Diazabicyclo [5.4.0] undec-7-ene
DPA	Dihydroxyphenylacetaldehyde
DPV	Differential pulse voltammetry
EDC	1-Ethyl-3-(3-dimethylaminopropyl) carbodiimide
EDL	The electrical double layer
EDLC	Electric double layer capacitance
EIS	Electrochemical impedance spectroscopy
EP	Epinephrine
FeOcPhOPc	Iron octacarboxyphenoxy phthalocyanine complex
FSCV	Fast scan cyclic voltammetry
GIT	Gastrointestinal tract
H_2OcPhOPc	Octacarboxyphenoxy phthalocyanines
HOMO	Highest occupied molecular orbital
HPLC-MS	High-performance liquid chromatography-Mass spectroscopy
IRMS	Isotope ratio mass spectrometer
LBD	Lewy body dementia
lcp	Left circularly polarized
LMCT	Ligand-Metal Charge Transfer
LSV	Linear sweep voltammetry
LUMO	Lowest unoccupied molecular orbital
MALDI/TOF	Matrix-assisted laser desorption/ionization mass spectrometer

MCD	Magnetic circular dichroism
MLCT	Metal-ligand charge transfer
$Mn(OAc)_2$	Manganese (II) acetate
Mn(OAc)OcPhOPc	Manganese octacarboxyphenoxy phthalocyanine complex
MOcPhOPc	Octacarboxyphenoxy metallophthalocyanines
MPc	Metallophthalocyanines
NEP	Norepinephrine
NHS	N-hydroxysuccinimide
OPD	Overpotential deposition
Pc	Phthalocyanines
PDT	Photodynamic therapy
PHA	Phenylhydroxylamine group
PNO_2	Phenylnitroso group
rcp	Right circularly polarized
Rct	Charge transfer resistance
R_s	Solution resistance
SAM	Self-assembled monolayer
SER	Serotonin
STD	Standard deviation
SWV	Square Wave Voltammetry
UPD	Under Potential Deposition
UV-Vis	Ultraviolet-visible

List of Symbols

E_c	Cathodic peak potential
D	Diffusion coefficient
E½	half-peak potential
E_a	anodic peak potential
$E^{o'}$	Formal potential
I_{pa}	anodic peak current
I_{pc}	cathodic peak current
Q	total charge
R^2	correlation coefficient
V	Volts
Γ_{ibf}	Ion barrier factor
ΔE_p	Potential difference
μMho	Conductivity standard
ν	Scan rate
Ω	Ohms

List of Figures

List of Tables

List of Schemes

1 CHAPTER ONE: INTRODUCTION AND LITERATURE REVIEW

1.1 Introduction

The increasing rate of neurodegenerative diseases and disorder globally called for improvement in the detection of the neurotransmitters that relatively cause the ill health. The treatment and the control of the illness have been a threat to public health and increased the global imparts finances. Neurotransmitters are biogenic chemical messengers with specific concentration which when altered results in neurodegenerative diseases such as Parkinson and Alzheimer diseases. The diseases can be repressed and controlled if detected early.

Among the many methods of detecting neurotransmitters, the electrochemical method was found to be efficient, simple, fast response, stable, produce qualitative and quantitative results without exhibiting fouling. The gold electrode used as the working electrode in the three electrodes electrochemical cell is a good conductor of heat and electricity (electrical connector) and highly resistant to corrosion and some chemical reactions. It exhibits good electrocatalytic activity towards the detection, and analysis of neurotransmitters. The working electrode used for electrochemical techniques is modified with octacarboxyphenoxy metallophthalocyanines pH-responsive, thin film layer for sensitivity, stability, and selectivity towards dopamine, epinephrine, serotonin and norepinephrine in the presence of interferents. The general challenge of the detection of neurotransmitters has been interference such as ascorbic acid, nitrite (NO_2), tryptophan and uric acid. The interferents co-exist in the nervous system with neurotransmitters. The interference of focus in this work is the ascorbic acid. Ascorbic acid is not a neurotransmitter but an isolated nutrient in vitamin C with similar oxidation potential with the neurotransmitters and higher concentration than that of the neurotransmitters in the same medium. The metallophthalocyanines thin film layer on the electrode, increase the gold electrode electroactivity, enhanced the current and lowered the redox potentials. The modified electrode thereby screened off the ascorbic acid and detected the neurotransmitters.

1.2 Literature review

The burden of mental disorder and neurodegenerative diseases (NDDs) are common problems causing significant impacts on human health around the world. Common conditions such as memory loss, autism, Alzheimer's, Parkinson's, and prion diseases are all caused by the malfunctioning of the chemistry in the brain **[1]**. These NDDs are caused by an imbalance of neurotransmitters (NTs) in the brain and body due to the damage or destruction of the nerve cells that control cognitive functions **[2]**. The WHO predicted an increase of 4.6 million cases annually in the cases of NDDs from 44 million in 2015 to 75 million by 2030, 81.1 million by 2040 and 132 million by 2050 **[3]**. It has been demonstrated in numerous studies that the development of NDDs begins 10 – 20 years prior to the clinical manifestation **[4]**. The diagnosis of NDDs at the preclinical manifestation stage would allow for the early treatment and efficient therapeutics outcome. However, it is extremely challenging to accurately diagnose disorders of the brain. Therefore, there is great interest in the design and optimization of diagnostic tools for the detection and quantification of chemical biomarkers implicated in neurological disorders to improve therapeutic outcome.

The imbalance of neurotransmitters (NTs) between the nerve cells and the brain have been implicated as the main cause of brain disorder and NDDs **[5]**. The NTs are chemicals that help to facilitate communication between nerve cells. They transfer synaptic information by the axis terminal of a neuron, activate and bind the receptor of the dendrites to another neuron throughout the brain and the body **[6]**. The NTs diffuse across the synapses and bind to the receptors in the cell membranes of the dendrites of the nerve cells. Upon binding, NTs can either inhibit or stimulate an electrical response in the receiving neuron's dendrites. The presynaptic neuron from the axon allows for the passage of electrical impulse across the

synaptic vesicle. The communication between two neurons occurs in the gap between the synapses of neurons called the synaptic cleft **[7]**. The pre-synaptic neuron is located before the synaptic cleft and communicates to the postsynaptic neuron (message receiver) across the synapse**.** Each of the NTs has a specific concentration level at which they demonstrate proper brain and body function. The sustained over- or under-production of NTs, leading to imbalances that could result in permanent neurodegenerative diseases such as Parkinson's disease, Alzheimer's disease, Lewy body dementia, Huntington's disease, prion disease, slowness, tremor, stiffness, shakiness, spinocerebellar ataxia and unsteady heartbeat rate **[8]**.

The maintenance of accurate levels of NTs within the central nervous system is very important to the stability and function of the body system. This is the principal motivation for the research on the quantification of NTs and their relationship to the optimal function of the body. The major challenges for the detection of NTs are the fact that the conventional sensors have limited target selectivity, undergo device fouling and degradation over time, and have large background noise signal. The diagnostic tools for the accurate monitoring of the level of brain chemicals, NTs in particular, need to be highly selective, sensitive and possess high spatial resolution. Recent advances in materials science are of help in the development of electrochemical sensors that can be extensively applied for the diagnosis of neurological disorder. Therefore, the improvement of the existing techniques or development of a new method that can sensitively and accurately detect NTs is highly necessary **[9]**.

The development of sensitive and highly selective diagnostic tools for the detection of NTs, especially the catecholamine and indoleamine NTs are the main focus of this thesis. The development of highly stable, selective and sensitive electrochemical biosensors with high resolution for screening off interfering analytes for the accurate detection of NTs would be presented.

1.3 Classification of NTs and their diagnostic values for NDDs

The classification of NTs depends on different aspects, such as the chemical structure, size and mode of action of NTs on each case. NTs are classified as small molecules (amino acids and monoamines) and neuropeptides neurotransmitters (somatostatin and endorphins) based on their sizes. **Table 1.1** shows the classification of NTs according to their chemical structures.

Table 1.1: Classification of neurotransmitters according to their chemical structures.

Class	**Examples**
Catecholamine	Epinephrine, Norepinephrine and Dopamine
Purinergic	Adenosine 5′-triphosphate (ATP), Uridine triphosphate (UTP) and Adenosine.
Amino acids	Glycine, Aspartate, Glutamate, Gamma Aminobutyric Acid
Indoleamine	Serotonin
Imidazoleamines	Histamine
Others	Acetylcholine

Monoamines are biogenic NTs that can be electrochemically oxidized and have an amine group attached to their structures. Catecholamine NTs are dopamine, epinephrine, and norepinephrine. Indoleamine NTs are serotonin and histamine **[10]**. The catecholamine NTs consists of the catechol chemical structure, as shown in **Figure 1.1**. All are synthesized from amino acids in the central nervous system in very low quantities. The monoamines undergo rapid metabolism and conversion into another type of NTs. They are broken down and

destroyed by monoamines oxidase inhibitors such as phenelzine, tranylcypromine, isocarboxazide and selegiline **[11].** They are absorbed in the gastrointestinal tract (GIT), liver, central nervous system and mitochondrion. Monoamines are electrochemically active and can be detected using electrochemical methods.

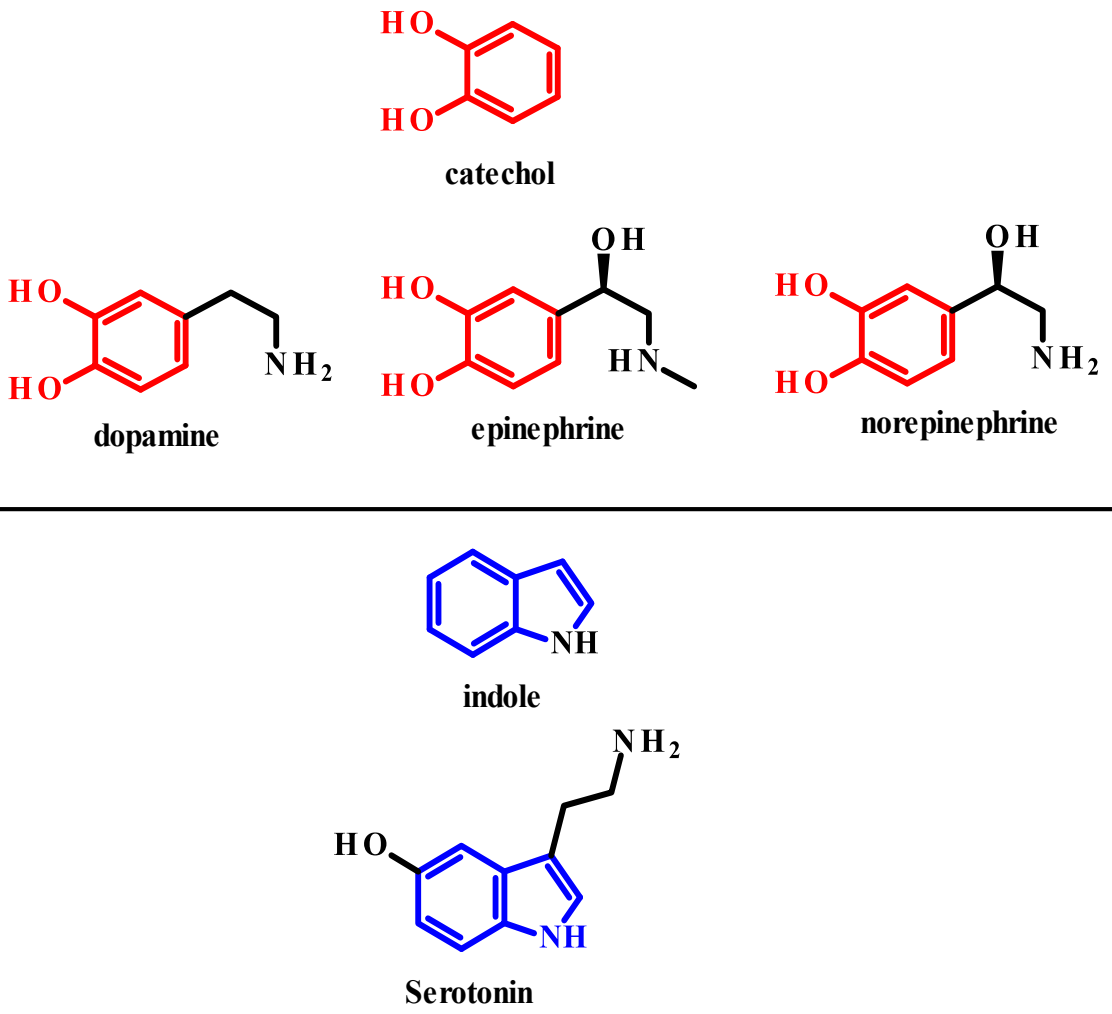

Figure 1.1: The structure of monoamine neurotransmitters, catecholamines (top) and indoleamines (bottom) with their core-structure highlighted **[12]**.

1.3.1 Dopamine (DA)

Dopamine (3, 4-dihydroxyphenethylamine) (DA) is a catecholamine NT that is widely present in the brain and the peripheral nervous system. DA is synthesized from the conversion of tyrosine to Levodopa (L-Dopa) by the enzyme hydroxylase, and L-dopa is converted to dopamine by the decarboxylase enzyme. DA is an inhibitory NT which plays an important role in the brain due to its involvement in cognitive and motor control. It reduces insulin production in the pancreases, reduces lymphocyte activity and reduces sodium excretion and urine output [**13]**. The normal DA concentration in the blood ranged from 0 to 30 pg. mL^{-1} (195.8 pmol. L^{1}; 0.1958 µmol. L^{-1}) in a healthy individual. Both excessively high levels of DA as well as very low levels in the brain cause serious impact to various brain functions and are related to different neurological diseases such Parkinson's disease, Huntington's disease, Schizophrenia and Drug addiction.

1.3.2 Norepinephrine (NE)

Norepinephrine (NE) also referred to as noradrenaline. It functions as a hormone and a neurotransmitter. It increases the force of the rate of contraction of the heart and thereby regulates the pumping of the blood. It regulates attention, releases glucose, promotes vigilance, contract muscle and increases the level of excitatory activity **[14]**. NE is synthesized from dopamine and its normal range in the blood is between 70 to 1700 pg. mL^{-1} (463.8 to 10048.7 pmol. L^{-1}; 0.4638 to 10.0487 µmol. L^{-1}) in a healthy adult. The imbalance in the level of norepinephrine in the brain and body results in memory loss, anxiety, high blood pressure, sleeplessness, and reduces blood flow.

1.3.3 Epinephrine (EP)

Epinephrine (EP) also called adrenaline. It is produced by adrenal glands and neurons. It is the last of the biosynthesis line of catecholamines that can be formed from NE by the enzyme phentolamine N-methyltransferase. Epinephrine is localized in the hypothalamus and the brainstem/medulla in the brains of various species, including mammals. EP increases blood flow to muscles and thereby causes fight-or-flight response, pupil dilation response, regulate sugar level and output of the heart **[15]**. The concentration of EP in the blood ranges from 0 to 140 pg. mL^{-1} (764.3 $pmol.L^{-1}$; 0.7643 $\mu mol.L^{-1}$) for healthy individual. Both epinephrine and norepinephrine control the stress systems in the human body. The instability of the concentration results in anxiety, nervousness and affect memory.

1.3.4 Serotonin (5-hydroxytryptamine)

Serotonin (5-hydroxytryptamine) is in the class indoleamine, produced from an amino acid called tryptophan. Serotonin is a chemical that controls mood, appetite, sleep, memory and contributes generally to the well-being and happiness. It relays messages from the brain cell. It is found mostly in the digestive system, blood platelets and in the nervous system **[16]**. The concentration in the adult blood is between 101 to 283 ng. mL^{-1} (1.01×10^5 - 2.83×10^5 pg. mL^1; 0.2269 – 0.6359 $\mu mol.\ L^{-1}$). **Table 1.2** shows the summary of the NTs, secretory site, function and normal levels in the body.

Table 1.2: Summary of the neurotransmitter's location, secretory site and their normal diagnostic range for normal body function.

NTs	Secretory Site	Functions	Normal range ($pg.mL^{-1}$)	Ref.
Dopamine	Blood	Perfect brain functioning	0 – 30	**[17]**
Epinephrine	Blood	Increased blood sugar and heart rate	0 – 140	**[17]**
Norepinephrine	Adrenal medulla	Maintain perfect heartbeat rate and blood pressure	70 - 1700	**[17]**
Serotonin	Blood	Regulate mood, appetite, and sleep	(1.01 - 2.83) x 10^5	**[18]**

1.4 Redox Reaction of Neurotransmitters

Scheme 1.1 shows the route for a two-electron transfer oxidation process of dopamine in which two protons are transferred resulting in the formation of dopamine-*o*-quinone (DAq). The dopamine-*o*-quinone undergoes an intermolecular addition reaction, which results in the cyclization reaction that results in the formation of leucodopaminechrome (LDAc). LDAc is oxidised further to dopamine-*o*-chrome via a two-electron transfer process. The dopamine*o*chrome is further oxidized to indolic-*o*-quinone to generate an insoluble melanin polymer. It is this melanin polymer that has been found to foul and poison electrode during the detection of dopamine. A similar redox process occurs for neurotransmitters **[19]** with different final products but similar steps. For the epinephrine redox process, the final products is

indolequinone and similar final product for norepinephrine. In the serotonin redox process, it is oxidized with the NH_2 on the serotonin structure, forming 5-hydroxy indole acetic acid (5HIAA) **[20]**.

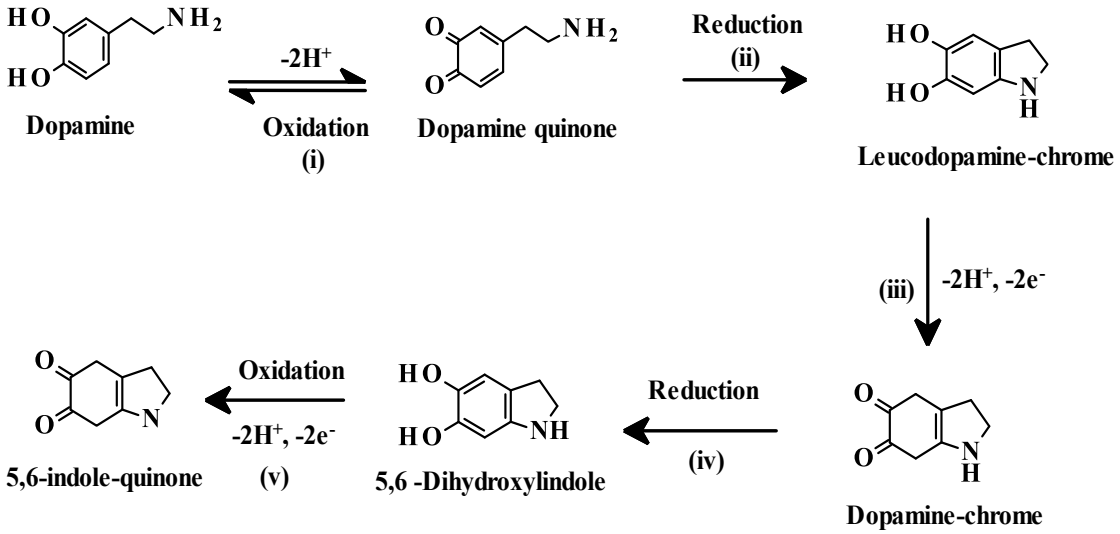

Scheme 1.1: The route for a two-electron transfer oxidation process of dopamine in which two protons are transferred resulting in the formation of dopamine-*o*-quinone (DAq) **[19].**

NTs co-exist with many interfering compounds in biological fluids. These interfering compounds are present at concentrations higher than NTs. Particularly, ascorbic acid (AA) exists at higher concentration than NTs and undergoes similar oxidation reaction as NTs. **Scheme 1.2** shows the schematic illustration for the oxidation of AA. The AA undergoes two electrons and two protons transfer process to form dehydroascorbic acid. Ascorbic acid releases H^+ that lowers the pH of the body fluids. Ascorbic acid transfers hydrogen atoms ($2e^- + 2H^+$) during cellular respiration. It is stable in acidic medium, but in neutral or basic solution, it is easily and rapidly oxidized by dissolved oxygen **[21].**

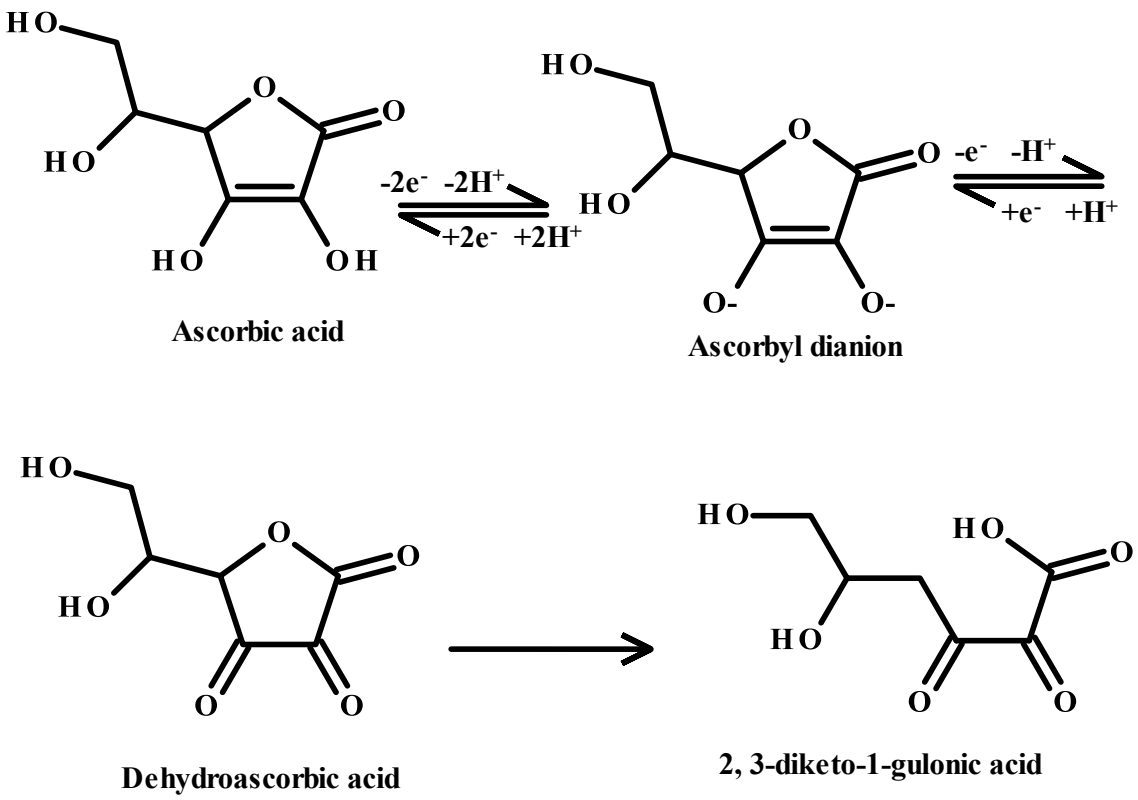

Scheme 1.2: Oxidation of ascorbic acid to form ascorbyl dianion and further oxidised to form dehydroascorbic acid (DHA) and finally, 2,3-diketo-1-glulonic acid **[22].**

1.5 Analytical methods for the detection and quantification of NTs

Both *in-vivo* and *in-vitro* diagnostic methods had been developed for the determination of NTs. The *in-vivo* methods include the microdialysis-capillary, capillary electrophoresis-laser induced fluorescence (CE-LIFD) **[24]**, the fast scan voltammetry **[25]**, neurochips **[26]**, wearable wireless electrochemical instruments **[27]**, and carbon nanotube on carbon fibre microelectrodes (CFME) **[28].** The *in-vivo* methods involve the immersion of a microdialysis probe into the brain **[23]**. This is invasive, painful to patients and expensive. The only advantage is the *in-vivo* measurements are online determination of neurotransmitters in that they measure

NTs as they are produced and in their natural environment. This is particularly important in monitoring the NTs is their natural environment.

The *in-vitro* methods detect NTs in biological fluids such as blood and neurological fluids. The fluids are drawn and analysed after treatment with fluids for specific analysis. This treatment introduces human and experimental errors (dilution, pH effect, stability) on the determination of the NTs. These errors must be accounted in the analysis and interpretation of results. The traditional *in-vitro* diagnostic methods for the detection and quantification are the high-performance liquid chromatography (HPLC) **[29]**, mass spectrometry (MS) **[30]**, and capillary electrophoresis and electroencephalography (CE-EE) **[31]**. These techniques require expensive instrumentation and reagents, they are laborious, tedious and require expertise to carry out and analyse result.

In recent time, electrochemical devices have received research attention for the detection of NTs **[32]**. The electrochemical detection is characterised by its simplicity, fast analytical response and generation of reproducible qualitative and quantitative results. Moreover, the catecholamine NTs are electrocatalytically active making their electrochemical detection easy to pursue. The catecholamines can be oxidised electrochemically at a potential ranging from 200 mV to 700 mV (Ag|AgCl) at physiological conditions. The current intensity or density (i_p) is a measure of NT concentration and the potential where the oxidation can be used for identifying NT under investigation. Randle-Sevcik equation in **Equation 1.1** is useful in relating the current to the concentration of the NT.

$$i_p = 2.69 \text{ x } 10^5 \, n^{3/2} A C D^{1/2} \upsilon^{1/2} \quad \text{.....} \mathbf{1.1}$$

In which n is the number of electrons transferred in the redox process, A is the electrode area in cm^2, C is the concentration of the NT in mol/cm^3, D is the diffusion coefficient in cm^2/s and υ is the scan rate in V/s.

Electrochemical detection of NTs has been challenging for the following reasons:

- The redox characteristics of catecholamine NTs are similar at physiological pH; thus, makes it difficult to electrochemically distinguish between the different NTs. This is the major challenge especially working with unmodified or solid electrodes.
- NTs coexists with other electroactive interfering compounds such as ascorbic acid (AA) and uric acid (UA) with similar oxidation potential as NTs.
- The fouling and poisoning of electrode surfaces by the formation of insoluble polymers as the by-product of NTs electrochemical oxidation. The polymers inhibit reusability of the electrode surfaces during the electrochemical detection of NTs.

Therefore, the modification of the electrode surface with materials that could improve the selectivity, prevent electrode fouling, and screen-off interfering substance has been the leading research interest in recent times **[33]**. Various materials have been used for the fabrication of chemically modified electrodes. The materials that have been investigated for electrode modification include metallophthalocyanines (MPcs), metalloporphyrins (MPPs), electroactive polymers and nanomaterials. The electrocatalytic properties of electrode modifiers enhance the current and lowers the potential of the analytes during the detection process **[34]**. The electrochemical sensor investigated in this study is a gold electrode modified with metallophthalocyanines complexes (MPc) film.

1.6 Metallophthalocyanines (MPcs) Complexes

Metallophthalocyanines (MPc) are blue-green anisotropic complexes with planar structure.

MPc is aromatic compounds, highly conjugated with 18 π-electrons in the macrocyclic ring [**35]**. The metal ion centre can contain transition metals known for its excellent electroactive properties. The transition metals have varied oxidation states and therefore improve the electrocatalytic activity of MPc-based electrochemical sensors **[36]**.

Figure 1.2 shows the structure of a typical MPc complex. MPc consists of four isoindole units fused at their 1,3-positions by nitrogen atoms of aza-bridges. They have a similar core structure of the naturally occurring metalloporphyrin complexes (MPP) but have an extended conjugation of benzene rings. The substituents attached to the ring and the sequestered metal ion at the core centre influence the intrinsic properties and increase the variety of metallophthalocyanines. The terminal ends of MPc can be substituted with functional groups like alkyl, aryl, amino, carboxyl, hydroxyl, thiol and azide **[37]**.

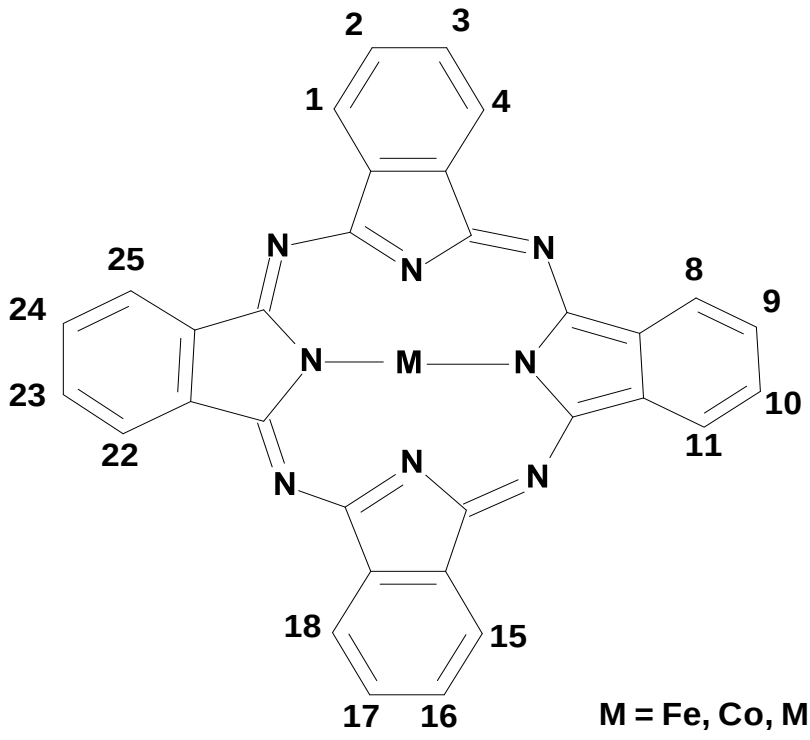

Figure 1.2: Molecular structure of metallophthalocyanines (MPc) with numbering (adopted from **[38]**.

The substitution in MPc complexes could be achieved either on the central metal ion or on the ring systems. The substituents on the ring could be mono, di, tetra or octa substituted groups. The substituent alters the properties of metallophthalocyanines, depending on their positions either at the non-peripheral (α) or peripheral (β) positions **[39]**. Also, the incorporation of different substituents, the positions of the substituents (either at α or β- positions) and the electron-withdrawing or donating effect of different substituents affect their properties and enhances the solubility **[40]**. The incorporation of different metal at the MPcs core often influences the electrical, optical and magnetic properties of MPc **[39]**, and they are excellent homogenous and heterogeneous catalysts for various applications**.** The flexibility, chemical, and thermal stability allow for their extensive application in the various areas of research, such as liquid crystal display devices **[39]**, photovoltaic cells **[41]**, fuel cells **[42]**, semiconductor

devices **[43]**and chemical sensors for various analytes. MPc is very stable and reusable electrocatalysts **[44]**. MPc with an octacarboxyphenoxy substituent group at the peripheral position and transition metals (Co, Fe, Mn) central metal substituents were employed in this work.

Scheme 1.3 shows the synthetic routes for unsubstituted metallophthalocyanines. Diverse types of precursors are used for the synthesis of the phthalocyanines. The formation of metallophthalocyanines involves cyclotetramerization reaction. The reactions are carried out with the starting material such as **(1)** phthalonitrile, **(2)** phthalic acid, **(3)** phthalimide, **(4)** phthalic anhydride, **(5)** dibromobenzene, **(6)** 1,3-diiminoisoindoline, and **(7)** O-cyanobenza - mide. A high boiling solvent such as 1-pentanol and 1-octanol is used in the presence of catalysts. The catalyst could be Li or Na metal, 1, 8-Diazabicyclo (5.4.0) undec-7-ene (DBU) or 1,5–Diazabicyclo [4.3.0] non-5-ene (DBN).

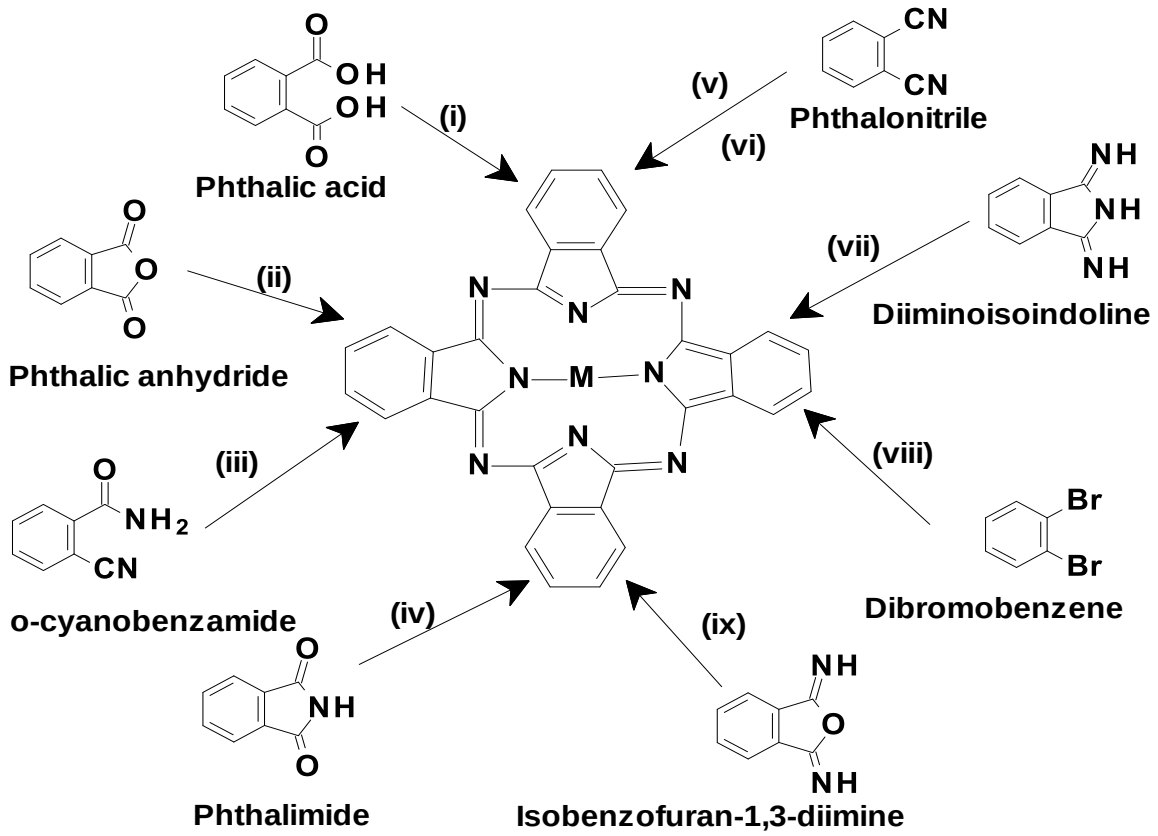

Scheme 1.3: The synthesis routes of metallophthalocyanines, reaction and conditions:**(i)** urea, metal salt, heat **(ii)** NH_3, metal salt, solvent, heat **(iii)** metal salt, solvent, 300ºC **(iv)** formamide, heat (v) ROH, metal salt, DBU, 130ºC **(vi)** ROH, solvent, Li metal, heat. **(vii)** Solvent, a metal salt **(viii)** CuCN, heat **(ix)** NH_3, metal salt, solvent, heat.

1.6.1 The Electrochemical properties of MPc

The redox activity of metal-free phthalocyanines was due to the conjugated π-electrons ring system**.** The redox reaction at the ring involves the removal of π-electrons from the highest occupied molecular orbital (HOMO). It also involves the addition of electrons to the lowest unoccupied molecular orbital (LUMO). In the neutral state, phthalocyanines exist as dianion in the form of Pc^{-2}. Each could undergo a redox process due to its ability to gain and donate electrons. Phthalocyanines lose two electrons to be Pc^{0} or one electron to Pc^{-1} cationic species.

In its reduced state, it becomes Pc^{-3}, Pc^{-4}, Pc^{-5} and Pc^{-6} due to the addition of electrons to the LUMO of the orbital **[45]**. The band energy between the first oxidation redox potential and the first reduction redox potential of the Pc ring is about 1.6 eV. The extended conjugation in the structure aids the electron transfers in the metallophthalocyanines ring. The bandgap can be tuned by the nature of the conjugation and the substituent attached to the Pc ring. As the conjugated Pi-system increases, the energy gap between the HOMO-LUMO decreases. The Q band also shifted to the longer wavelength **[46]**. The substituents affect the electrochemical properties of the MPc. The substituents that are electron-donating would thereby reduce the HOMO-LUMO gap. In addition, the electron-withdrawing substituents would increase the width of the HOMO-LUMO gap.

1.6.2 The metallophthalocyanines modified electrode for detection of neurotransmitters

Modification of electrodes with MPcs protects the electrode surfaces from chemical fouling**,** provides enhanced catalytic properties**,** improves sensitivity and selectivity towards the analyte of interest **[47**]. **Table 1.3** shows the summary of MPcs modified electrodes for the detection of neurotransmitters. The majority of the reported MPc-modified electrodes were used for the detection of dopamine. As shown in **Table 1.3**, the limit of detection varies depending on the MPcs used and the method of MPcs immobilization.

Table 1.3: Metallophthalocyanine-based Electrochemical Sensors for the Detection of Neurotransmitters.

Analytes	MPc materials	Method of modification	LOD (μM)	Ref.
Dopamine	• Tetraaminophthalocyanatonickel(II) (p-NiTAPc) film	Dip dry	0.09	**[48]**
	• Azo-bridged tetracarboxylic metallophthalocyanines (Ni, Co and Cu)	Drop dry	0.33	**[49]**
	• Nickel tetrasulphonated phthalocyanines (NiTsPc)	Drop dry	0.10	**[50]**
	• Cobalt teratsulphonated phthalocyanines (CoTsPc)	Electrodeposition	0.87	**[51]**
	• Copper tetrasulphonated phthalocyanines (CuTsPc)	Deposition	10.00	**[52]**
Epinephrine	• Metal-octacarboxyl phthalocyanines (M-Fe, Co, Mn)	Au-Cyst SAM	0.013	**[53]**
	• 1,8,15,22-tetraamino-phthalocyanatonickel (II) (Ni^{II}TAPc	amide coupling	0.05	**[54]**
	• Cobalt phthalocyanines	Drop dry	0.04	**[55]**
	• Iron phthalocyanines	Deposition	0.5	**[56]**
Norepinephrine	MWCNT/ZnO/29H,31H-Pc	Adsorption	1.7	**[57]**
Serotonin	Cobalt (II) phthalocyanine and tyrosinase	Drop and dry	0.84	**[58]**

The most widely reported method for MPcs immobilisation onto the electrode surface is via dip and drop dry method. Unfortunately, these methods suffer from high irreproducibility and poor stability **[59].** Also, the MPcs layer thickness on the electrode surface cannot be controlled and film reproducibility is a major challenge. Agboola and Ozoemena **[60]** fabricated a sensitive epinephrine electrochemical sensor using gold electrode-prefunctionalized with cysteamine for the covalent immobilisation of octacarboxylcobalt phthalocyanine via amide bonding. The MPcs modifications via self-assembled monolayer technique (SAM) are not stable and have limited pH range applicability. The SAM layer has low shelf-life and therefore, has limited reliability. The stability of the MPc modified electrode, shelf life, reliability and reproducibility of results depends on the immobilization technique employed.

In this work, the method targets immobilization technique that would be novel with high stability and longer shelf-life. This work therefore investigated the synthesis of octacarboxyphenoxy metallophthalocyanines and the covalent immobilization onto gold electrode. The gold electrode was chosen due to its excellent electrochemical activity. The stability of the octacarboxyphenoxy metallophthalocyanines complexes at the electrode surface at wider pH would be demonstrated. The stable thin film on the electrode would be employed for the identification and selective detection of specific NTs. The MPcs modified electrode would be used for the screening out of the interferents. It is expected that the MPc would provide enhanced sensitivity.

1.7 Electrode modification techniques

1.7.1 Electrochemical grafting technique for pre-modification of electrode

Electrochemical grafting of aryldiazonium salts has been widely explored for the functionalization of conducting surfaces with aromatic molecules. **Scheme 1.4** shows the schematic illustration of the reductive electrochemical grafting of phenyldiazonium groups onto a gold surface **[61].** The reduction of the phenyldiazonium is believed to involve a two-electron reduction to produce a phenyl radical and loss of nitrogen gas (N_2). A covalent bond is formed between the electrode surface and the phenyl radical. The bond formed is strong and stable compared to SAM. The phenyldiazonium (R-NOx, R-NH_2) formed an active aryl radical with the loss of nitrogen (N_2).

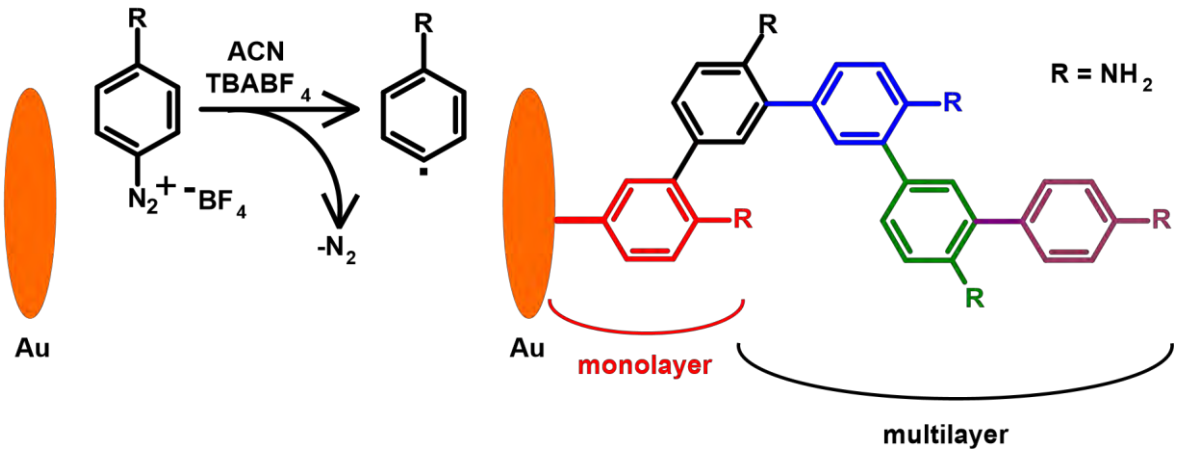

Scheme 1.4: Electrochemical grafting of diazonium salt onto conductive surface, for mono or multilayer thin films **[62].**

1.7.2 Amide coupling

Amide coupling formed a strong covalent bond between the carboxylic acid and amine functional groups. The process occurred through a nucleophilic substitution reaction. The COOH group is activated with EDC and NHS to form an amine-reactive succinimide ester as shown in **Scheme 1.5.** The mixture of the EDC/NHS was used to activate the carboxyl group

to obtain unstable and highly reactive NHS esters. In **Scheme 1.5**, the carboxylic acid reacted with the EDC to form an intermediate O-acrylisourea (urea derivative). NHS reacts with the O-acrylisourea to form NHS ester which conveniently reacted with the amine to form amide bond. The addition of NHS improved the efficiency of the amide formation **[63].**

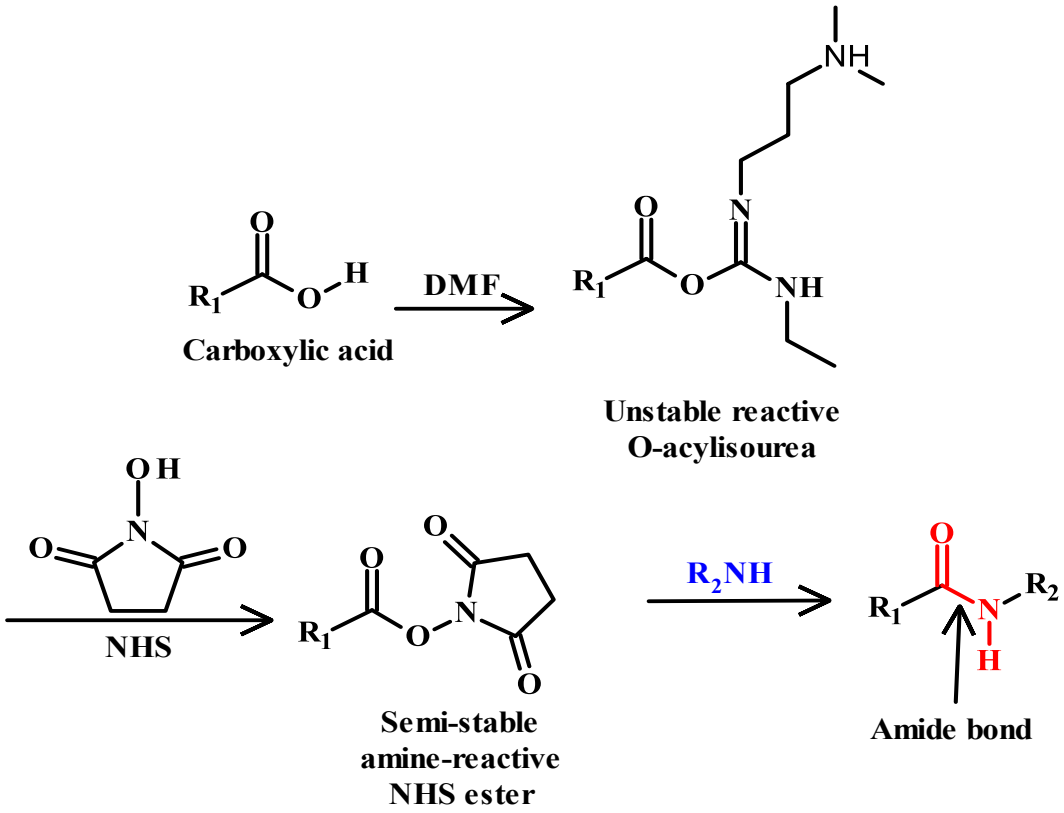

Scheme 1.5: Amide coupling mechanism of nucleophilic substitution reaction using EDC (1-Ethyl-3-(3-dimethylaminoppropylcarbodiimide) and NHS (N-Hydroxysuccinimide). **[64]**

1.8 Aims and research objectives of the thesis:

This study aim is to design pH-sensitive electrochemical sensors for the detection and quantification of electroactive neurotransmitters and screening off of ascorbic acid as strong interferent.

The specific objectives are to:

(a) Synthesise and characterise thoroughly octacarboxyphenoxy metallophthalocyanines complexes containing iron (Fe), cobalt (Co) and Mn (manganese) central metal ions;

(b) Covalently immobilise octacarboxyphenoxy metallophthalocyanines onto the gold electrode surface in a stable manner and study its electrochemical properties;

(c) Study the effect of pH of the modified phthalocyanines gold electrodes using negative and positively charged electroactive redox species;

(d) Investigate the electroactive detection and quantification of neurotransmitters such as dopamine (DA), serotonin (SE), epinephrine (EP), and norepinephrine (NEP); and

(e) Study the screening off of ascorbic acid, a strong interference for the detection of neurotransmitters (DA, SE, EP and NEP).

1.9 Thesis Outline

- **Chapter One: Introduction**

  This chapter introduces neurotransmitters, neurodegenerative diseases and disorder, method of neurotransmitters detection, chemically modified electrode, electrografting process, amide bond coupling and electroanalytical method metallophthalocyanines. It also includes aim and specific objectives of the study.

- **Chapter Two: Experimental**

  The chapter discusses the experimental procedure, synthesis, characterization of octacarboxyphenoxy metallophthalocyanines and characterization.

- **Chapter Three: Characterization of synthesized complexes**

  This chapter explains the characterization of metallophthalocyanines with electrochemical methods.

- **Chapter Four: Electrode fabrication and characterization using various surface techniques**

  The chapter presents the innovative immobilization of metallophthalocyanines on the electrode surface. Techniques used for the characterization of the surfaces are also discussed. The electrocatalysis and the electroanalysis of the sensors towards dopamine, serotonin, and norepinephrine are discussed. The screening out of the ascorbic acid was also investigated.

- **Chapter 5: Comparative studies of the electroanalysis studies in this work on the neurotransmitters and different MPcs used for NTs detections.**

  The results obtained were compared with other results from other research work on NT detections using metallophthalocyanines.

- **Results and Discussion:**

  This chapter discusses the findings and compares the results in line with the effectiveness of different materials used for the modification of the gold electrode.

- **Conclusions and Recommendations**

  This chapter concludes the findings and compares the results in line with the effectiveness of different materials used for the modification of the gold electrode.

- **References**

  This section list in detail the references cited in the whole thesis.

2 CHAPTER TWO: EXPERIMENTAL

2.1 Materials and Reagents

Tetrabutylammonium tetrafluoroborate ($TBABF_4$), 4-Nitroaniline ($C_6H_6N_2O_2$), L-Ascorbic acid (AA), epinephrine hydrochloride (EP), 1,8-diazabicylo-[5,4,0]-undec-7-ene (DBU), dopamine hydrochloride (DA), serotonin hydrochloride (SE), 1-ethyl-3-(3-dimethyl aminopropyl) carbodiimide (EDC), N-hydroxysuccinimide (NHS), 4,5-dichlorophthalic acid, trifluoroacetic acid (TFA), 2,5-dihydroxybenzoic acid, 1-pentanol, and potassium ferrocyanide $K_4[Fe(CN)_6]$ and potassium ferricyanide ($K_3[Fe(CN)_6]$) were obtained from Sigma-Aldrich. Iron (II) chloride ($FeCl_2$), manganese (II) acetate ($Mn(OAc)_2$), acetonitrile (ACN), and potassium chloride (KCl), tetrahydrofuran (THF), Hydrochloric acid (HCl) were obtained from Minema. Potassium carbonate (K_2CO_3), 25% ammonium hydroxide, sodium chloride (NaCl) and Silica Gel 60P F254 (Thin layer chromatography) were purchased from Merck. Potassium dihydrogen orthophosphate (KH_2PO_4), dimethyl formamide (DMF), dimethyl sulfoxide (DMSO), and dipotassium hydrogen orthophosphate (K_2HPO_4) and cobaltous acetate tetrahydrate ($Co(OAc)_2.4H_2O$) were purchased from Associated Chemical Enterprises (ACE). Hydrogen peroxide (H_2O_2) and sodium hydroxide pellet were purchased from B & M Scientific. Absolute ethanol (C_2H_6O) was purchased from SAARChem. Alumina powder was purchased from Allied High Tech. Silica Gel 60 (0.04-0.063 mm) for Column chromatography was obtained from Fluka. All other reagents were of analytical grade. Ultra-pure Milli-Q Water (18.2 MΩ. cm resistivity at 25ºC) was obtained from the Milli – Q water system (Millipore Corp., Bedford, MA, USA) and was used to prepare all aqueous solutions.

Phosphate buffers saline (PBS) were prepared with ultrapure Millipore water, using appropriate amounts of KH_2PO_4 (90.0 mg; 0.70 mmol), K_2HPO_4 (1.63 g; 9.4 mmol), sodium chloride salts (8.0 g; 0.10 mmol) and KCl (20.0 mg; 0.30 mmol) for 100 ml. The quantities can be altered depending on the desired pH and the molarity. The activation buffer used was 2-(N-

morpholine) ethanesulfonic acid (MES) buffer (10 mM, pH 6.5). The pH was adjusted using 0.10 M HCl, and 0.10 M NaOH. The gold and reference electrodes were purchased from BioAnalytical Systems Incorporation (BASi).

2.2 Experimental Techniques and Equipment

The electrochemical techniques employed in this study include cyclic voltammetry (CV), electrochemical impedance spectroscopy (EIS), and differential pulse voltammetry (DPV). The electrochemical measurements were conducted using an Autolab PGSTAT 302N equipped with Nova 1.10 software (FRA 32M). The conventional three-electrode electrochemical cell consists of gold working electrode (1.6 mm diameter), Ag|AgCl, 3M KCl reference electrode (6 mm diameter, 7.5 cm long with coral or frit at the tip) and platinum wire as counter electrode. The electrochemical impedance spectroscopy (EIS) measurements were carried out on the mirror polished bare, electrografted and modified electrode surfaces in 2.0 mM (1:1) $K_3[Fe(CN)_6]$ and $K_4[Fe(CN)_6]$ containing 0.10 M KCl. Metrohm 827 pH meter was used for the pH measurements. Hettich Zentrifugen MIKRO 220 Labotec was used for the centrifugation studies. Branson 1800 was used for ultrasonication studies.

2.3 Spectroscopic Characterization of Synthesized Compounds and Complexes

2.3.1 Fourier transforms infrared (FT-IR) spectroscopy

The various complexes were characterized using FTIR data obtained from Bruker Alpha-model FT-IR Spectrometer (4000 - 650 cm^{-1}) or Perkin-Elmer Spectrum 100 FT–IR Spectrometer (4000 - 400 cm^{-1}) equipped with the diamond-attenuated total reflectance (ATR) sampling accessory. The two instruments were utilized interchangeable and there was no discrepancy for the data obtained. All measurements were recorded at room temperature. 100 Scans were taken

for each interferogram at 4 cm^{-1} resolutions. The background spectrum in the air was recorded and automatically subtracted from the sample spectrum by the appropriate software (Bruker OPUS 6.5 software) and (Perkin Elmer Spectrum One software).

2.3.2 Nuclear magnetic resonance spectroscopy (NMR)

NMR is a technique used for the determination of the structure of an organic compound and to confirm its purity. It involves the exposure of certain atomic nuclei notably ^{13}C, ^{1}H, ^{19}F and ^{31}P to an external magnetic field. The ^{1}H chemically equivalent hydrogen will give signals in the ^{1}H NMR. By integrating the area under the ^{1}H signal, the number of chemically equivalent protons can be determined, hence revealing how many numbers of hydrogen atoms are present in a compound. In this study, ^{1}H NMR was employed to elucidate the structure of the synthesised compounds and metallophthalocyanines and confirms the purity. The peaks were recorded in deuterated solvents of choice depending on the solubility of the compound or materials investigated. Solvents such as $CDCl_3$ or DMSO-d_6 were used and a Bruker 300MHz and 400MHz NMR spectrometer.

2.3.3 Elemental analysis

The elemental (CHN) and isotopic compositions in each of the prepared samples were conducted with a Vario-Elemental Microcube ELIII.

2.3.4 Ultraviolet/visible absorption spectroscopy (UV-Vis)

The spectra were recorded using a Perkin Elmer Lambda 25 Spectrometer and Multiskan sky Thermo Scientific UV equipment. The sample solution of 1 cm path length was used in the

cuvette cell. The equipment measures the absorbance of ultraviolet or visible light by the sample. This could be either at a single wavelength or by performing a scan over a range of wavelengths in the spectrum. The radiation causes an electronic transition within the structure of a molecule or ion to exhibit absorption in the visible or ultraviolet region.

2.3.5 Magnetic circular dichroism (MCD)

The MCD spectra were recorded with MCD Applied Photophysics Chirascan plus spectropolarimeter equipped with a permanent magnet, producing a magnetic field of 1 Tesla. The MCD spectra gives the differential absorption of left (lcp) and right (rcp) circularly polarized light. The light-induced in a sample by a strong magnetic field is oriented parallel to the direction of light propagation. It measures the difference in intensity between left and right. The magnetic dipole moment was used to determine the intensity of MCD spectra, which gave better resolution than UV absorbance spectroscopy. The combination of UV-Vis and MCD spectroscopy provides direct information about the energies and degeneracies of the state that are responsible for the major spectral bands in the UV-Vis.

2.3.6 Mass spectroscopy (MS)

The mass spectra were recorded with Bruker AutoFLEX III smartdata beam MALDI/TOF (Matrix-assisted laser desorption/ionization/ time of flight) mass spectrometer. The matrix used in the positive ion mode was 2,5-dihydroxybenzoic acid. The technique ionizes chemical species and sorts the ions into a spectrum detector based on their mass-to-charge ratio. The matrix (0.10 mg, 0.60 mmol) was dissolved in 1 mL of acetonitrile:TFA (v:v 30:70). Other solvents that can be used for the preparation of the matrix are methanol, acetone, chloroform,

and water. Metallophthalocyanine complexes (5.0 µL) was mixed with matrix (20.0 µL) and spotted on the equipment's stainless-steel plate and inserted into the instrument for analysis. The decoded results with relative intensity were interpreted.

2.4 Synthesis of metallophthalocyanines

2.4.1 Synthesis of 4,5-di(4-carboxyphenoxy) phthalonitrile

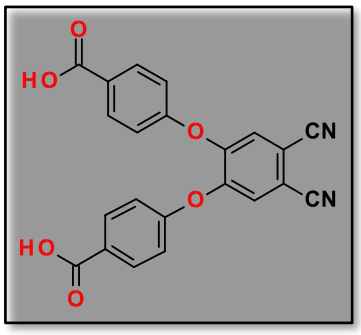

The synthesis of 4, 5-di(carboxylphenoxy) phthalonitrile was carried out following the previously reported methods with slight modification **[65].** A mixture of 4,5-dichlorophthalo-nitrile (0.50 g; 2.5 mmol) and 4-hydroxybenzoic acid (1.0 g; 7.5 mmol) was stirred in dry DMSO (20.0 mL) at 50°C for 48 hours under Argon gas. Dried fine powdered of K_2CO_3 (8 x 0.70 g; 5.0 mmol) and 8 x (1.40 g, 10.0 mmol) every 5 minutes was added. The reaction was cooled and added to ice. The precipitate formed was filtered off, washed with ice water, recrystallized with methanol and air-dried to obtain a white crystal of 4,5-di(4-carboxyphenoxy) phthalonitrile.

Yield (0.80 g; 98.1%),

- ^{1}HNMR (DMSO-d_6) δ (ppm); 7.21-7.18 (4H, d, Ar-H); 7.79 (2H, s, Ar-H); 8.01, 7.18 (4H, d, Ar – H), 8.44 (2H, s, $(COOH)_2$).
- FT-IR (ATR), υ_{max} (cm^{-1}): 3088 (O-H_{str}) (and C-H_{str}); 2234 (C≡N); 1679(C = O); 1285 (C-O_{str}) and 1082 (C–O–C).

2.4.2 Synthesis of 2,3,9,10,16,17,23,24-octacarboxyphenoxy phthalocyanines (H_2OcPhOPc)

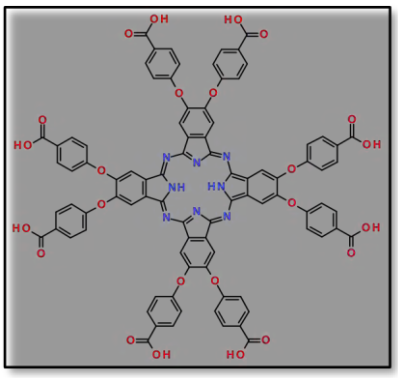

A mixture of 4,5-di(4-carboxyphenoxy) phthalonitrile (0.30 g; 0.70 mmol), and lithium metal (40.0 mg) in 1- pentanol (3.0 mL) was refluxed under argon gas at 130°C for 16 hours. The green precipitate was obtained, and the lithium metal was removed from the precipitate with 50% aqueous acetic acid (1.0 mL). This was followed by successive purification under centrifugation using methanol and 1 M HCl. The product was dried and further purified with a silica gel packed column eluting with a mixture of methanol:THF (1:5).

Yield 0.10 g (33%).

- FT-IR (ATR), υ_{max} (cm^{-1}); 3413 (N-H_{str}), 1717 (C=O_{str}), 1454 (C-H_{str}), 1064 (C-O-C).
- UV-Vis (DMSO), λ_{max} nm (ϵ): 674 (3.43), 618 (4.30), 342 (4.90).
- MALDI-TOM MS (m/z): Calc.1602.01. Found 1601.52. [M^+].

2.4.3 Synthesis of 2,3,9,10,16,17,23,24-octacarboxyphenoxy metallophthalocyanines (MOcPhPc), **Scheme 3.1**

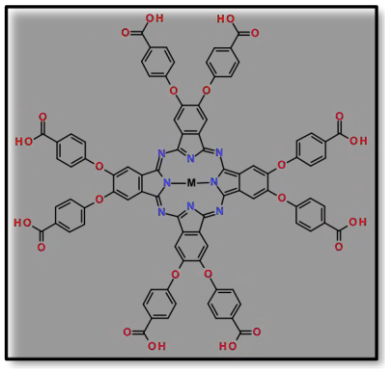

The mixture of 4,5-di (4-carboxyphenoxy) phthalonitrile (0.3 g; 0.7 mmol), 1-pentanol (3.0 mL), DBU (0.04 mL, 0.3 mmol) and metal salt (0.4 mg; 2.0 mmol) and refluxed under argon gas at 130°C for 16 hrs. After cooling to room temperature, the reaction mixture was precipitated by the addition of methanol, filtered and dried in air. The precipitate was treated with 1M HCl. The phthalocyanines were purified using silica gel column chromatography and

methanol: THF (1:5) as eluent system. The solvent was evaporated and the product was dried to yield **FeOcPhOPc**.

Yield 60.0 mg (19%).

- FT-IR (ATR), υ_{max} (cm^{-1}): 3264 (O-H), 2956 (Ar-C-H), 1714 (C=O), 1065 (C-O-C) and 1601 (Ar-C=C-C).
- UV-Vis (DMSO) λ_{max} (nm) (ε): 631 nm (4.30).
- MALDI-TOF MS (m/z): Calc.1655.84, [M^+]. Found 1653.71, [M – $2H^+$].

The metal salts used were iron (II) chloride (0.40 mg, 2.0 mmol), cobaltous acetate tetrahydrate (0.40 mg, 2.2 mmol) and manganese (II) acetate (0.40 mg; 2.3 mmol) to give three complexes.

2.4.4 Synthesis of CoOcPhOPc

Yield 90.0 mg (30 %).

- FT-IR (ATR), υ_{max} (cm^{-1}); 3256 (O-H), 2932 (C-H), 1717 (C=O), 1095 (C–O-C) and 1604 (Ar-C=C-C).
- UV-Vis (DMSO) λ_{max} (nm) (ε): 661 (4.25), 338(2.54).
- MALDI-TOF MS (m/z): Calc.1654.93 [M^+]. Found 1653.63 [M-H^+].

2.4.5 Synthesis of Mn(OAc)OcPhOPc

Yield 70.0 mg (23 %).

- FT-IR (ATR), υ_{max} (cm^{-1}): 3382 (O-H), 1716 (C=O), 1083 (C-O-C) and

1601 (Ar-C=C-C).

- UV-Vis (DMSO) λ_{max} (nm) (ε): 715 (4.27), 499 (4.17), 376 (1.56).
- MALDI-TOF MS (m/z): Calc.1656.93 [M^+]. Found 1654.06 [$M-2H^+$].

2.5 Synthesis of 4-nitrobenzene tetrafluoroborate diazonium salt

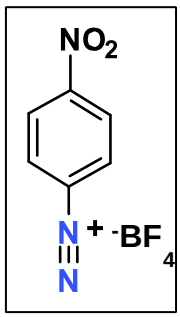

The synthesis of diazonium salt followed a reported method **[66]** with slight modification. Briefly, the 4-nitrobenzenediazonium tetrafluoroborate was synthesized by reacting 4-nitroaniline (1.04 g, 15.0 mmol) with HBF_4 (3.0 mL) and stirred for 15 minutes in an ice bath at -5°C. Ice cold solution of $NaNO_2$ (1.04 g, 30.0 mmol) was added drop wisely. The mixture was stirred vigorously for 40 minutes. The precipitate formed and was filtered, washed with petroleum ether and vacuum dried. The product was stored in the dark and frozen.

Yield 0.84 g (82%).

- FT-IR (ATR) ν_{max} (cm^{-1}): 3381 (N-H), 3107 (Ar-CH), 2307 (N≡N), 1615 (C=C-C).

2.6 Electrode modification with diazonium and metallophthalocyanines

2.6.1 Electrode cleaning and pre-treatment

The gold electrode was first polished with aqueous slurries of alumina powder (< 2 µm) on a SiC emery paper (type 2400 grit). After which it was washed with a copious amount of Millipore water, and mirror-polished on a Buehler felt pad with various aqueous alumina

slurries of 1.0 μm, 0.3 μm and 0.065 μm, respectively. The gold electrode was then subjected to ultrasonic vibration in absolute ethanol to remove residual alumina powder. The organic contaminant on the electrode surface was etched in a "Piranha" solution (1:3 (v/v) 30% H_2O_2 and concentrated H_2SO_4) for about 2 minutes. Gold electrode was then rinsed with a copious amount of Milli-Q water and finally rinsed with absolute ethanol. The cleanliness was confirmed with cyclic voltammetry by subjecting the electrode to multiple cycle scans in 0.50 M H_2SO_4. The scanned potential was between -0.5 and 1.5 V (versus Ag|AgCl) at a scan rate of 50 mV/s until a reproducible scan was achieved.

2.6.2 Pre-modification of gold electrode using electrochemical grafting method

The reductive electrodeposition of the synthesized 1.0 mM 4-nitrobenzene tetrafluoroborate diazonium salt (1.18 mg, 5.0 μmol) in ACN (5.0 mL) containing 0.1 M $TBABF_4$ (164.0 mg, 0.50 mol) was carried out. The cyclic voltammetry was run at four cycles at the potential range of + 0.40 V to - 0.40 V and at the fixed scan rate of 100 mV/s. Phenylnitro formed on the gold surface (Au-PNO_2). Au-PNO_2 was electrochemically reduced to phenylamino (Au-PA) group in aprotic solvent (ethanol/water) (1:9 v:v) containing 0.10 M KCl solution at the potential range between + 0.40 and -1.25 V at the fixed scan rate of 100 mV/s.

2.6.3 Immobilization of MOcPhOPc complexes onto Au-PA to yield Au-PA-MOcPhOPc

The immobilization of MOcPhOPc was carried out after the electrografting process and following amide coupling. The phenylamino modified surface of the electrode (Au-PA) was dipped into DMF solution containing the EDC/NHS activated MOcPhOPc. EDC and NHS are coupling agent. A mixture of MOcPhPc (5.0 mg, 6.0 μmol), NHS (57.5 mg, 49.7 mmol) and EDC (96.0 mg, 50.1 mmol) was dissolved in PBS pH 7.4 (5.0 ml) and allowed to react to form

an active carbodiimide esters for 6 hours. The electrografted electrode (Au-PA) was immersed in the solution and kept for 6 hours. The active carbodiimide esters underwent a condensation reaction with the amino groups. The reaction resulted in the formation of amide bonds between the activated carboxylic acid functional groups of the phthalocyanine complexes and terminal amine functional groups on the electrode surface (Au-PA). The modified electrode was stored rinsed with phosphate buffer pH 4.0 to yield Au-PA-MOcPhOPc surfaces (M = Co, Fe, and Mn(OAc)].

2.7 Analysis of neurotransmitters and ascorbic acid

The neurotransmitters (DA, EP, NEP, SER) with final concentration of 0.10 mM was prepared in 10 mL of PBS (pH 7.4) solution. The bare and modified electrodes were scanned between -0.20 V to +0.60 V and at the scan rate 50 mV/s for electrooxidation of NTs. Cyclic and differential pulse voltammetry methods were used for the detection and quantification of the neurotransmitters. The concentration range for the analysis was 30.0 to 70.0 μM. The signals were observed and recorded after the addition of the 3.0 μM in 5.0 mL PBS (pH 7.4) solution. The selectivity of the modified electrode was demonstrated towards the NTs using cyclic and differential pulse voltammetry methods with ascorbic acid as a strong interferent. Ascorbic acid (17.60 mg, 0.10 mM) was dissolved in 10 mL PBS (pH 7.4). Cyclic and differential pulse voltammetry methods were used at the potential range of -0.20 V to + 0.60 V at the scan rate 50 mV/s.

3 CHAPTER THREE: SYNTHESIS AND CHARACTERIZATION

3.1 Synthesis of octacarboxyphenoxy metallophthalocyanines

Scheme 3.1 shows the schematic illustration of the synthesis of octacarboxyphenoxy metallophthalocyanines **(4), (5)** and **(6)**. The first step involved the synthesis of 4,5-di(4-carboxyphenoxy) phthalonitrile **(3)**. The synthesis of **(3)** involve nucleophilic aromatic substitution reaction between 4,5-dichlorophthalonitrile **(1)** and 4-hydroxybenzoic acid **(2)** in the presence of K_2CO_3 as a base. The octacarboxyphenoxy phthalocyanine complexes **(4), (5)** and **(6)** were synthesised by cyclotetramerization of **(3)** in the presence of the corresponding metal salts (Fe, Mn, Co) using 1-pentanol as a refluxing solvent and catalytic amount of DBU refluxed at 130 ^{o}C.

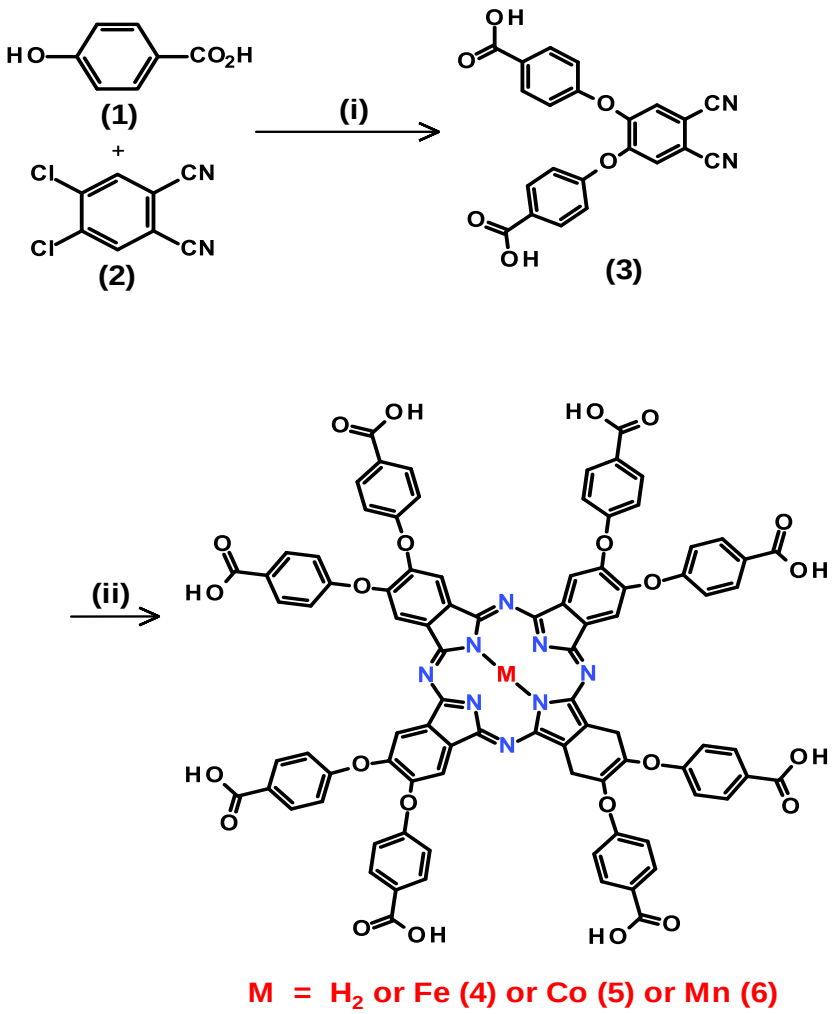

Scheme 3.1: The synthesis route for octacarboxyphenoxy metallophthalocyanines (MOcPhOPc) complexes. (i) Dry DMSO, Ar gas, K_2CO_3, 50 °C, 48 hrs; and (ii) 1pentanol, metal salt, DBU, 130 °C, 16 hrs.

3.2 Characterization of MPc complexes

3.2.1 FT-IR characterization of metallophthalocyanines

Figure 3.1 shows the FT-IR spectra of (i) 4-hydroxybenzoic acid (**1**), (ii) 4,5-dichlorophthalonitrile (**2**) and (iii) 4,5-di(4-carboxyphenoxy) phthalonitrile (**3**). The observed changes in the FTIR spectra shows the disappearance of hydroxyl (OH) stretch at

3400 cm^{-1} for 4-hydroxybenzoic acid (**1**) and a shift of the carbonyl (C=O) from 1669 cm^{-1} to 1680 cm^{-1}. The disappearance of the C-Cl at 829 cm^{-1} for 4,5-dichlorophthalonitrile (**2**) was observed. This was observed with an emergence of C-O ether stretch at 1161 cm^{-1} confirming to formation of 4,5-di(4-carboxyphenoxy) phthalonitrile (**3**). The retention of the characteristic nitrile (C≡N) functional group at 2234 cm^{-1} was observed. The FTIR results confirm the functional groups for the successful synthesis of 4,5-di(4-carboxyphenoxy) phthalonitrile (**3**).

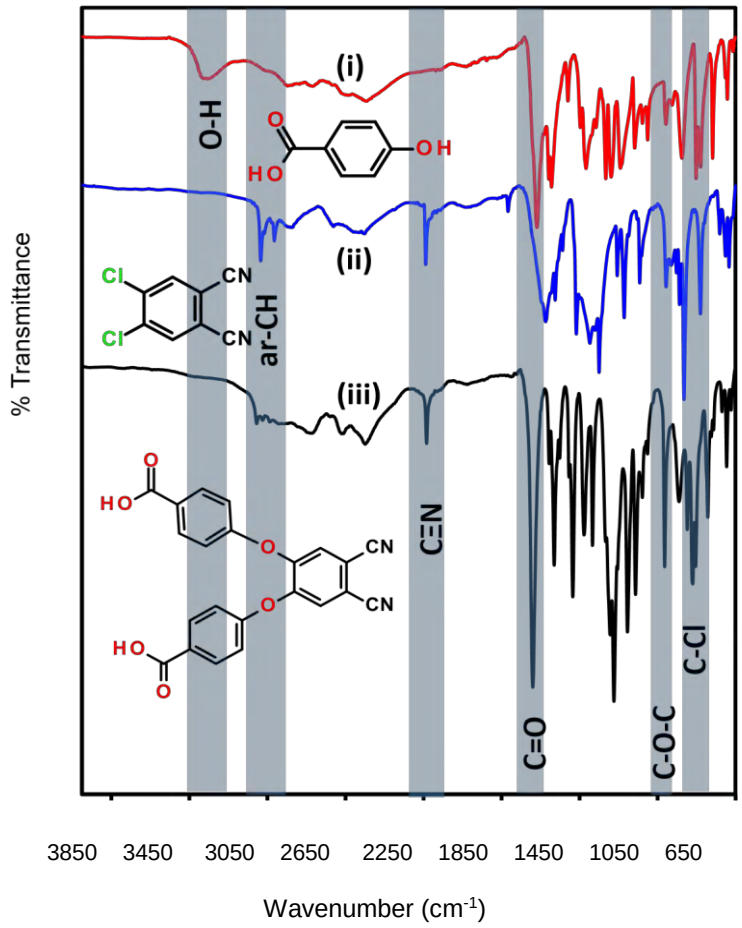

Figure 3.1: FT-IR spectra of (i) 4-hydroxybenzoic acid (**1**), (ii) 4,5-dichlorophthalonitrile (**2**) and (iii) 4,5-di(4-carboxyphenoxy) phthalonitrile (**3**).

Figure 3.2 shows the FT-IR spectra of (a) FeOcPhOPc (**4**), (b) CoOcPhOPc (**5**) and (c) Mn(OAc)OcPhOPc (**6**). The FTIR spectrum of FeOcPhOPc exhibited the OH stretch at 3332 cm^{-1}. The C=O stretch of the carboxylic acid was observed at 1714 cm^{-1}. The OH and C=O

bands confirmed the presence of COOH of the carboxylphenoxy substituents on the FeOcPhOPc complex. The significant ar-C=C stretch from the aromatic ring was also observed at 1596 cm^{-1} and ar-CH was also observed at 3080 cm^{-1}. The disappearance of the characteristic C≡N peak of the precursor at 2234 cm^{-1} was also observed. The peak of the split C-O-C stretching frequencies for the ether groups at 1208 – 1161 cm^{-1} was observed. In addition **Figure 3.2** shows the FT-IR spectra of (b) CoOcPhOPc (**5**) and (c) Mn(OAc)OcPhOPc (**6**). The spectra for both complexes exhibited OH stretching peaks for the carboxylic acid group was observed at 3259 cm^{-1} for CoOcPhOPc (**5**) and at 3382 cm^{-1} for Mn(OAc)OcPhOPc (**6**). The C=O stretch of the carboxylic acid was observed at 1717 cm^{-1} for CoOcPhOPc (**5**) and at 1716 cm^{-1} for Mn(OAc)PhOPc (**6**). These confirmed the presence of COOH of the carboxylphenoxy substituents on the CoOcPhOPc (**5**) and Mn(OAc)OcPhOPc (**6**). The ar-CH peak at 2930 cm^{-1} for the aromatic ring was observed. Similar to the FTIR for the FeOcPhOPc (**4**), the disappearance of the characteristic C≡N peak of the precursor at 2234 cm^{-1} was also noticed for CoOcPhOPc (**5**) and Mn(OAc)OcPhOPc (**6**). The significant ar-CH peaks for the aromatic ring was observed at 1598 cm^{-1} and at 1597 cm^{-1}, respectively for CoOcPhOPc (**5**) and Mn(OAc)OcPhOPc (**6**). The C-O stretch peak was observed at 1272 cm^{1}. The peak of the split C-O-C stretching frequencies for the ether groups was observed at 12061161 cm^{-1} for CoOcPhOPc (**5**) and at 1207 – 1084 cm^{-1} for Mn(OAc)OcPhOPc (**6**).

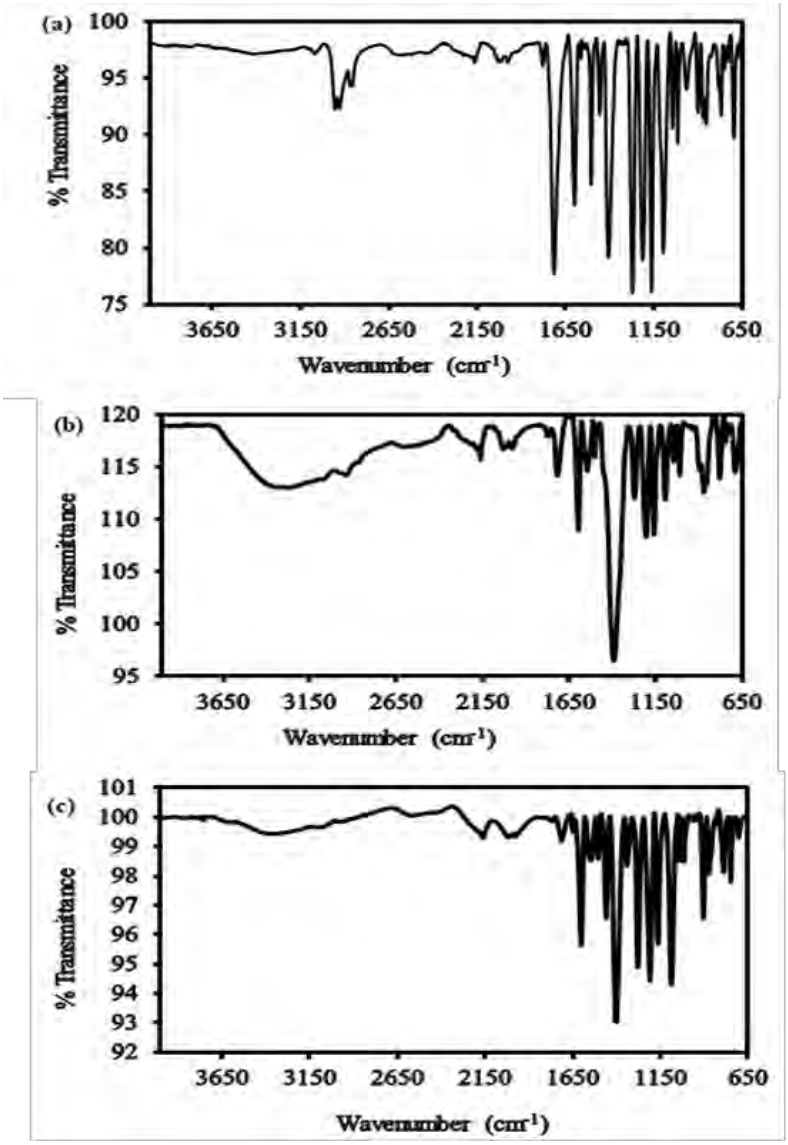

Figure 3.2: FT-IR spectroscopic characterization of **(a)** FeOcPhOPc (**4**), **(b)** CoOcPhOPc (**5**), and **(c)** Mn(OAc)OcPhOPc (**6**).

3.2.2 Ultraviolet-visible (UV-Vis) characterization of MOcPhOPc

Figure 3.3 shows the UV-Vis absorption spectra of 12 nM of **(a)** FeOcPhOPc, **(b)** CoOcPhOPc, and **(c)** Mn(OAc)OcPhOPc complexes in DMSO. The electronic ground state absorption spectra of complexes FeOcPhOPc **(4),** CoOcPhOPc **(5),** and Mn(OAc)OcPhOPc **(6)** showed monomeric behaviour with a single Q-band at 663 nm, 667 nm and 728 nm respectively. The single Q-bands are characteristics of metal containing phthalocyanines with degenerate e_g

orbital. This reflects the transitions between the highest occupied molecular orbital (HOMO) to the lowest unoccupied molecular orbital (LUMO) of the delocalized phthalocyanines. The red shift in the position of the Q-band of the Mn(OAc)OcPhOPc complex relative to FeOcPhOPc and CoOcPhOPc could be attributed to increase in oxidation state Mn(III) and a decrease in the energy band gap between the HOMO and the LUMO orbitals after the insertion of the transition metal. The B-band of the complexes (**5**) and (**6**) were observed at 338 nm and 376 nm; respectively. The B-bands are a resultant transition from the b_2u and a_2u transitions to e_g. For the Mn(OAc)OcPhOPc (**6**) there was an additional band at 498 nm due to the metal-to-ligand (MLCT) or ligand-to-metal (LMCT) charge transfer. These are due to the Mn metal orbitals lying between the HOMO and LUMO orbital of the phthalocyanine ring allowing for transitions from the Pc ligand to metal orbitals or from metal orbitals to Pc ligand.

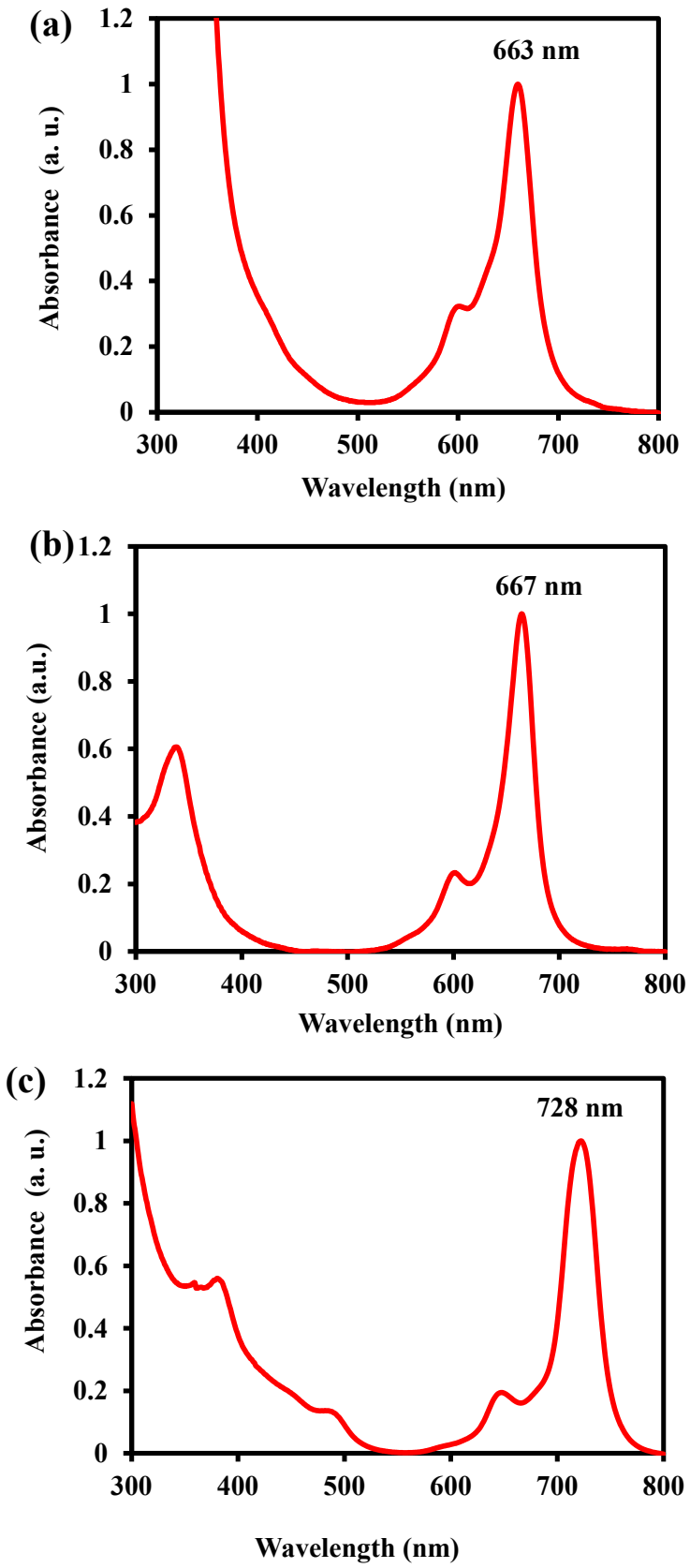

Figure 3.3: UV-Vis absorption spectra of 12 nM of **(a)** FeOcPhOPc, **(b)** CoOcPhOPc, and **(c)** Mn(OAc)OcPhOPc complexes in DMSO.

The molecular interaction of the complex monomers could result in aggregation, thereby causing a decrease in intensity and broadening of Q-band. The aggregation behaviour of the complexes was further investigated with different concentrations of complexes (**4**), (**5**), and (**6**) in DMSO. **Figure 3.4** shows the UV-Vis absorption spectra of different concentrations of **(a)** FeOcPhOPc, **(b)** CoOcPhOPc, and **(c)** Mn(OAc)OcPhOPc complexes in DMSO. The UV-Vis of complex (**4**) in **Figure 3.4 (a)** showed a broad Q-band even at lower concentrations, which suggested that the complex (**4**) aggregates in DMSO. The aggregation behaviour of complex (**4**) could be attributed to the formation of π- π interaction and could account for the absence of the B-band in complex (**4**). The UV-Vis spectra of complexes (**5**) and **(6)** in **Figure 3.4 (b)** and **(c)** showed a sharp Q-band even at higher concentrations up to 15.1 nM. This confirmed that complexes **(5)** and **(6)** are monomeric and no aggregation was observed in DMSO.

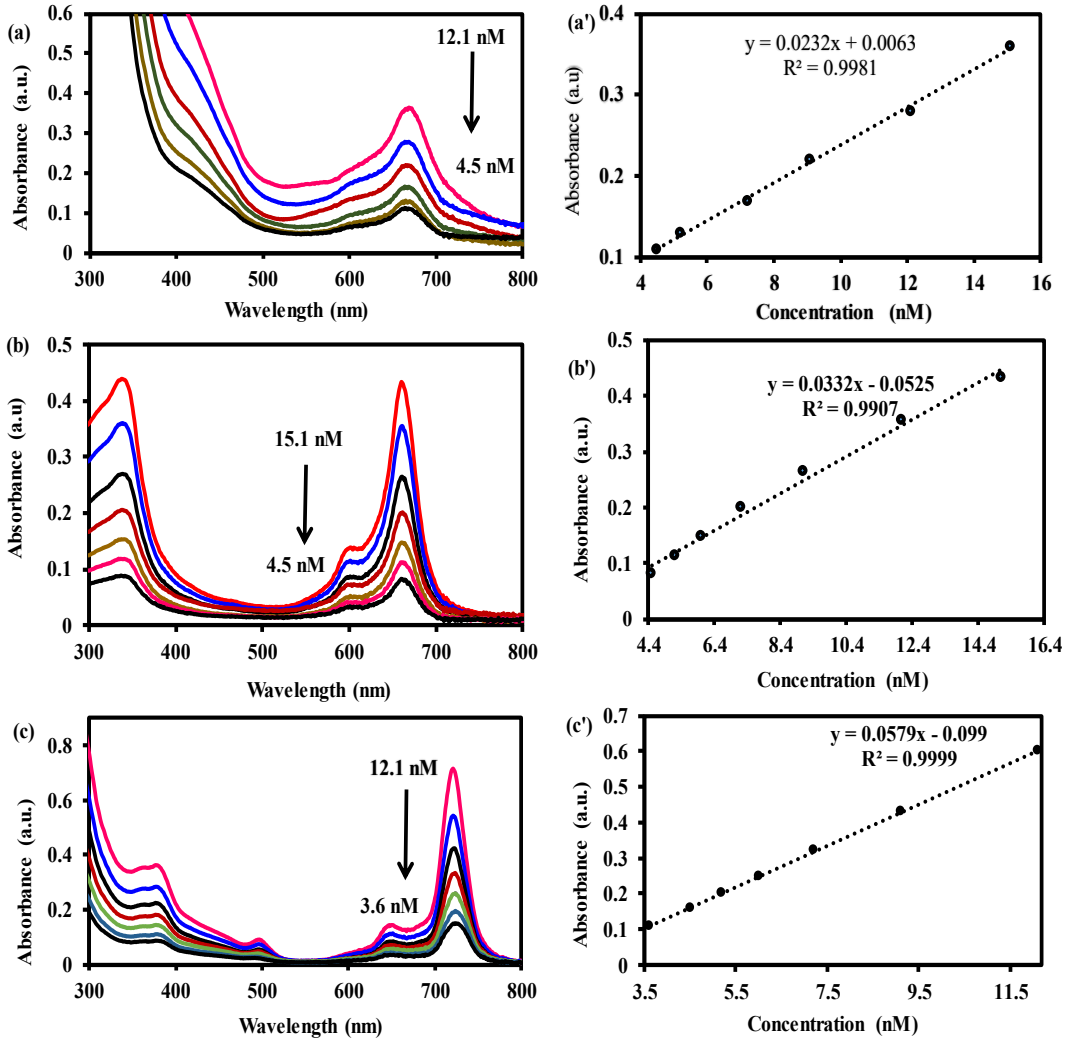

Figure 3.4: Aggregation studies relationship between absorbance for different concentrations of **(a)** FeOcPhOPc, **(b)** CoOcPhOPc, **(c)** Mn(OAc)OcPhOPc complexes in DMSO.

3.2.3 Magnetic circular dichroism (MCD) characterization of complexes

Figure 3.5 shows the MCD and UV-Vis spectra of 12 nM **(a)** H_2OcPhOPc, **(b)** FeOcPhOPc, **(c)** CoOcPhOPc, and **(d)** Mn(OAc)OcPhOPc. The split peaks in the H_2OcPhOPc MCD in **Figure 3.5 (a)** confirmed the Faraday B terms, which correspond to the two separate peaks of the Q-band in the UV-Vis absorption spectrum of H_2OcPhOPc. This is normally expected for metal-free phthalocyanines. The Faraday B term arises from the effects of Zeeman splitting of

the zero-field states through magnetic dipole moments transitions **[67]**. The MCD transition for FeOcPhOPc **(4)** in **Figure 3.5 (b)** indicated a pseudo –Faraday A term. It arises from the π→ π* transition in a degenerate state. The energy splitting transition is small, the MCD curve observed appear like a Faraday A term but differs. The absorbance of the MCD band at 631 (-) cm^{-1} corresponds to the absorbance of the UV-Vis Q-band at 631 nm. The absorbance of the UV-Vis and MCD for CoOcPhOPc **(5)** at room temperature in **Figure 3.5 (c)** indicated a Faraday A terms. The peaks correspond to the absorption peaks, which confirmed the D_{4h} symmetry. The MCD observed Faraday A terms at 661 and 600 (-) cm^{-1} corresponding to the Q-bands at 661 nm and 600 nm. The band at 339 (-) cm^{-1} which corresponds to 338 nm (Soret band) of the UV-Vis bands at room temperature. It confirmed the D_{4h} symmetry for complex **(5)**. The MCD spectrum of Mn(OAc)OcPhOPc **(6)** in **Figure 3.5 (d)** clearly showed a single Q band corresponding to a Faraday A term. The peaks correspond to the absorption peaks, which confirmed the D_{4h} symmetry. MCD spectrum of the π →π* transition was observed at 718 (-) cm^{-1} which corresponds to 715 nm (Q-band). Ligand-to-metal charge transfer (LMCT) and metal-to-ligand charge transfer (MLCT) at 496 cm^{-1} correspond to 498 nm. The B band observed at 376 nm corresponds to 374 (-) cm^{-1} in the MCD spectra. This confirmed the D_{4h} symmetry for complex **(6)**. This allowed the identification of specific transitions that may have overlapped in the absorption spectra.

3.2.4 Mass spectrometry characterization of MPc

The octacarboxyphenoxy metallophthalocyanines complexes were characterized using MALDI-TOF mass spectrometer. **Table 3.1** summarized the theoretical and experimental molecular mass of the synthesised complexes. The mass spectra for FeOcPhOPc showed a molecular ion peak at m/z = 1653.71 $[M-2H]^+$, CoOcPhOPc peaks at 1661.67 $[M+3H]^+$ and

Mn(OAc)OcPhOPc peak m/z at 1653.90 $[M-H]^+$. The mass spectroscopy results shown in **Table 3.1** confirmed the successful formation of the complexes.

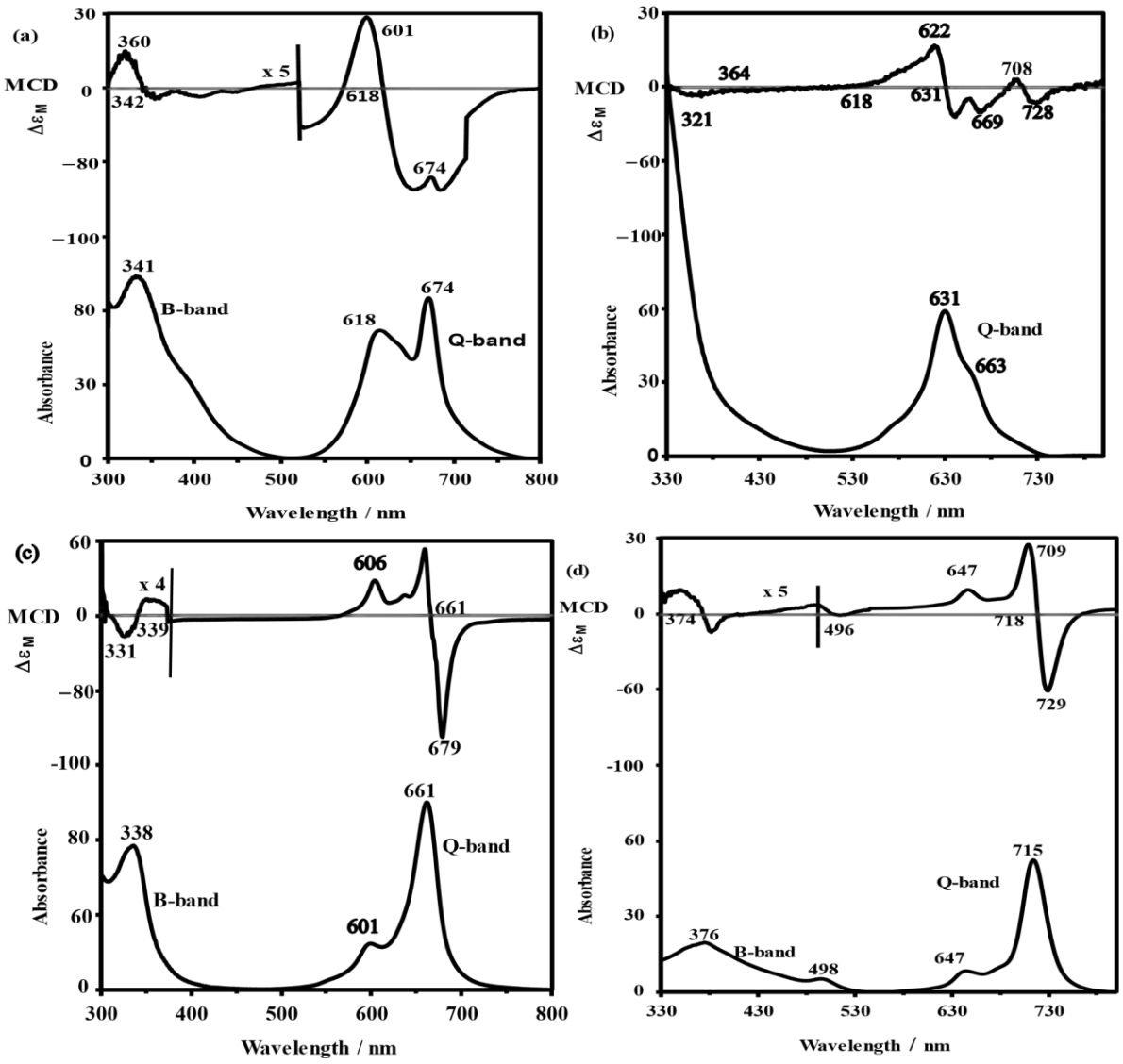

Figure 3.5: MCD and UV-Vis spectra of 12 nM of **(a)** H_2OcPhOPc, **(b)** FeOcPhOPc, **(c)** CoOcPhOPc and **(d)** Mn(OAc)OcPhOPc in THF.

Table 3.1: Summary of characterization of the complexes with FT-IR, UV-Vis, MCD, MS, and Elemental analysis.

Complexes	FT-IR (cm^{-1})		UV-Vis (nm)		MS (m/z)		Elemental					
	Groups	Wavenumber	Wavelength (λ, nm), log ε	Assigned bands	Expected	Found	Expected (%)			Found (%)		
							C	H	N	C	H	N
FeOcPhOPc	OH	3332	663	Q band	1656.2131 $[M]^+$	1653.71 $[M-2H]^+$	59.45	3.67	6.86	59.9	4.2	8.1
	arCH	3020	608	Vibronic band								
	C=O	1714										
	ar-C=C	1596										
	C-O-C	1208-1161										
CoOcPhPc	OH	3259	667	Q band	1659.2113 $[M]^+$	1661.67 $[M+3H]^+$	63.8	3.1	6.7	49.1	1.5	7.4
	C=O	1717	607	Vibronic band								
	ar-CH	2930										
	arC=C	1598										
	C-O	1272	343	B (Soret) band								
	C-O-C	1206-1161										
Mn(OAc)OcPhOPc	OH	3382	728	Q band	1655.2162 $[M]^+$	1653.70 $[M-2H]^+$	63.9	3.1	6.7	59.2	3.7	5.3
	arCH	3020										
	C=O	1716	655	Vibronic band								
	ar-C=C	1597	495	MLCT/LMCT								
	C-O-C	1207-1084	386	B (Soret) band								

4 CHAPTER FOUR: ELECTRODE MODIFICATION, ELECTROCATALYSIS AND ELECTROANALYSIS

4.1 Electrode modification and surface characterisation

Scheme 4.1 shows the schematic illustration of the immobilisation of the octacarboxyphenoxy metallophthalocyanines complexes (**4**), (**5**) and (**6**) onto the gold electrode surface. The first step involves the formation of a thin-film of phenylamino functional group on the gold electrode, represented as Au-PA. This was achieved via electrochemical grafting of 1.0 mmol. L^{-1} 4-nitrobenzene tetrafluoroborate diazonium salt in a solution of 0.10 mol.L^{-1} $TBABF_4$. This process involves the electrochemically reduction of 4-nitrobenzene tetrafluoroborate diazonium to form phenylnitro radical. Upon scanning to more negative potential, the phenylnitro radical was then grafted onto the gold electrode surface. The phenylnitro modified gold electrode surface was represented as Au-PNO_2. Subsequently, the Au-PNO_2 surface was electrochemically reduced by cycling between +0.25 to -1.25 V vs Ag|AgCl in (1:10 by v: v) ethanol/water mixture containing 0.10 mol.L^{-1} KCl. The Au-PNO_2 surface was reduced to the phenylamino group functionalized gold surface (Au-PA). The Au-PA have terminal NH_2 group.

The immobilisation of the synthesised FeOcPhOPc **(4),** CoOcPhOPc **(5),** and Mn(OAc)OcPhOPc **(6)** onto the Au-PA electrode was achieved via EDC/NHS carbodiimide crosslinking reaction. The crosslinking reaction involves the activation of the terminal carboxylic acid groups of the complexes with EDC and NHS to form an amine reactive succinimide ester group (semi-stable NHS-activated complexes). The NHS-activated complex reacts with the amine groups of the Au-PA electrode via amide bond formation. A similar immobilisation process was used for covalent attachment of all the complexes onto the gold electrode surface to yield, Au-PA-CoOcPhOPc, Au-PA-FeOcPhOPc and Au-PAMnOcPhOPc.

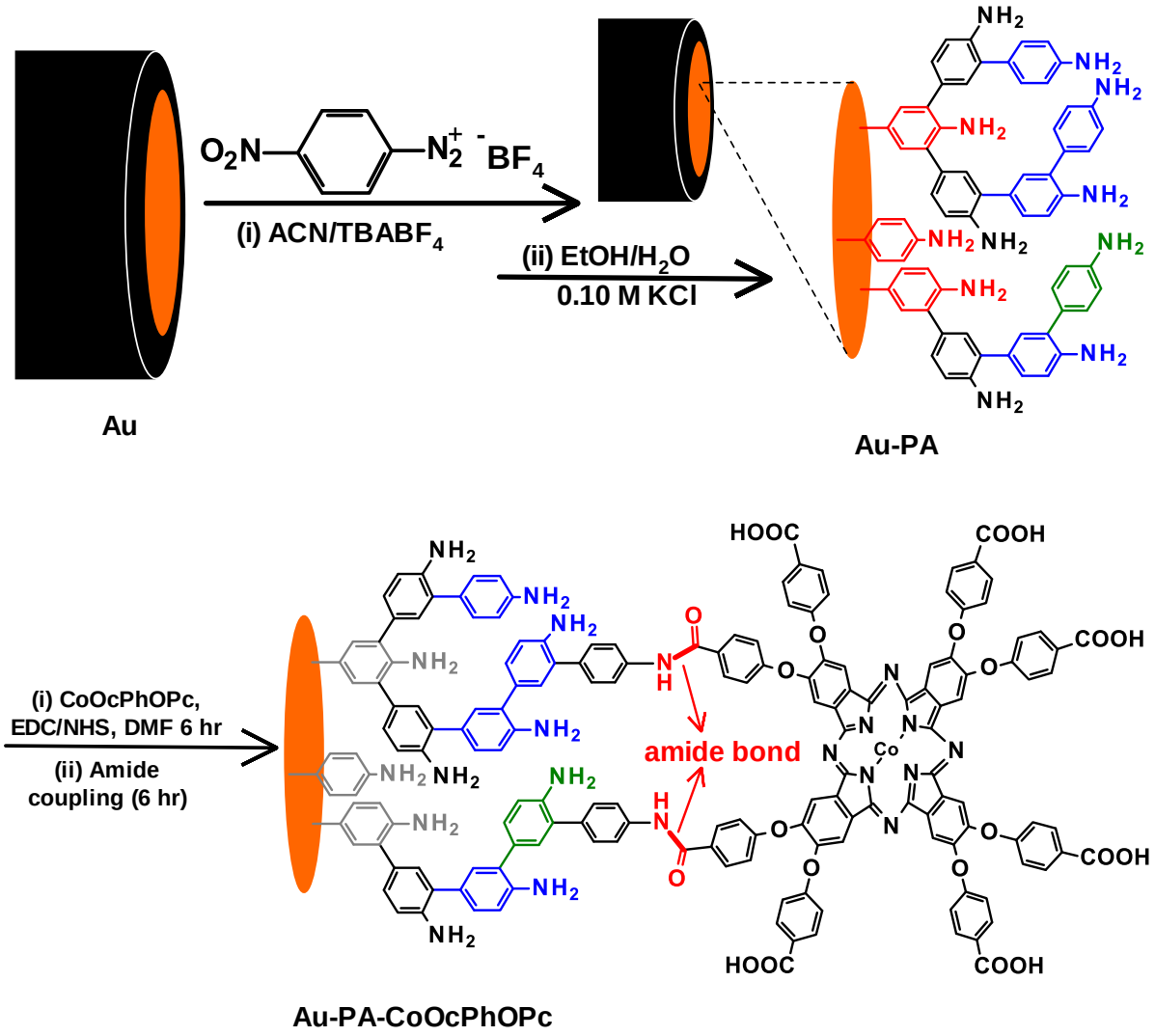

Scheme 4.1: Procedure for the electrochemical grafting and immobilisation of CoOcPhOPc onto gold electrode surface premodified with phenylamine represented as Au-PA-CoOcPhOPc. Similar procedure was used for the immobilisation of FeOcPhOPc (Au-PA-FeOcPhOPc) and Mn(OAc)OcPhOPc (Au-PA-Mn(OAc)OcPhOPc).

4.2 Electrografting and characterization of Au, Au-PA and Au-PA-CoOcPhOPc surfaces

4.2.1 Cyclic voltammetry of electrode modified with phenylamino (Au-PA)

Figure 4.1 shows the cyclic voltammograms for **(a)** electrochemical reduction of 4-nitrobenzene diazonium salt, and (**b**) electrochemical reduction of phenylnitro group to form phenylamino group. The first scan in the voltammograms in **Figure 4.1 (a)(i)** showed a cathodic peak at 0.31 V. This reduction peak corresponds to the electrochemical reduction of the diazonium and the formation of the phenylnitro radical with loss of N_2. The radical attached to the gold electrode and formed a thin film of phenylnitro (Au-PNO_2) on the electrode surface when the potential was scanned to the potential that is more negative. The cathodic peak disappeared during the subsequent scans due to the grafting of the radical onto the electrode surface. This confirmed the formation of phenylnitro layer on the Au electrode surface. The use of three CV scans was employed to achieve a thin of monolayer or few multilayers. The formation of a monolayer is idealistic but not achievable even though some reports have claimed the formation of a monolayer **[68]**. It is possible to form a thin multilayer film and a study of distinct number of layer deposition is ideal but not a subject of this work.

Figure 4.1 (b) shows the cyclic voltammograms for electrochemical reduction of phenylnitro to form phenylamino groups. The first scan in the voltammograms in **Figure 4.1 (b)(i)** showed intense cathodic peak at -0.92 V (labelled **II**). This cathodic peak corresponds to the reduction of the phenylnitro group (PNO_2) to phenylhydroxylamine group (PHA). The PHA oxidizes to phenylnitroso group and the CV in **Figure 4.1 (b)(ii)** showed an oxidation peak at -0.27 V (labelled **III**). The peak at -0.42 V in **Figure 4.1 (b) (iii)** was due to the reduction of PHA to

phenylamino group (PA) thus the formation of Au-PA. On subsequent scans, the reduction peak at -0.92 V disappeared, confirming the conversion of the phenylnitro groups to phenylamino group. The peak at -0.92 V was preceded by a peak at -0.63 V (labelled **I**) attributed to the reduction of the physiosorbed phenylnitro on the phenylnitro modified surface.

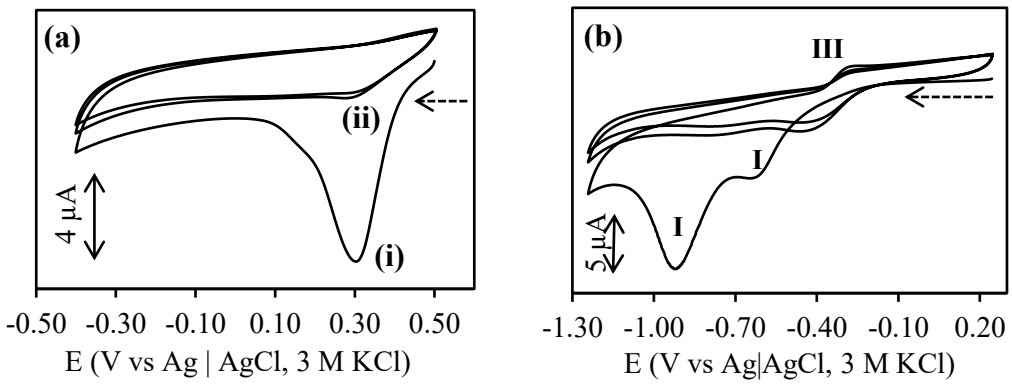

Figure 4.1: Cyclic voltammograms of **(a)** the electroreduction and grafting of phenylnitro from 1.0 mM 4-nitrobenzene diazonium salt tetrafluoroborate in ACN containing 0.10 M $TBABF_4$ in 3 cycles and **(b)** reduction of NO_2 to NH_2 in ethanol/water (1:9) solution containing 0.10 M KCl. Scan rate 100 $mV.s^{-1}$.

4.2.2 Cyclic voltammetry and electrochemical impedance spectroscopy studies

Figure 4.2 shows the cyclic voltammograms (CV) and the electrochemical impedance spectroscopy (EIS) of the **(i)** bare Au, **(ii)** Au-PA and **(iii)** Au-PA-CoOcPhOPc in **(a)** 2.0 $mmol.L^{-1}$ $K_3/K_4[Fe(CN)_6]$ and **(b)** 2 $mmol.L^{-1}$ $[Ru(NH_3)_6]$ containing 0.10 $mol.L^{-1}$ KCl at a scan rate of 50 $mV.s^{-1}$. The CV of the bare Au electrode in $K_3/K_4[Fe(CN)_6]$ in **Figure 4.2 (a) (i)** showed Fe^{II}/Fe^{II} reversible redox couple of $[Fe(CN)_6]^{3-/4-}$ with a peak-to-peak separation (ΔE) of 73 ± 4.4 mV. The CV of the Au-PA electrode in **Figure 4.2 (ii)** showed a decrease in peak current when compared to the bare Au electrode. The cathodic peak shifted to higher

potential and the anodic peak was not observed. This showed that the PA-layer passivates the Au surface and blocks electron transfer process. The CV of the Au-PA-CoOcPhOPc showed restoration (to some extent) of the Fe^{II}/Fe^{II} reversible redox couple of $[Fe(CN)_6]^{3-/4-}$. At Au-PA-CoOCPhOPc, the ΔE was 154 ± 4.53 mv. The restoration of the redox process at the Au-PA-CoOcPhOPc surface was attributed to the electrocatalytic properties of CoOcPhOPc towards $[Fe(CN)_6]^{3-/4-}$ redox couple. The anodic and cathodic current at the Au-PA-CoOcPhOPc were very small compared to the bare Au surface but much higher compared to Au-PA surface.

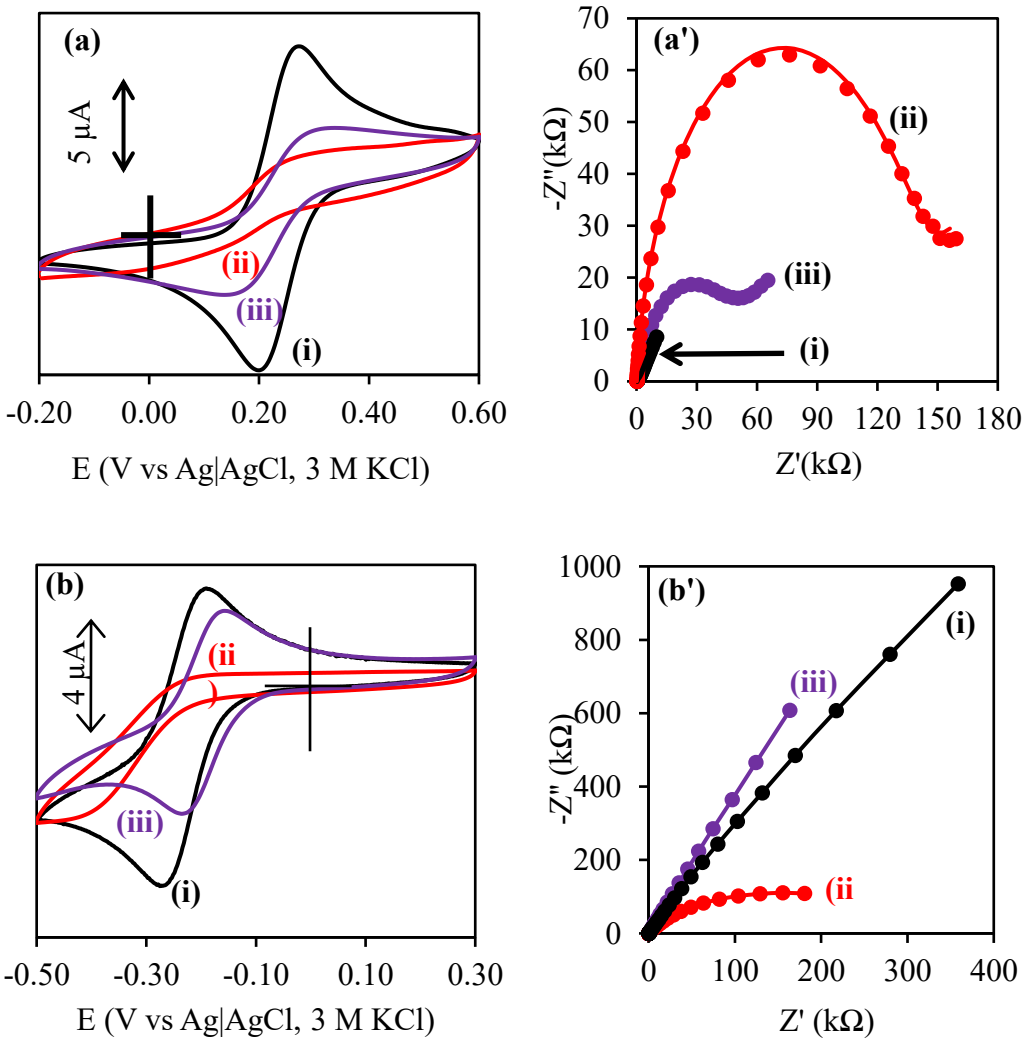

Figure 4.2: CV and EIS of **(i)** bare Au, **(ii)** Au-PA and **(iii)** Au-PA-CoOcPhOPc in **(a)** 2.0 mM $K_3/K_4[Fe(CN)_6]$ and **(b)** 2.0 mM $Ru(NH_3)_6$ containing 0.10 M KCl. Scan rate = 50 $mV.s^{-1}$.

The slow electrode kinetics results from the slight repulsive effect of the negatively charged carboxyl (COO^-) groups of Au-PA-CoOcPhOPc or delayed electron transfer due to the Au-PA thin film. Both these phenomena are possible, the pH studies will be investigated later. The restoration of the Fe^{II}/Fe^{III} redox couple due to $[Fe(CN)_6]^{3-/4-}$ was observed for the Au-PA-FeOcPhOPc and Au-PA-Mn(OAc)OcPhOPc with the peak to peak separation of 127 ± 2.52 mV and 188 ± 2.56 mV respectively. The restoration of the redox couple is due to the observed phenomena for the Au-PA-CoOcPhOPc as discussed above. The redox properties of the bare and modified electrodes were studied with a positive redox probe using Ruthenium hexamine, $[Ru(NH_3)_6]^{2+/3+}$, solution. The cyclic voltammograms of the bare Au electrode in 2.0 $mmol.L^{-1}$ $Ru(NH_3)_6$ containing 0.10 M KCl are shown in **Figure 4.2 (b)(i).** A characteristic $[Ru(NH_3)_6]^{+2/+3}$ redox couple with an anodic potential at 170 mV and a cathodic peak at –260 mV was observed. The peak-to-peak separation (ΔE) was 90 mV. The CV of the Au-PA in the $[Ru(NH_3)_6]$ solution in **Figure 4.2 (b)(ii)** showed a complete blockage of the electrode surface and no observable cathodic or anodic peak observed. This was attributed to the thin PA layer coating the gold electrode surface. The CV of the Au-PA-CoOcPhOPc in **Figure 4.2 (b)(iii)** showed restoration of $[Ru(NH_3)_6]^{2+/3+}$ redox couple with an increase in cathodic and anodic peak currents. The immobilization of CoOcPhOPc to form Au-PA-CoOcPhOPc onto the Au-PA layer was confirmed and the catalytic nature of the CoOcPhOPc also catalyzed the $[Ru(NH_3)_6]^{2+/3+}$ redox couple. The anodic and cathodic peaks shifted to lower potential in comparison to the bare Au surface with a ΔE of 92 mV. The effect resulted from the electrostatic attraction between the positively charged $[Ru(NH_3)_6]^{2+/3+}$ and the negative charge carboxylic acid (COO^-) of the Au-PA-CoOcPhOPc. The Au-PA-FeOcPhOPc and Au-PA-Mn(OAc)OcPhOPc sensors also displayed anodic and cathodic peaks that shifted to lower potentials with increase in currents.

The ΔE were summarized in **Table 4.1**. Furthermore, the electrochemical impedance characteristics of the modified surfaces were recorded to investigate the electron transfer properties on modified gold surfaces. **Figure 4.2 (a')** show the Nyquist plot of **(i)** Au, **(ii)** Au-PA and **(iii)** Au-PA-MOcPhPc in 2.0 mmol.L^{-1} $K_3/K_4[Fe(CN)_6]$ containing 0.10 mol.L^{-1} KCl. The charged transfer resistance (R_{CT}) for the bare Au electrode was 0.67 kΩ.cm^{-2}. The R_{CT} increased significantly to 139 kΩ.cm^{-2} and attributed to the inhibition of electron transfer process after the formation of the Au-PA thin film. The Nyquist plot of Au-PA-MOcPhPc in **Figure 4.2 (a') (iii)** showed a decrease in the R_{CT} from 139 kΩ.cm^{-2} for Au-PA to 9.01 kΩ cm^2 for Au-PA-CoOcPhOPc. The decrease was due to the conductivity of CoOcPhOPc. For the other MPc complex modified electrodes similar trends were observed and R_{CT} decreased to 25.10 kΩ.cm^{-2} for Au-PA-Mn(OAc)OcPhOPc and 27.70 kΩ.cm^{-2} for Au- PA-FeOcPhOPc. The impedance data was accepted when the error (% error) of all the circuit elements was less than 5% and are summarized in **Table 4.1**. The Nyquist plot of the (i) bare Au, (ii) Au-PA, and (iii) Au-PA-CoOcPhOPc in 2.0 mmol.L^{-1} $Ru(NH_3)_6$ solution are shown in **Figure 4.2(b')**. The Nyquist plot of the bare Au in $Ru(NH_3)_6$ in **Figure 4.2 (b')(i)** had R_{CT} of 0.010 kΩ.cm^{-2}. The R_{CT} for the Au-PA increased to 0.26 kΩ.cm^{-2} due to the passivation of the PA thin film after formation of Au-PA. On Au-PA-CoOcPhOPc, the R_{CT} decreased to 0.17 kΩ.cm^{-2} due catalytic effect or conductivity of the CoOcPhOPc layer. For the Au-PA-FeOcPhOPc the R_{CT} was 0.69 kΩ.cm^{-2} and 1.10 kΩ.cm^{-2} for Au-PA-Mn(OAc)OcPhOPc. The increase in the RCT was observed for Au-PA-FeOcPhOPc and Au-PA-Mn(OAc)OcPhOPc and this was attributed to the fitted circuit elements were summarized in **Table 4.1**.

The real surface area of the gold electrode represents the actual are of gold surface after mechanical treatment by polishing in aqueous alumina slurries of 1.0, 0.30 and 0.065 micron. The geometric area calculated using the active surface diameter is 0.0201 cm^2 and represent an

underestimation of the actual electrode surface. Using the electrochemical measurement to calculate the actual surface area and was found to be 0.0413 cm^2 using **Equation 4.1**

$$I_{pa} = (2.69\ X\ 10^5)\ n^{3/2}\ AD^{1/2}\ Cv^{1/2} \ldots\ldots\ldots\ldots\ldots\ldots\ldots\ldots\ldots\ldots\ldots\ldots\ldots\ldots (\mathbf{4.1})$$

where 'n' is the number of electrons involved (n = 1); A is the geometric surface area of gold electrode (A = actual surface area calculated); C is the concentration of the $K_3Fe(CN)_6$ is (2.0 $mmol.L^{-1}$), D is the diffusion coefficient of $K_3Fe(CN)_6$ is 7.6 X 10^{-6} cm^2s^{-1} and ν is the scan rate (0.050 $V.s^{-1}$). The surface roughness, is the ratio of the real surface area (0.0413 cm^2) and the geometric area (0.0201 cm^2) is 2.05. The real surface area was used in all other surface area calculations.

Table 4.1: The CV and EIS results of the characterization of the bare Au, Au-PA and Au-PA-MOcPhPc (M = Fe, Co, and Mn) in 2.0 mM $K_3/K_4[Fe(CN)_6]$ containing 0.10 $mol.L^{-1}$ KCl.

Electrode	Cyclic voltammetry		Nyquist plot				
	△E (mV)	$E_{½}$ (mV)	R_S (kΩ)	R_{CT} (kΩ)	CPE (μF)	n	Z_W (μΩ)
Au	73 ± 4.40	205	0.26	0.67	3.75 ± 0.28	0.84	99.50
Au-PA	-	-	0.24	139	1.61 ± 0.11	0.93	64.90
Au-PA-FeOcPhOPc	127 ± 2.52	199	0.07	27.7	1.91 ± 0.70	0.77	61.90
Au-PA-CoOcPhOPc	154 ± 4.53	195	0.28	9.01	0.78 ± 0.14	0.89	67.50
Au-PA-MnOcPhOPc	188 ± 2.56	244	0.06	25.1	1.89 ± 0.10	0.78	56.90

4.2.3 Under potential deposition of copper (Cu-UDP) and gold oxidation

Figure 4.3 shows the cyclic voltammograms of the **(i)** bare Au, **(ii)** Au-PA, and **(iii)** Au-PA-CoOcPhOPc in (a) in 2.0 mmol.L^{-1} $CuSO_4$ containing 0.50 mol.L^{-1} H_2SO_4 and (b) 0.01 mol.L^{1} KOH solution. In **Figure 4.3(a)(i),** the bare gold electrode displayed two reduction peaks (**I)** due to metal reduction from Cu^{II} to Cu^{I} at 0.225 V. The second reduction peak (**II)** was observed at -0.015 V due to the metal reduction of Cu^{I}/Cu^{0}. The metallic Cu^{0} deposits onto the gold electrode surface, thereby forming Cu ad-atom formation. The return scan displayed a notable large anodic peak at 0.020 V due to the stripping of metallic (Cu^{0}) copper layer from the gold surface and oxidation Cu^{0} to form Cu^{I} and dissolving back into solution. Upon scanning further in the oxidation potential, Cu^{I} to Cu^{II} peak was observed at 0.242 V. In **Figure 4.3(a)(ii)** for Au-PA, the copper reduction-oxidation peaks at similar potential values were observed with decreased currents. The decrease in peak currents was due to PA thin layer that was electrografted onto the gold electrode surface. The deposited copper was at pinholes. In Figure **4.3(a)(iii)**, Au-PA-CoOcPhOPc, the reduction and stripping of $CuSO_4$ solution was blocked and very small redox peak due to copper were observed. The further decrease was due to the deposited CoOcPhOPc thin monolayer film after amide coupling reaction. The results confirmed the presence of PA (Au-PA) and PA-CoOcPhOPc onto gold electrode surface, establishing the presence of material (thin film layer of the complex) on the electrode surface. The complete suppression of the Cu reduction and oxidation reaction was also observed at Au-PA-FeOcPhOPc and Au-PA-Mn(OAc)OcPhOPc surfaces.

The oxidation and reduction reaction of the bare and modified electrodes were studied in 0.010 mol.L^{-1} KOH solution. The cyclic voltammograms of the bare Au in **Figure 4.3(b)(i)** shows the gold oxidation peak at 0.57 V and the reduction peak 0.18 V. The bare gold electrode surface in KOH forms a monolayer of oxygen in the form of gold (I) hydroxide on the forward scan.

On the reverse scan, the gold oxide layer was stripped off from the surface of the gold resulting in the broad reduction peak at 0.18 V. After the modification of the surface with phenylamino (Au-PA) and with PA-CoOCPhOPc thin films, the CVs in **Figure 4.3(b)(ii)** and **(iii)** shows that the oxidation and reduction peak currents decreased. The small peak currents were due to solution permeability and reaction at the pin-holes. Both the Au-PA and Au-PACoOcPhOPc showed reactions at pin-holes. The decrease in currents was due to the thin films blocking to some extent the solution ions from reaching the underlying gold surface for oxidation and reduction reactions to occur. The decrease in currents confirmed the formation of PA and PA-CoOcPhOPc thin films. Similar behaviour to Au-PA-CoOcPhOPc was observed for the Au-PA-FeOcPhOPc and Au-PA-Mn(OAc)OcPhOPc surfaces confirming the surface modification.

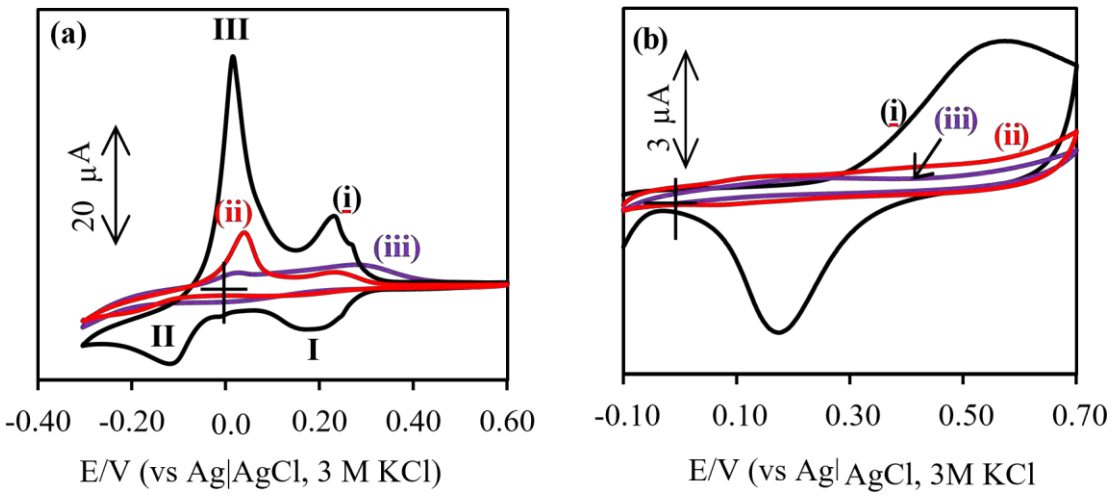

Figure 4.3: Cyclic voltammograms of **(i)** Au, **(ii)** Au-PA, **(iii)** Au-PA-CoOcPhOPc in (**a**) 2.0 mM $CuSO_4$ in 0.50 mol.L^{-1} H_2SO_4 and **(b)** 0.010 mol.L^{-1} KOH solution. Scan rate 100 mVs^{-1}.

The ion barrier factor (Γ_{ibf}), the measure of electrode modification and its interaction with solution ions was measured and calculated using **Equation 4.2.**

$$\Gamma_{ibf} = 1 - \frac{Q_{PA-MOcPhOPc}}{Q_{bare\ Au}} \quad \ldots\ldots\ldots\ldots\ldots\ldots\ldots\ldots\ldots\ldots\ldots\ldots\ldots\ldots (\mathbf{4.2})$$

The total charge (Q) of the bare and the modified surfaces were obtained by integrating the currents under the peak. $Q_{bare\ Au}$ for the bare was integrated and obtained to be 6.38 x 10^{-7} C and the $Q_{PA\text{-}MOcPhOPc}$ or Q_{PA} for the modified was for the PA and MOcPhOPc modified electrode. For Au-PA-CoOcPhOPc the $Q_{PA\text{-}CoOcPhOPc}$ was obtained to be 1.53 x 10^{-7} C. The Γ_{ibf} was calculated to be 0.76 for Au-PA-CoOcPhOPc and Au-PA-FeOcPhOPc, and 0.77 for AuPA-Mn(OAc)OcPhOPc. The surface coverage of the complexes on the gold electrode was also calculated using **Equation 4.3**

$$\Gamma_{MPc} = \frac{Q_{MOcPhOPc}}{nFA} \ldots\ldots\ldots\ldots\ldots\ldots\ldots\ldots\ldots\ldots\ldots\ldots\ldots\ldots\ldots\ldots\ldots\ldots (\mathbf{4.3})$$

Where Q is the charge under the reduction peak (Coulombs), F is the Faraday constants (96485 $C.mol^{-1}$), n is the number of electrons transferred (1.0) during the redox reaction, A is the geometric area of the gold electrode (0.0201 cm^2). The surface coverage was estimated to be 7.93 x 10^{-11} $mol.cm^{-2}$ for Au-PA-FeOcPhOPc, 7.98 x 10^{-11} $mol.cm^{-2}$ for Au-PA-CoOcPhOPc and 7.69 x 10^{-11} $mol.cm^{-2}$ for Au-PA-Mn(OAc)OcPhOPc. The values obtained are lower than those of phthalocyanines lying flat on the electrode surface or forming an umbrella orientation know to be 1.0 x 10^{-10} $mol.cm^{-2}$. The values cover a small surface area and therefore suggesting the perpendicular or vertical orientation of the MPc complexes on the gold electrode surface as previously reported **[69]**.

4.2.4 Buffer (pH 7.4) studies

Figure 4.4 shows the CVs of the **(i)** bare Au, **(ii)** Au-PA, and **(iii)** Au-PA-CoOcPhOPc. The CV for the bare Au showed no peak at the studied potential scan range. The Au-PA-CoOcPhOPc surface showed a metal ion redox process ($Co^{III}Pc^{-2}/Co^{II}Pc^{-2}$) with an oxidation peak at 250 mV and reduction peak at 120 mV. The formal potential ($E_{½}$) was found to be 185 mV. Metal redox processes were observed for Au-PA-FeOcPhOPc as $Fe^{II}Pc/Fe^{III}Pc^{-2}$ and Au-PA-Mn(OAc)OcPhOPc as $Mn^{III}Pc^{2}/Mn^{IV}Pc^{-2}$. The oxidation and reduction peaks observed for Au-PA-Mn(OAc)OcPhOPc were 239 mV and 127 mV with $E_{½}$ = 183 mV. The redox peaks observed on the modified surfaces confirmed the presence of the thin layer film on the electrode surface and was not observed at Au-PA surface.

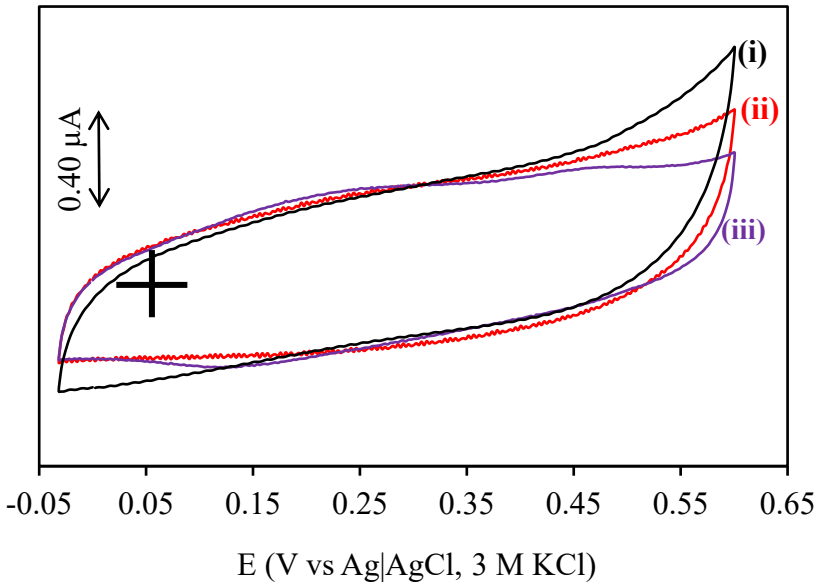

Figure 4.4: Cyclic voltammograms of **(i)** bare Au, **(ii)** Au-PA, and **(iii)** Au-PA-CoOcPhOPc in 0.10 M phosphate buffer saline (PBS) solution, pH 7.4. Scan rate = 100 $mV.s^{-1}$.

4.3 Effect of pH studies of Au-PA-MOcPhOPc towards $[Fe(CN)_6]^{3-/4-}$ redox couple

Figure 4.5 shows the effect of pH changes for **(a)** Au-PA-FeOcPhOPc, **(b)** Au-PA-CoOcPhOPc and **(c)** Au-PA-Mn(OAc)OcPhOPc surfaces in 2.0 mmol.L^{-1} $K_3/K_4[Fe(CN)_6]$ containing 0.10 mol.L^{-1} KCl at different pH solutions ranging from (5.0 to 8.0). For all the complex modified electrodes, the CV showed a decrease in current and an increase in peak-to-peak separation (ΔE) as the pH increased from 5.0 to 8.0. The decrease was attributed to the deprotonation of carboxylic acid functional group (COO^-) repelling the negatively charged redox probe, $[Fe(CN)_6]^{3-/4-}$. The pKa of the carboxylic acid on the peripheral position of the phthalocyanine complexes is 4.59. Therefore, at pH > 4.59 the COOH is negatively charged (COO^-). **Figure 4.5 (a' – c')** shows Impedance data represented as Nyquist plots for (a) Au-PA-FeOcPhOPc, (b) Au-PA-CoOcPhOPc and (c) Au-PA-Mn(OAc)OcPhOPc surfaces in 2.0 mmol.L^{-1} $K_3/K_4[Fe(CN)_6]$ containing 0.10 mol.L^{-1} KCl at different pH solutions ranging from (5.0 to 8.0). The Nyquist plots shows the increase in the R_{CT} with the increase in pH further confirming pH sensitive and responsive nature of Au-PA-MOcPhOPc surfaces. The pH effect of Au-PA-MOcPhOPc (M = Co, Fe and Mn(OAc)) was further investigated against the positively charged redox probe, $[Ru(NH_3)_6]^{2+/3+}$.

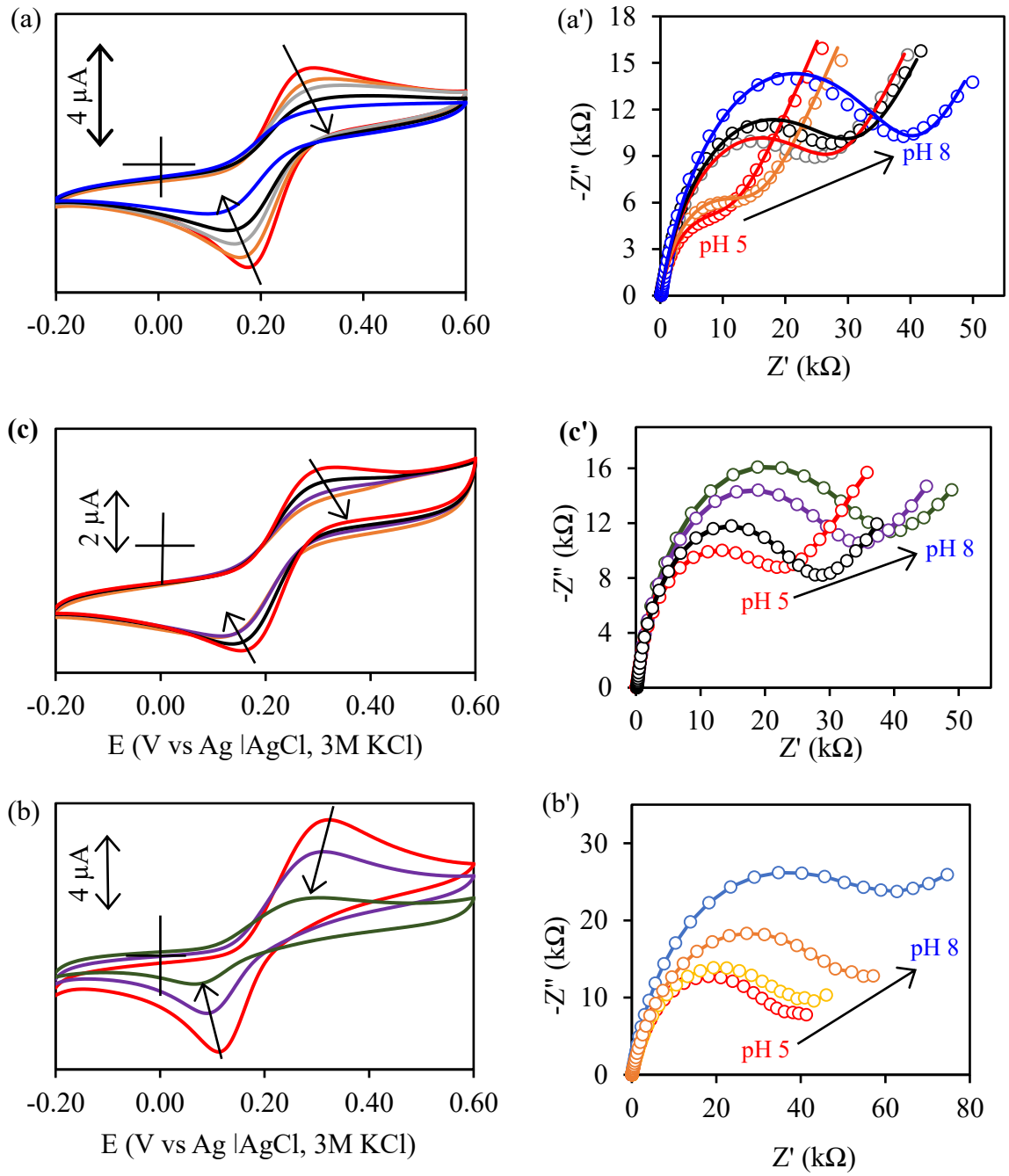

Figure 4.5: Cyclic voltammograms and impedance spectroscopy (Nyquist plot) for **(a)** Au-PA-FeOcPhOPc, **(b)** Au-PA-CoOcPhOPc, and **(c)** Au-PA-Mn(OAc)OcPhOPc in 2.0 mmol.L^{-1} $K_3/K_4[Fe(CN)]_6$ containing 0.10 mol.L^{-1} KCl at varied pH conditions.

4.4 Effect of pH changes of Au-PA-MOcPhOPc towards $[Ru(NH_3)_6]^{2+/3+}$ redox probe

Figure 4.6 shows the effect of pH changes for Au-PA-CoOcPhOPc, (a) the cyclic voltammograms, and (b) Impedance spectroscopy (Nyquist plots) in 2.0 $mmol.L^{-1}$ $Ru(NH_3)_6$ containing 0.10 $mol.L^{-1}$ KCl at different pH ranging from (3.0 to 8.0). There were no changes in the cyclic voltammograms and impedance spectroscopy (Nyquist plot representation) for all the electrodes. The lack of changes is due to the fact that the pKa values for carboxylic acid of the metallophthalocyanines are 4.57. This means that at pH < pKa, the carboxylic acid functional groups are neutral (COOH). At pH values > pKa, the carboxylic acid functional groups are deprotonated (COO^-). There is therefore attractive forces between the COO^- and $[Ru(NH_3)_6]^{2+/3+}$ and hence the observed redox couple due at Au-PA-CoOcPhOPc. The COOH functional groups behave the same for the MOCPhOPc modified electrodes (Au-PA-MOcPhOPc, M = Co, Fe and Mn). The impedance spectroscopy (Nyquist plot representation) showed a Wardburg Impedance (Z_w) with semi-infinite straight line. The observation confirms the oxidation and reduction of $Ru(NH_3)_6$ at electrodes even after modifying with octacarboxyphenoxy phthalocyanine complexes. This is preliminary to the eletrocatalysis and shows the pH sensitive effect of the modified gold electrodes with complexes bearing carboxylic acid functional groups.

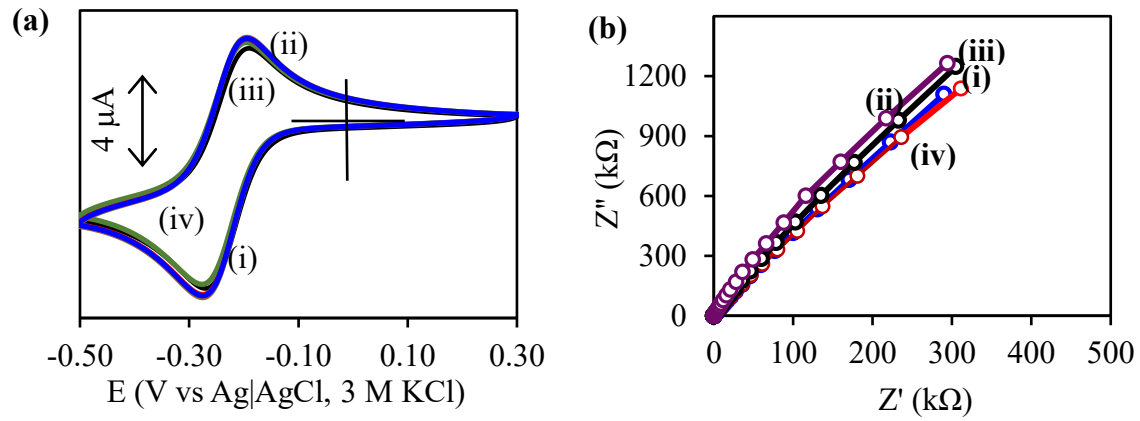

Figure 4.6: (a) Cyclic voltammograms (CVs) and (b) Impedance spectroscopy (Nyquist plots) of the effect of pH on 2.0 mM $[Ru(NH_3)_6]^{2+/3+}$ containing 0.10 M KCl at Au-PA-CoOcPhOPc.

4.5 Electrocatalysis of neurotransmitters and ascorbic acid at bare Au and Au-PA

The major aim of the research was to design a pH sensitive electrochemical sensor capable of detecting neurotransmitters (epinephrine, norepinephrine, dopamine and serotonin) but screen off ascorbic acid. The investigation of the detection of neurotransmitters at bare Au and Au-PA as underlying surface was important. Therefore, **Figure 4.7** shows the CVs (i) bare Au and (ii) Au-PA surfaces in the presence of 0.10 mM (a) epinephrine, (b) serotonin, (c) dopamine, (d) norepinephrine, and (e) 0.10 mM of ascorbic acid at pH 7.4 PBS. The CVs, in **Figure 4.7 (i)** for all the neurotransmitters and including ascorbic acid (a strong interfering species) showed peaks at the bare gold electrode. When the gold was coated with phenylamine (Au-PA) in **Figure 4.7** (ii), the peaks disappeared and this was due to the blockage of the gold surface by phenylamine thin film. The phenylamine thin film is not conducting and hence no electrooxidation and electroreduction of neurotransmitters and ascorbic acid was observed. The phenylamine therefore silenced the electrooxidation and electroreduction of neurotransmitters and ascorbic acid.

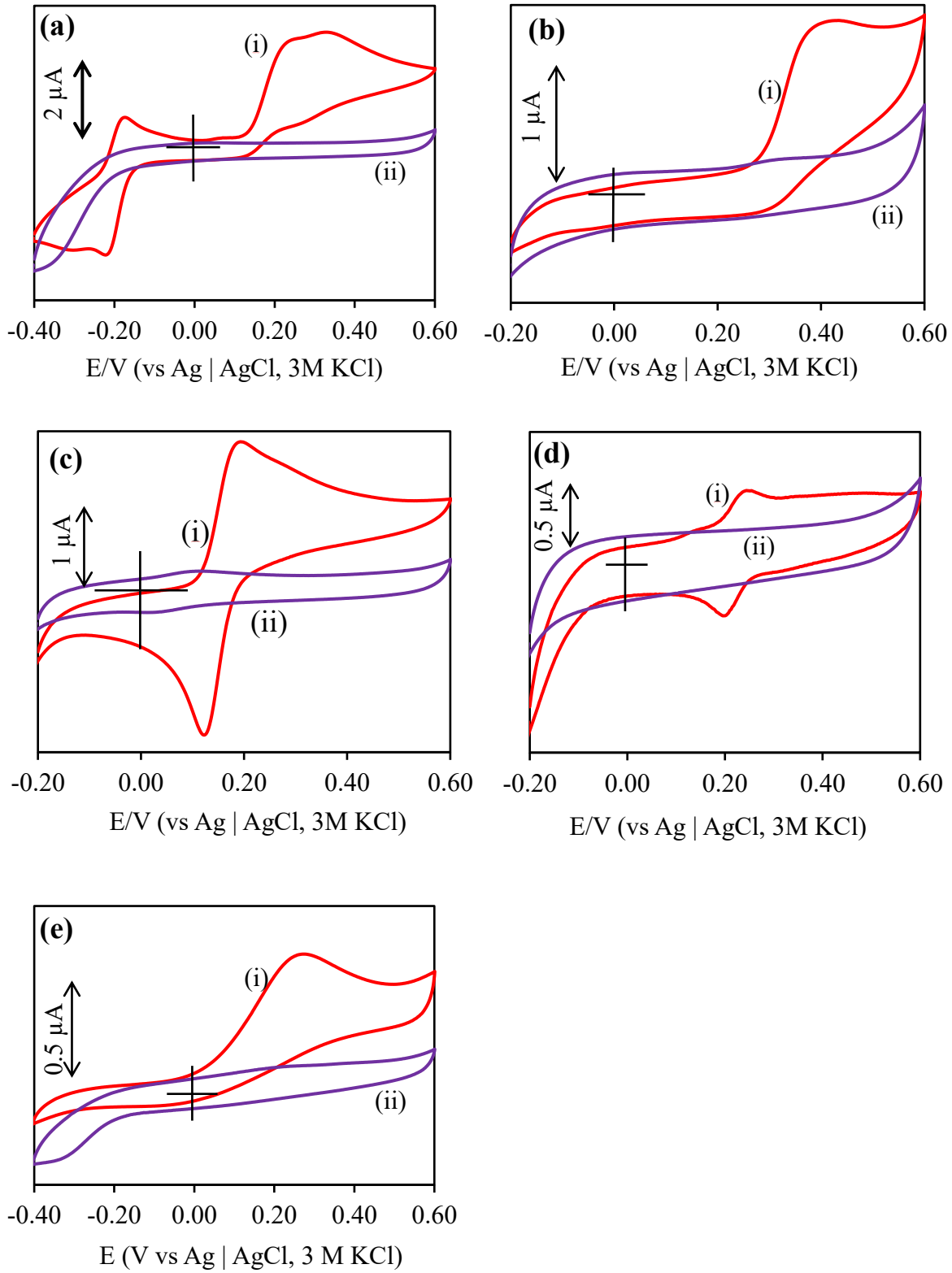

Figure 4.7: Cyclic voltammograms of 0.10 mM of **(a)** epinephrine, **(b)** serotonin, **(c)** dopamine **(d)** norepinephrine, **(e)** ascorbic acid at **(i)** bare Au and **(ii)** Au-PA surfaces.

The peak potentials for the electrooxidation and electroreduction of neurotransmitters on bare Au electrode are summarized in **Table 4.2**. The oxidation peak potential for ascorbic acid is in the same potential range as the neurotransmitters making their detection complicated. In addition, ascorbic acid concentration is always higher (100-fold) than the neurotransmitters in bodily fluids. Therefore, there is a need to design electrochemical sensors that can block of ascorbic acid during the detection of neurotransmitters which are of importance in the diagnosis of neurodegenerative diseases. The modification of gold electrode with PA-MOcPhOPc seeks to achieve this goal by introducing carboxylic acid functional groups on the electrode surface to screen the ascorbic acid. The effect of pH was studies and showed that the negatively charged redox species, $[Fe(CN)_6]^{3-/4-}$ redox couple was suppressed at Au-PA-MOcPhOPc due to the negatively charged COO^- functional group at pHs > 5 (pKa of COOH). Ascorbic acid has pKa of 4.2 and exists as an ascorbate anion at pH > 4.2.

Table 4.2: Summary of electrooxidation and electroreduction peak potentials.

	E^1_{pa} (V)	E^2_{pa} (V)	E_{pc} (V)	Onset E (V)
Epinephrine (EP)	-0.161	0.249	-0.219	0.130
Serotonin (SER)	-	0.432	-	0.274
Dopamine (DA)	-	0.208	0.127	0.098
Norepinephrine (NEP)	-	0.261	0.202	0.171
Ascorbic Acid (AA)	-	0.289	-	0.000

4.6 Electrocatalysis and analysis of neurotransmitters at Au-PA-CoOCPhOPc

4.6.1 Electrocatalysis of neurotransmitters at Au-PA-CoOcPhOPc at physiological pH

Figure 4.8 shows the cyclic voltammograms of Au-PA-CoOCPhOPc in (i) pH 7.4 PBS and (ii) pH 7.4 PBS + 0.10 mM of **(a)** epinephrine (EP), **(b)** norepinephrine (NEP), **(c)** dopamine (DA), and **(d)** serotonin (SER). **Figure 4.8(i)** shows the Au-PA-CoOcPhOPc in the buffer solution alone. There was a small metal redox peak due Co^{II}/Co^{III} in the centre of phthalocyanine ring as observed before in **Figure 4.4**. In the present of 0.10 mM of neurotransmitters (EP, NEP, DA, SER), in **Figure 4.8(ii)**, there was an increase in currents and peak due to each analyte. The presence of 0.10 mM epinephrine, in **Figure 4.8(a)(ii)**, the two oxidation peaks were observed at -0.217 V and 0.259 V with the reduction peak at -0.268 V. The oxidation peak at 0.259 V had an onset potential at 0.086 V. The lower onset potential confirmed the excellent electrocatalyst (CoOcPhOPc) immobilized onto the phenylamine (AuPA). For norepinephrine in **Figure 4.8(b)(ii)**, the oxidation peak was observed at 0.183 V and the reduction peak was observed at 0.086 V. For the oxidation peak the onset was at a low 0.022 V confirming the excellent CoOcPhOPc as an electrocatalyst. In Figure **4.8(c)(ii)**, the electrocatalytic detection of dopamine was observed with the oxidation peak at 0.217 V and reduction peak at 0.042V. The onset potential for the oxidation peak was at 0.061 V confirming excellent electrocatalyst (CoOcPhOPc). **Figure 4.8(d)(ii)** showed an increase in the current with serotonin oxidation with a peak at 0.344 V and an onset potential at 0.169 V. The oxidation peak potentials were in the range for metal ion oxidation (Co^{II}/Co^{III}) and therefore the metal redox couple is involved in the electrocatalysis of the neurotransmitters.

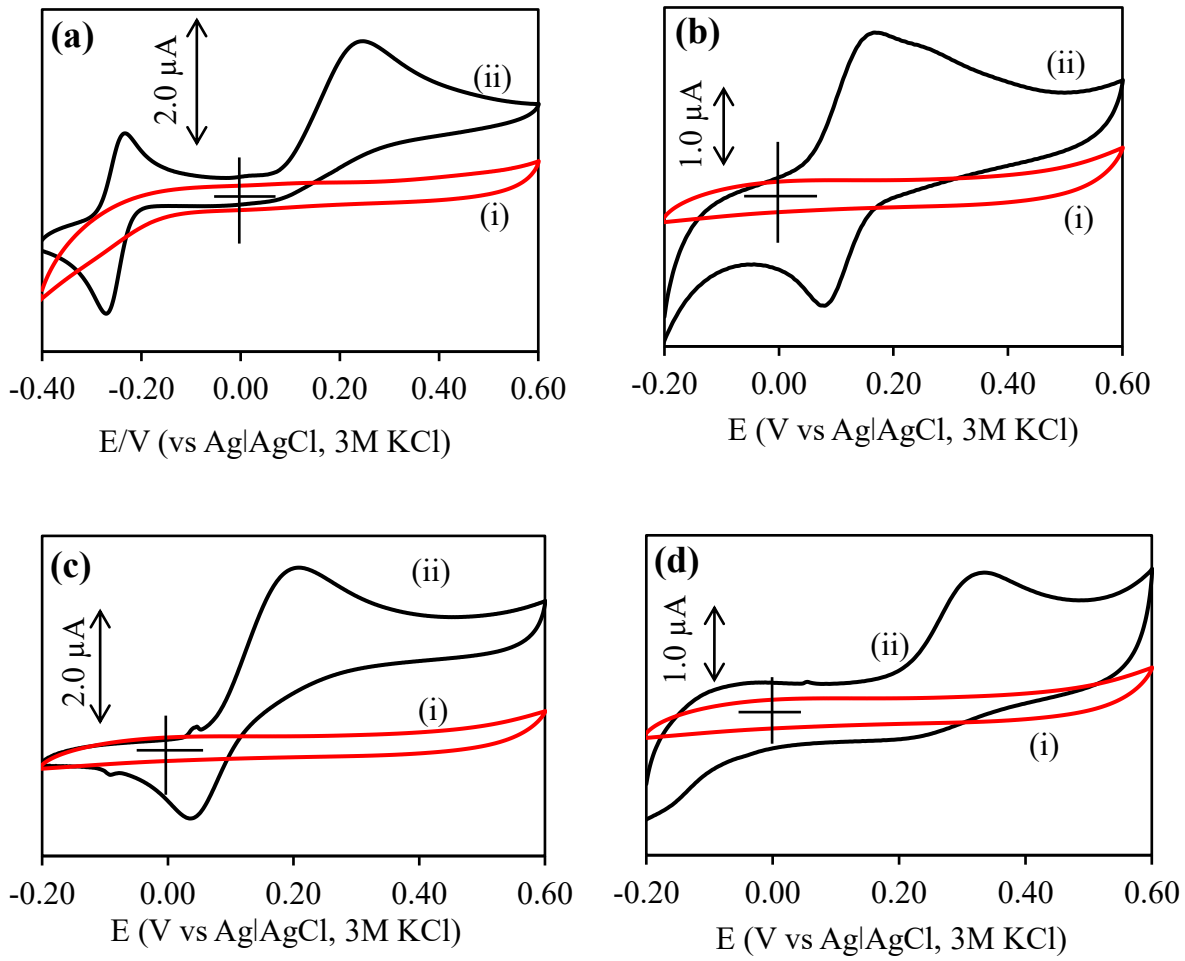

Figure 4.8: Cyclic voltammograms of Au-PA-CoOCPhOPc in (i) pH 7.4 PBS and (ii) pH 7.4 PBS + 0.10 mM of **(a)** epinephrine (EP), **(b)** norepinephrine (NEP), **(c)** dopamine (DA), and **(d)** serotonin (SER).

The electrooxidation and electroreduction potentials are summarized in **Table 4.3**. A pH 7.4 PBS solution of ascorbic acid (0.10 mM) was also investigated at the Au-PA-CoOcPhOPc. The CVs were the same as in **Figure 4.8(i)**. No oxidation or reduction peak was observed at pH 7.4 PBS. At bare Au, the oxidation of ascorbic acid was observed with a peak at 0.289 V. The Au-PA also showed no oxidation or reduction peak due to the passivation of the phenylamine thin film layer. At the Au-PA-CoOcPhOPc, the onset potential for the electrooxidation of neurotransmitters shifted to lower potential values. This was due to the electrocatalytic effect

of CoOcPhOPc. The analysis of neurotransmitters was investigated following the electrooxidation peak above 0.20 V as it showed sensitivity to the changes in concentrations.

Table 4.3: Summary of the electrocatalytic properties of bare Au and Au-PA-CoOcPhOPc.

Electrodes		E^1_{pa} (V)	E^2_{pa} (V)	E_{pc} (V)	Onset E (V)
bare Au	Epinephrine (EP)	-0.161	0.249	-0.219	0.130
	Serotonin (SER)	-	0.432	-	0.274
	Dopamine (DA)	-	0.208	0.127	0.098
	Norepinephrine (NEP)	-	0.261	0.202	0.171
	Ascorbic Acid (AA)	-	0.289	-	0.000
Au-PA-CoOcPhOPc	Epinephrine (EP)	-0.217	0.259	-0.268	0.086
	Serotonin (SER)	-	0.344	-	0.169
	Dopamine (DA)	-	0.217	0.086	0.022
	Norepinephrine (NEP)	-	0.183	0.202	0.171
	Ascorbic Acid (AA)	-	-	-	-

At the Au-PA-CoOcPhOPc modified surface, the epinephrine redox process was restored due to the electrocatalytic activity of the CoOcPhOPc. The electrocatalysis of the Au-PACoOcPhOPc caused an enhancement in the peak current of epinephrine, compare with the EP response at the bare Au electrode as shown in **Figure 4.9(a).** The oxidation potential of epinephrine shifted to 0.254 V and the reduction peak potential also shifted to -0.249 V. The electrocatalysis of Au-PA-FeOcPhOPc and Au-PA-Mn(OAc)OcPhOPc towards epinephrine was further investigated and well-defined anodic peaks of epinephrine were observed at the potential values of 0.103 V and 0.191 V respectively. In **Figure 4.9 (b) (i),** norepinephrine

oxidation peak was observed on the bare Au at 0.222 V with a reduction peak at 0.159 V. In **Figure 4.9 (b) (iii),** on Au-PA-FeOcPhOPc, two redox peaks were observed on norepinephrine at 0.154 V and 0.283 V with a reduction peak at 0.083 V. The norepinephrine voltammograms shifted to lower potential value of 0.120 V and 0.132 V for Au-PA-CoOcPhOPc and Au-PAMn(OAc)OcPhOPc compare with bare Au. In **Figure 4.9 (c) (i)**, dopamine oxidation peak was observed on the bare Au at peak at 0.188 V and reduction peaks 0.127 V. In **Figure 4.9 (c) (iii),** the voltammograms of dopamine at the Au-PA-FeOcPhOPc showed an oxidation peak at 0.181 V and reduction peak at 0.056 V. In **Figure 4.9 (c) (ii), a**t Au-PA surface, no peak was displayed, due to the insulating property of the PA thin film. The dopamine peak current enhancement was observed on Au-PA-FeOcPhOPc compare with the current on bare Au. For the Au-PA-FeOcPhOPc and Au-PA-CoOcPhOPc the redox potential for dopamine was lowered to 0.186 V and 0.169 V; respectively. In **Figure 4.9 (d) (i),** serotonin displayed irreversible voltammograms with the oxidation peak on bare Au at 0.388 V, attributed to the oxidation of serotonin to 5-hydroxyindoleacetic acid. In **Figure 4.9 (d) (ii),** no redox peak was observed due to the passivation at the Au-PA surface. At the Au-PA-CoOcPhOPc in **Figure 4.9 (d) (iii)**, the oxidation peak was restored and a lowered redox potential for serotonin was observed at 0.371 V. The voltammograms of serotonin on Au-PA-FeOcPhOPc and Au-PAMn(OAc)OcPhOPc, were observed at low potentials values of 0.286 V and 0.383 V compare with serotonin on bare electrode surface.

In **Figure 4.9**, dopamine gave its best response on Au-PA-FeOcPhOPc in terms of enhancement of current. Epinephrine is best detected on Au-PA-CoOcPhOPc with a better peak current. While serotonin and norepinephrine were best detected on Au-PA-FeOcPhOPc electrodes with enhanced current. The lowering of the potential values and the enhanced current confirmed the electrocatalytic behaviour of the octacarboxyphenoxy metallophthalocyanines on the electrode surface towards the neurotransmitters.

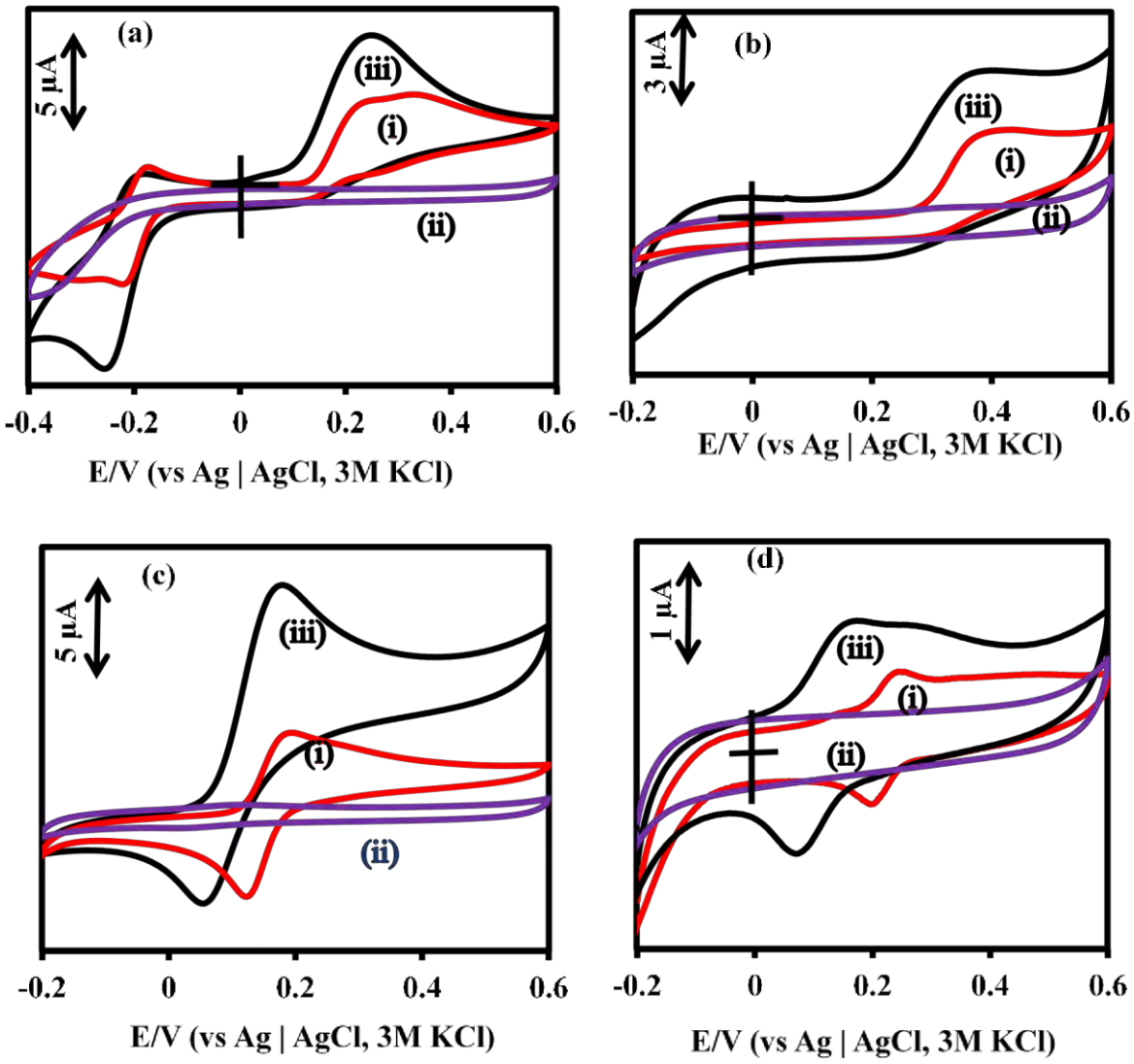

Figure 4.9: Cyclic voltammograms of 0.10 mM of **(a)** epinephrine, **(b)** norepinephrine, **(c)** dopamine, and **(d)** serotonin on **(i)** Bare **(ii)** Au-PA **(iii)** Au-PA-MOcPhOPc.

4.6.2 Electrocatalysis of Au-PA-MOcPhOPc towards ascorbic acid (AA)

In **Scheme 4.2,** the illustration of the reaction at the electrode surfaces was demonstrated in PBS pH 7.4. The carboxylate ions (COO^-) at the terminal end of the thin film of MOcPhOPc electrodes displayed an electrostatic attraction toward the cationic neurotransmitters. Therefore, neurotransmitters were detected at the Au-PA-MOcPhOPc modified electrode surfaces. The anionic ascorbic acid was repressed at the anionic COO^- surface of the electrode due to the

electrostatic repulsion thus the ascorbic acid was not detected. Therefore, the AuPA-MOcPhOPc modified electrode offered an advantage for accurate neurotransmitters detection.

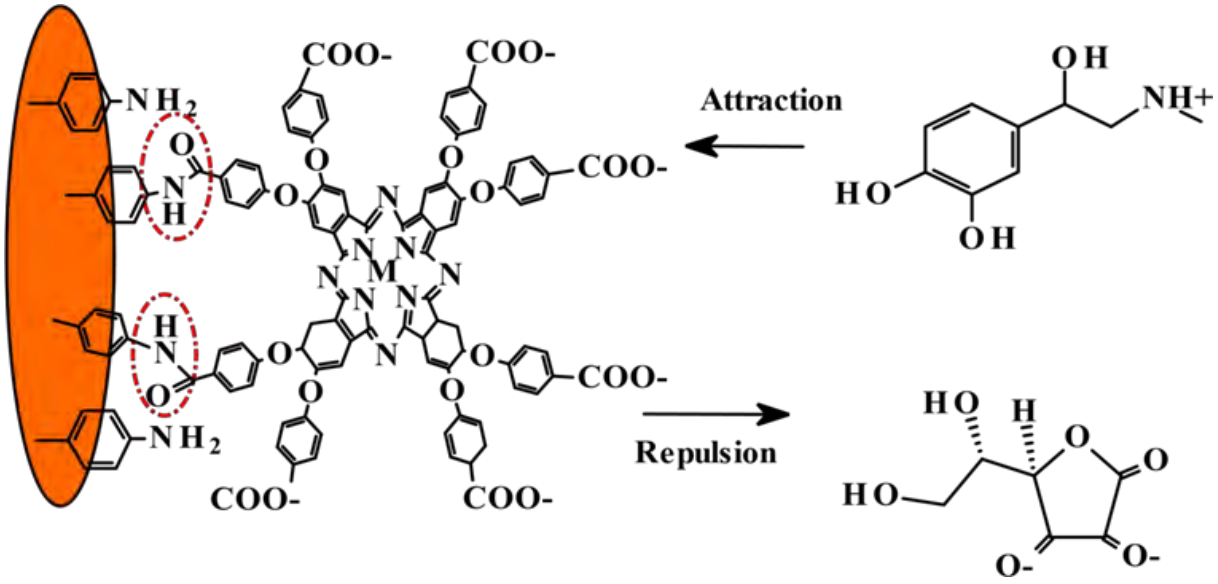

Scheme 4.2: Mechanism of the detection of epinephrine (electrostatic attraction) and screening of ascorbic acid (charge repulsion) in physiological pH conditions by Au-PA-MOcPhOPc surface**.**

Figure 4.10 shows cyclic voltammograms of 0.1 mM of ascorbic acid at the bare gold surface and at **(a)** Au-PA-CoOcPhOPc **(b)** Au-PA-Mn(OAc)OcPhOPc and **(c)** Au-PA-FeOcPhOPc surfaces. In **Figure 4.10 (i)**, on bare gold electrode surface, an oxidation peak of ascorbic acid was observed at 0.289 V. In **Figure 4.10 (ii) (a) (b) and (c)**, the oxidation peak of the ascorbic acid was suppressed. This clearly show that ascorbic acid was not detected on the AuPACoOcPhOPc, Au-PA-Mn(OAc)OcPhOPc and Au-PA-FeOcPhOPc surfaces. The oxidation process of ascorbic acid was inhibited on the Au-PA-MOcPhPc surfaces. Therefore,

the modified surfaces could be employed for the neurotransmitter's detection without the problem of interference.

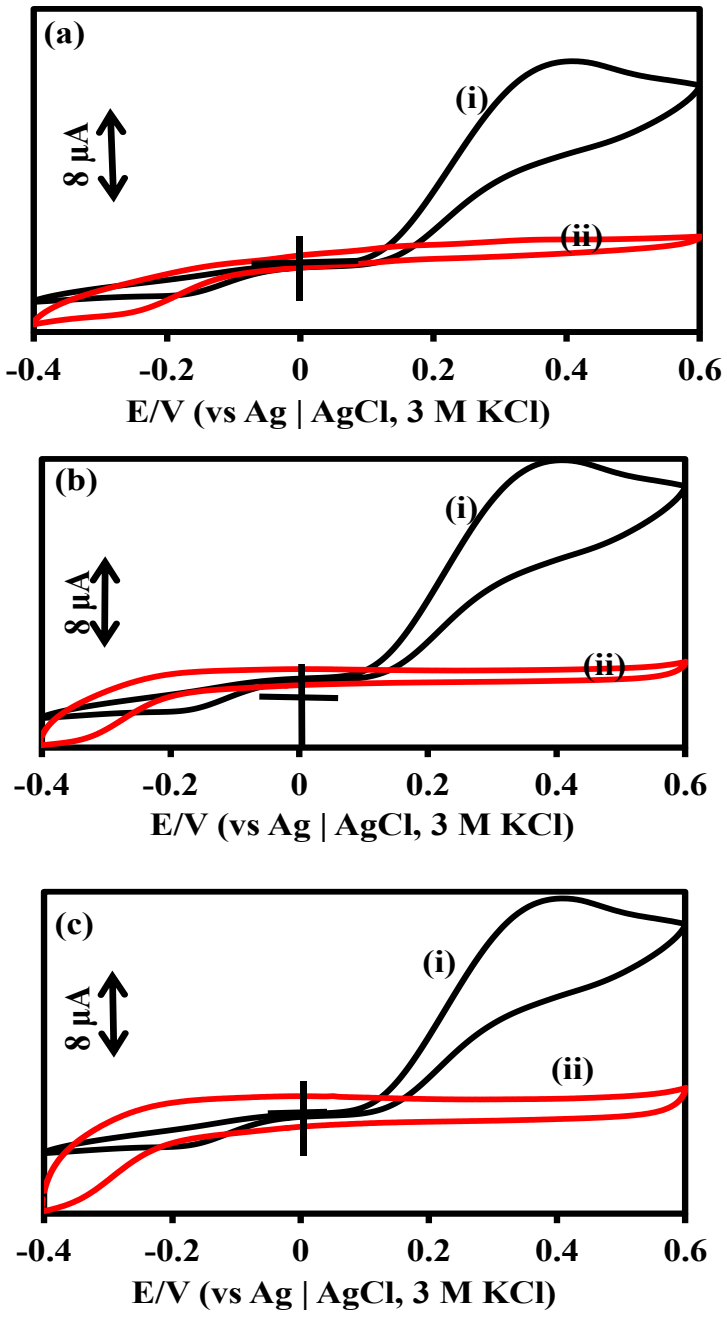

Figure 4.10: Cyclic voltammograms of 0.1 mM ascorbic acid at **(i)** bare Au and **(ii) (a)** Au-PA-CoOcPhOPc, **(b)** Au-PA-Mn(OAc)OcPhOPc and **(c)** Au-PA-FeOcPhOPc sensors.

Figure 4.11 shows the cyclic voltammograms of **(a) (i)** ascorbic acid (0.10 mM) on (0.10 mM) of **(b) (ii)** epinephrine, norepinephrine, dopamine and serotonin. In **Figure 4.11 (i)** the ascorbic acid voltammograms displayed no redox peak. This confirmed the screening out of the ascorbic acid on the sensors. **Figure 4.11 (ii)** shows the voltammograms of the neurotransmitters with the redox peaks, confirming the high response of the sensors towards the neurotransmitters. A similar trend was observed on Au-PA-Mn(OAc)OcPhOPc and Au-PA-FeOcPhOPc sensors. Therefore, the modified electrodes could be used for the detection of neurotransmitters in the presence of ascorbic acid.

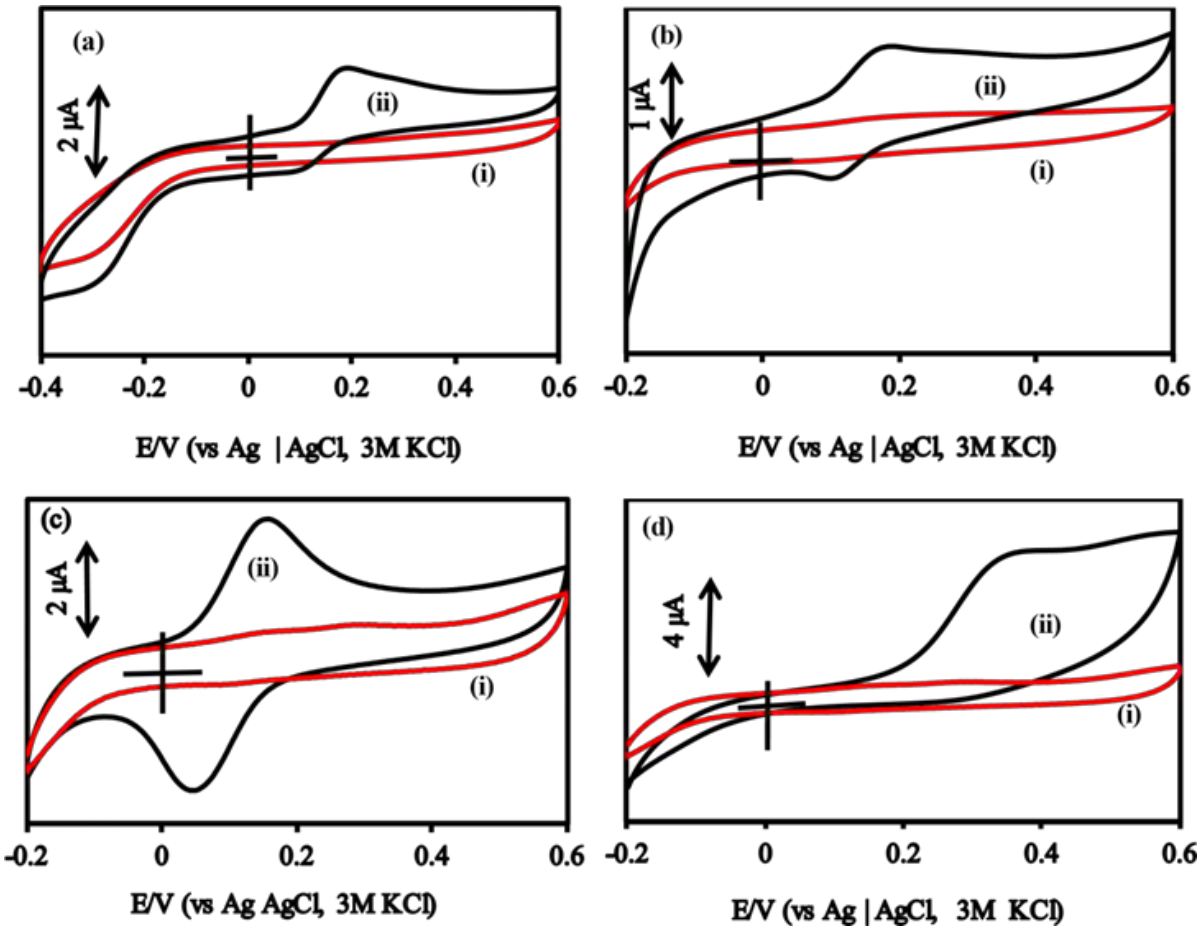

Figure 4.11: The cyclic voltammograms of **(i)** 0.10 mM ascorbic acid on 0.10 mM of **(ii) (a)** epinephrine, **(b)** norepinephrine, **(c)** dopamine and **(d)** serotonin.

In **Figure 4.12,** the response of the Au-PA-CoOcPhOPc sensor towards neurotransmitters and ascorbic acid was further studied using chronoamperometry. Chronoamperometry method was used for more information on the detection of neurotransmitters and screening out of ascorbic acid using the modified electrode. Chronoamperometry method has a better signal-to-noise ratio than most techniques **[66].** In **Figure 4.12 (ii),** the response of the Au-PA-CoOcPhOPc towards the addition of each 20 µL epinephrine, measured at 50 seconds interval caused the potential at the working electrode stepped with the resulting current at a function of time. The current increased at the increasing concentration of the epinephrine. In **Figure 4.12 (i),** the Au-PA-CoOcPhOPc sensor on ascorbic acid using similar method was not stepped. The stepped confirmed the high response of the sensor towards epinephrine and the unstepped chronoamperometry confirmed the screen out of the ascorbic acid at the electrode surface.

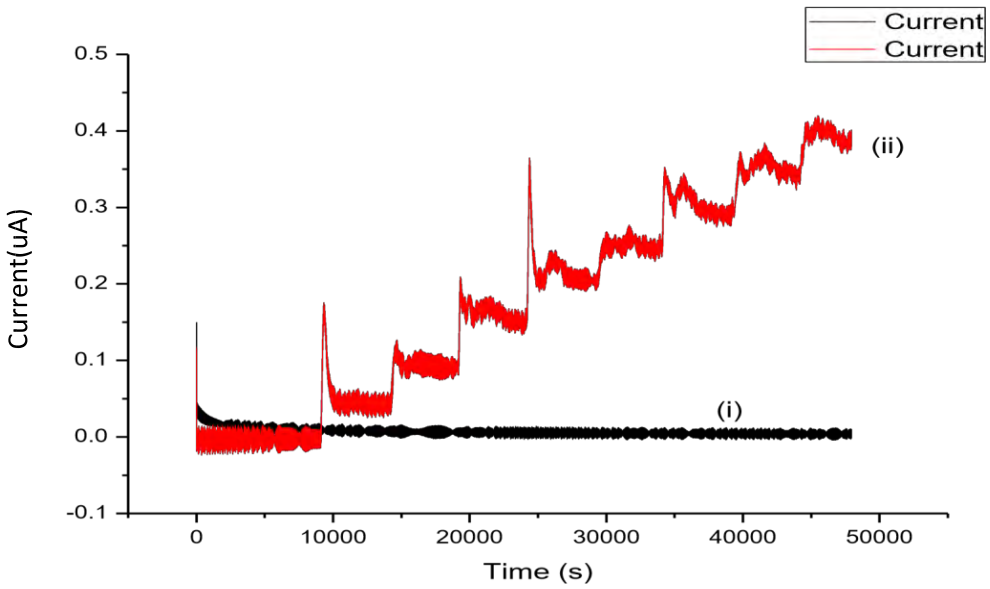

Figure 4.12: Chronoamperometry of the Au-PA-CoOcPhOPc on **(i)** ascorbic acid and **(ii)** epinephrine.

4.7 Electroanalysis of neurotransmitters at Au-PA-MOcPhPc

4.7.1 Cyclic voltammetry detection of neurotransmitters employing Au-PA-FeOcPhOPc

Figure 4.13 shows the cyclic voltammograms of the increasing concentration of 0.10 mM **(i)** epinephrine, **(ii)** norepinephrine **(iii)** dopamine and **(iv)** serotonin on Au-PA-FeOcPhOPc. The corresponding linear calibration curves of I_{pa} vs concentrations at the concentration range of 3.0 – 70.0 µM were obtained. In **Figure 4.13 (a),** the current (I_{pa}) increased with increasing concentration of epinephrine. The LoD, LoQ and the sensitivity obtained for epinephrine were 7.93 ± 0.05 µM, 26.44 ± 0.05 µM and 1.27 mA. $\mu M^{-1}.cm^{-2}$. In **Figure 4.13 (b),** at the increased concentration of norepinephrine showed an increase in current. The LoD, LoQ and the sensitivity obtained for norepinephrine at Au-PA-FeOcPhOPc were 8.64 ± 0.03 µM, 28.82 ± 0.03 µM and 1.16 mA. $\mu M^{-1}.cm^{-2}$. **Figure 4.13 (c)** shows the voltammograms of dopamine increased in current with the increasing concentration of dopamine. The plot of change in peak current is proportional to the concentration.

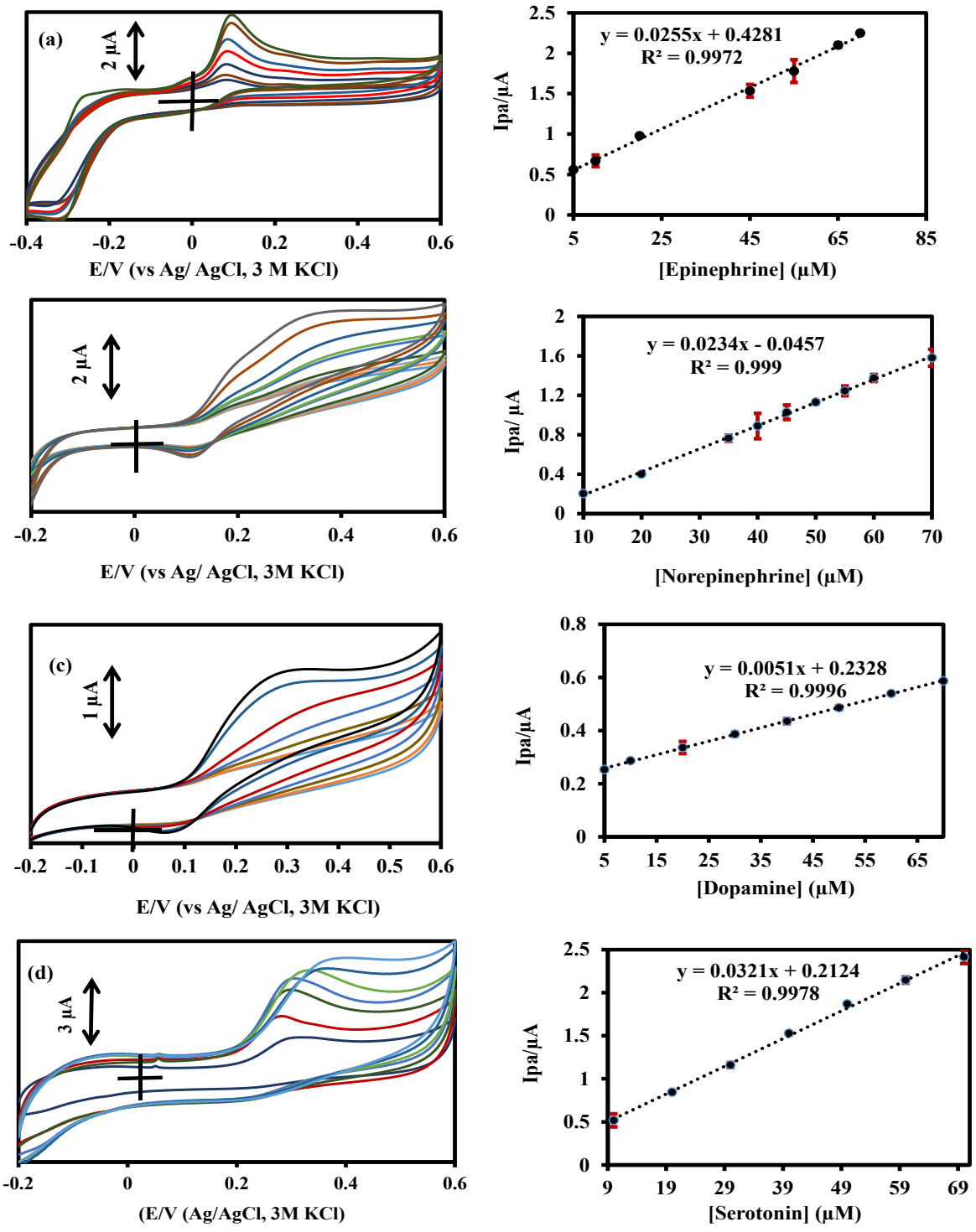

Figure 4.13: Cyclic voltammograms of 0.10 mM **(a)** epinephrine, **(b)** norepinephrine, **(c)** dopamine, and **(d)** serotonin at increase concentration at the range of 3.0 -70.0 µM at Au-PA-FeOcPhOPc.

The LoD, LoQ and the sensitivity obtained for dopamine at Au-PA-FeOcPhOPc were 39.66 ± 0.05 µM, 132.20 ± 0.05 µM, and 0.25 mA. $\mu M^{1}.cm^{-2}$. In **Figure 4.13 (d),** at the increased concentration of serotonin, an increase in current was observed. The LoD, LoQ and the sensitivity obtained for serotonin at Au-PA-FeOcPhOPc were 6.30 ± 0.03 µM, 21.01 ± 0.03 µM and 1.60 $mA.\mu M^{-1}.cm^{-2}$

In **Figure 4.13,** the linear regression equations obtained for epinephrine, norepinephrine, dopamine and serotonin showed in **equations (4.4)** to **(4.7)**.

$$Ipa\ (\mu A) = 0.026\ [Epinephrine] + 0.428,\ R^2 = 0.99 \qquad (4.4)$$

$$Ipa\ (\mu A) = 0.023\ [Norepinephrine] - 0.046,\ R^2 = 0.99 \qquad (4.5)$$

$$Ipa\ (\mu A) = 0.005\ [Dopamine] + 0.233,\ R^2 = 0.99 \qquad (4.6)$$

$$Ipa\ (\mu A) = 0.032\ [Serotonin] + 0.212,\ R^2 = 0.99 \qquad (4.7)$$

4.7.2 Differential pulse voltammetry detection of neurotransmitters using Au-PA-FeOcPhOPc

Differential pulse voltammetry (DPV) was used for the electroanalysis of epinephrine, norepinephrine, dopamine and serotonin employing Au-PA-FeOcPhOPc sensors. The concentration range used was from 3.0 – 70.0 µM. The DPV was used for the estimation of limit of detection (3σ), the limit of quantitation (10σ), and the sensitivity. **Figure 4.14 (a)** shows increasing current at the increased concentration of epinephrine. The LoD, LoQ and the sensitivity were calculated to be 1.44 ± 0.02 µM, 4.78 ± 0.02 µM and 1.15 mA. μM^{-1}. cm^{-2} respectively. **Figure 4.14 (b),** displayed an increase in peak current of norepinephrine as the concentration increases. The LoD, LoQ and the sensitivity were obtained to be 7.37 ± 0.005 µM, 24.56 ± 0.005 µM and 0.22 mA. $\mu M^{-1}cm^{-2}$ respectively. **Figure 4.14 (c)** shows increased

in the peak current of dopamine at the increasing concentration The LoD, LoQ and the sensitivity were calculated to be 19.50 ± 0.009 µM, 65.00 ± 0.009 µM and 0.08 mA. μM^{-1} cm^2 respectively. **Figure 4.14 (d)** shows increased in the peak current of serotonin as the concentration increases. The LoD, LoQ and the sensitivity were calculated to be 2.01 ± 0.009 µM, 6.70 ± 0.009 µM and 0.82 mA. $\mu M^{-1} cm^{-2}$ respectively.

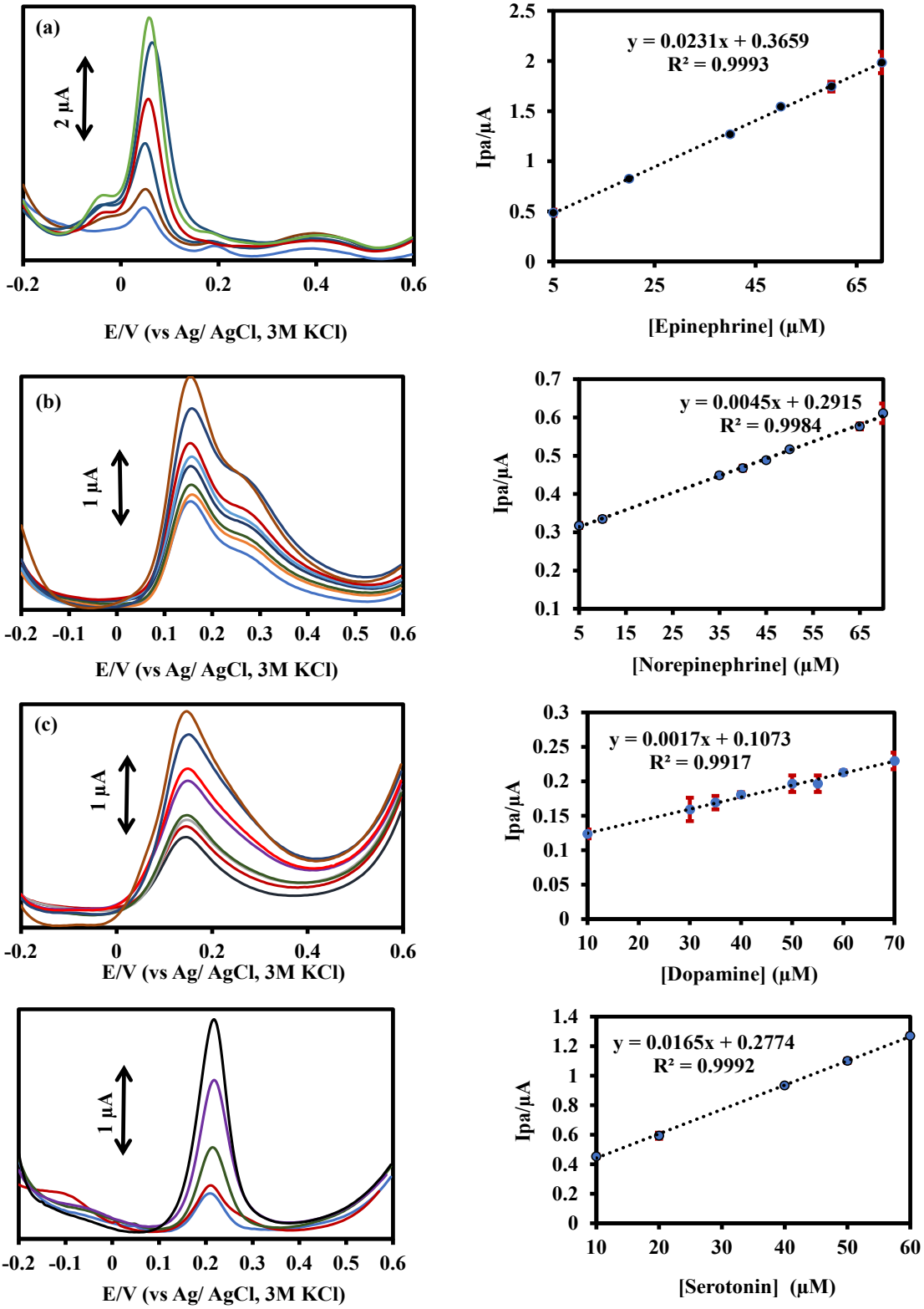

Figure 4.14: Differential pulse voltammograms of 0.10 mM **(a)** epinephrine, **(b)** norepinephrine, **(c)** dopamine, and **(d)** serotonin on Au-PA-FeOcPhOPc at increase concentration at the range of 3.0 – 70.0 µM.

In **Figure 4.14,** the linear regression equations obtained for epinephrine, norepinephrine, dopamine and serotonin showed in **equations (4.8) to (4.11).**

$$Ipa\ (\mu A) = 0.023\ [Epinephrine] + 0.366, R^2 = 0.99 \quad (4.8)$$

$$Ipa\ (\mu A) = 0.005\ [Norepinephrine] + 0.292, R^2 = 0.99 \quad (4.9)$$

$$Ipa\ (\mu A) = 0.002\ [Dopamine] + 0.107, R^2 = 0.99 \quad (4.10)$$

$$Ipa\ (\mu A) = 0.017\ [Serotonin] + 0.277, R^2 = 0.99 \quad (4.11)$$

4.7.3 CV method for the detection of neurotransmitters employing Au-PA-CoOcPhOPc

Figure 4.15 shows the cyclic voltammograms of 0.10 mM of **(a)** epinephrine, **(b)** norepinephrine **(c)** dopamine and **(d)** serotonin at the Au-PA-CoOcPhOPc sensor in PBS pH 7.4. The electroanalysis was carried out at the concentration ranges of 3.0 µM – 70.0 µM. The corresponding linear calibration curves of anodic peak current (Ipa) against concentrations of the neurotransmitters were plotted. In **Figure 4.15 (a)** the peak current (I_{pa}) increased with increasing concentration of epinephrine. The limit of detection (LoD), limit of quantification (LoQ) and the sensitivity for epinephrine obtained were 0.32 ± 0.03 µM, 1.06 ± 0.03 µM and 1.0 mA. $\mu M^{-1}.cm^{-2}$; respectively. **Figure 4.15 (b)** shows the increasing current of norepinephrine at the increasing concentration. The LoD, LoQ and the sensitivity obtained for norepinephrine at Au-PA-CoOcPhOPc were 0.22 ± 0.04 µM, 0.75 ± 0.04 µM and 1.41 mA. $\mu M^{-1}.cm^{-2}$. The LoD, LoQ and the sensitivity obtained for dopamine at Au-PA-CoOcPhOPc were 0.73 ± 0.009 µM, 2.44 ± 0.009 µM, and 0.43 mA. $\mu M^{-1}.cm^{-2}$ in **Figure 4.15 (c)**. In **Figure 4.15 (d),** at the increased concentration of serotonin from 3.0 – 70.0 µM. The LoD, LoQ and the sensitivity obtained for serotonin at Au-PA-CoOcPhOPc were 0.56 ± 0.001 µM, 1.86 ± 0.001 nM and 0.57 mA. $\mu M^{-1}.cm^{-2}$. The linear regression equations obtained for epinephrine, norepinephrine, and dopamine is presented in **Equations (4.12) to (4.15)**.

$$Ipa\ (\mu A) = 0.020\ [Epinephrine] + 0.334,\ R^2 = 0.99 \quad (4.12)$$

$$Ipa\ (\mu A) = 0.028\ [Norepinephrine] - 0.209,\ R^2 = 0.99 \quad (4.13)$$

$$Ipa\ (\mu A) = 0.009\ [Dopamine] + 0.191,\ R^2 = 0.99 \quad (4.14)$$

$$Ipa\ (\mu A) = 0.011\ [Serotonin] + 0.110,\ R^2 = 0.99 \quad (4.15)$$

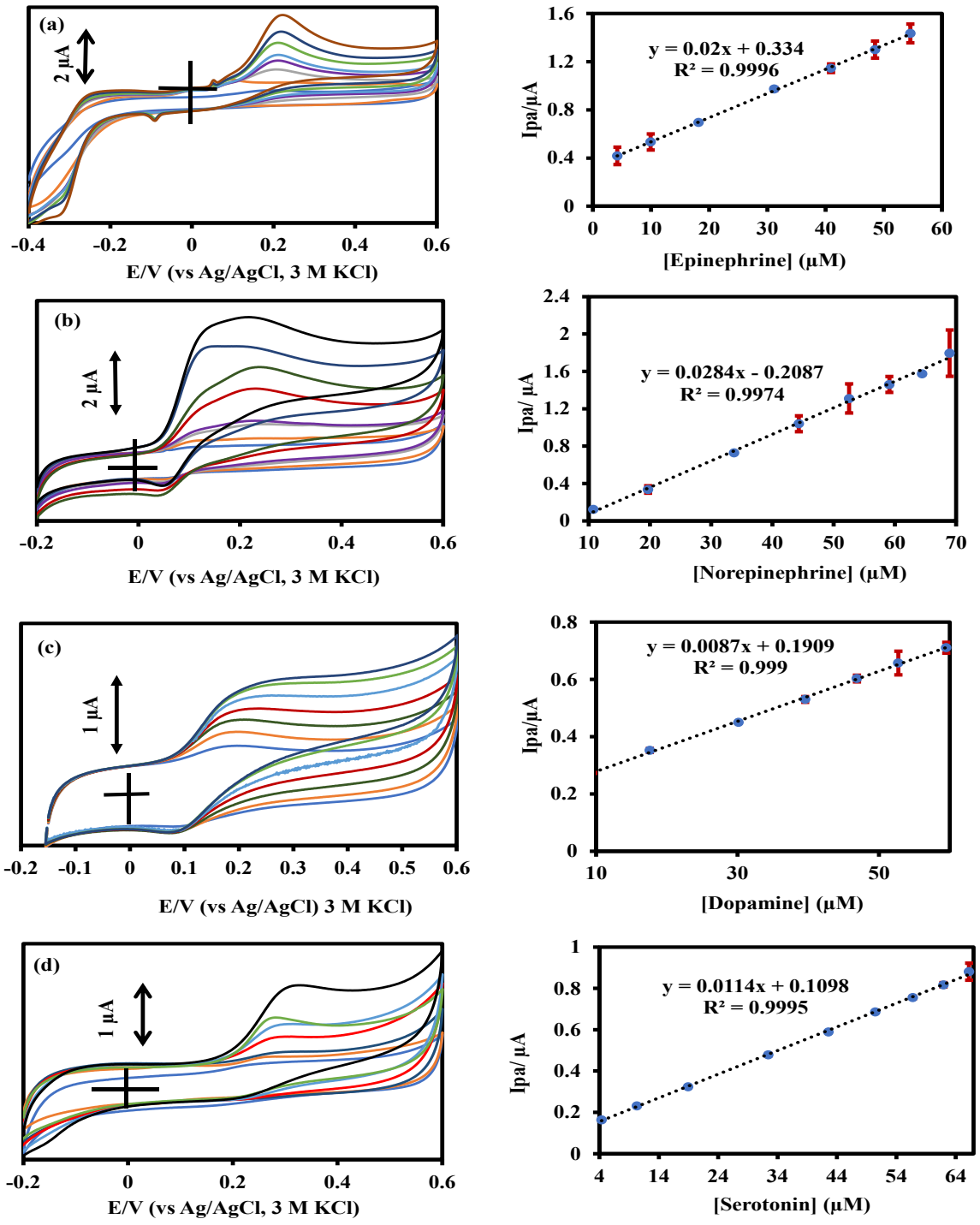

Figure 4.15: Cyclic voltammograms of 0.10 mM **(a)** epinephrine, **(b)** norepinephrine, **(c)** dopamine, and **(d)** serotonin at increase concentration at the range of 3.0 µM – 70.0 µM at Au-PA-CoOcPhOPc sensor.

4.7.4 Differential pulse voltammetry detection of neurotransmitters using Au-PA-CoOcPhOPc

Differential pulse voltammetry (DPV) was used for the determination of epinephrine, norepinephrine, dopamine and serotonin at the Au-PA-CoOcPhOPc sensors. The current output increased with increasing concentrations of all the neurotransmitters from 3.0 -70.0 μM. The DPV was used for the estimation of LoD, LoQ and the sensitivity. **Figure 4.16 (a)** shows the DPV and corresponding calibration curves for the determination of epinephrine. The LoD, LoQ and the sensitivity were calculated to be 1.01 ± 0.04 μM, 3.35 ± 0.04 μM and 1.03 mA. $\mu M^{-1}.cm^{-2}$ respectively for epinephrine. In **Figure 4.16 (b)**, the LoD, LoQ for norepinephrine were calculated to be 0.99 ± 0.06 μM, 3.31 ± 0.06 μM and 1.04 mA. $\mu M^{-1}.cm^{2}$ respectively. **In Figure 4.16 (c)**, the LoD, LoQ and the sensitivity were calculated to be 0.25 ± 0.08 μM, 0.83 ± 0.08 μM and 4.16 mA. $\mu M^{-1}.cm^{-2}$; respectively for dopamine. While in **Figure 4.16 (d)**, the LoD, LoQ and the sensitivity for serotonin were calculated to be 1.12 ± 0.05 μM, 3.74 ± 0.05 μM and 0.92 mA. $\mu M^{-1}.cm^{-2}$ respectively. The linear regression equation for the epinephrine, norepinephrine, dopamine, and serotonin were given by **Equation (4.16)** to **(4.19)**.

$$Ipa\ (\mu A) = 0.021\ [Epinephrine] + 0.473, R^2 = 0.99 \quad (4.16)$$

$$Ipa\ (\mu A) = 0.021\ [Norepinephrine] + 0.559, R^2 = 0.99 \quad (4.17)$$

$$Ipa\ (\mu A) = 0.084\ [Dopamine] + 2.113, \quad R^2 = 0.99 \quad (4.18)$$

$$Ipa\ (\mu A) = 0.019\ [Serotonin] + 2.294, \quad R^2 = 0.99 \quad (4.19)$$

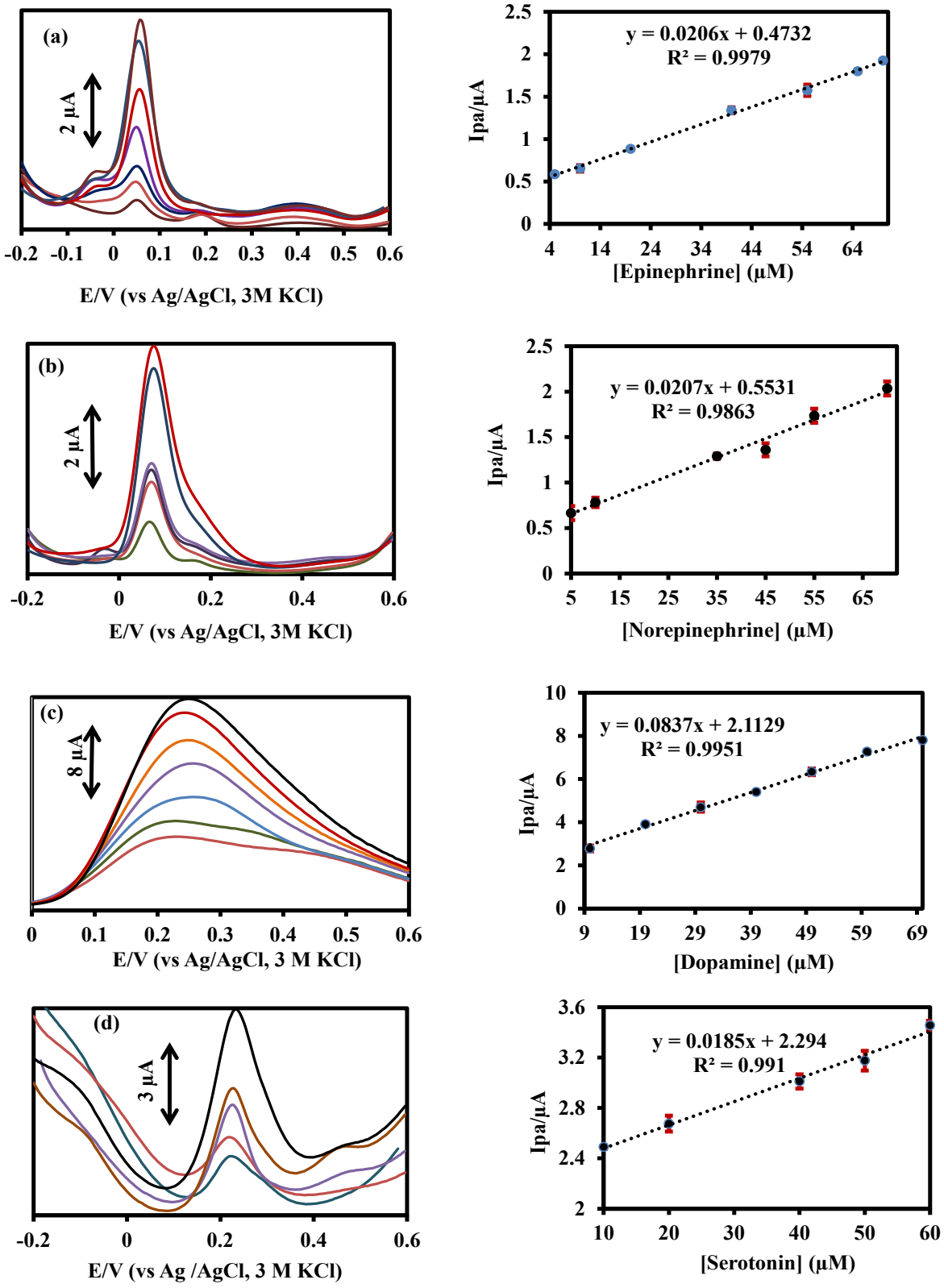

Figure 4.16: Differential pulse voltammograms of **(a)** epinephrine, **(b)** norepinephrine, **(c)** dopamine, and **(d)** serotonin on Au-PA-CoOcPhOPc at increase concentration at the range of 3.0 – 70.0 µM at the fixed potential at the scan rate of 50 $mV.s^{-1}$.

4.7.5 CV determination of neurotransmitters using Au-PA-Mn(OAc)OcPhOPc

Figure 4.17 shows the cyclic voltammograms of the increasing concentration of **(i)** epinephrine, **(ii)** norepinephrine **(iii)** dopamine and **(iv)** serotonin on Au-PAMn(OAc)OcPhOPc. The analyses were run in PBS pH 7.4 with their corresponding linear calibration curves of Ipa vs concentrations at the concentration range of 3.0 -70.0 μM. In **Figure 4.17 (a),** the current (Ipa) increased with increasing concentration of epinephrine. The LoD, LoQ and the sensitivity obtained for epinephrine were 0.696 ± 0.03 μM, 2.32 ± 0.03 μM and 1.93 mA. $\mu M^{-1}.cm^{-2}$. In **Figure 4.17 (b),** the LoD, LoQ and the sensitivity obtained for norepinephrine at Au-PA-Mn(OAc)OcPhOPc were 1.0 ± 0.04 μM, 3.32 ± 0.04 μM and 1.35 mA.$\mu M^{-1}.cm^{-2}$. **Figure 4.17 (c)** showed the LoD, LoQ and the sensitivity obtained for dopamine at Au-PA-Mn(OAc)OcPhOPc were 1.71 ± 0.08 μM, 5.70 ± 0.08 μM, and 0.79 mA. $\mu M^{-1}.cm^{-2}$. The LoD, LoQ and the sensitivity obtained for norepinephrine in **Figure 4.17 (d)** for Au-PA-Mn(OAc)OcPhOPc were 1.67 ± 0.01 μM, 5.56 ± 0.01 μM and 0.81 mA. $\mu M^{1}.cm^{2}$. The linear regression equations obtained for epinephrine, norepinephrine, dopamine and serotonin showed in **Equations (4.20) to (4.23).**

$$Ipa\ (\mu A) = 0.039\ [Epinephrine] + 0.875,\ R^2 = 0.99 \quad (4.20)$$

$$Ipa\ (\mu A) = 0.027\ [Norepinephrine] + 2.236,\ R^2 = 0.99 \quad (4.21)$$

$$Ipa\ (\mu A) = 0.016\ [Dopamine] + 2.536,\ R^2 = 0.99 \quad (4.22)$$

$$Ipa\ (\mu A) = 0.016\ [Serotonin] - 0.137,\ R^2 = 0.99 \quad (4.23)$$

The correlation coefficient obtained established a strong and positive relationship between the current and the concentration of the neurotransmitters.

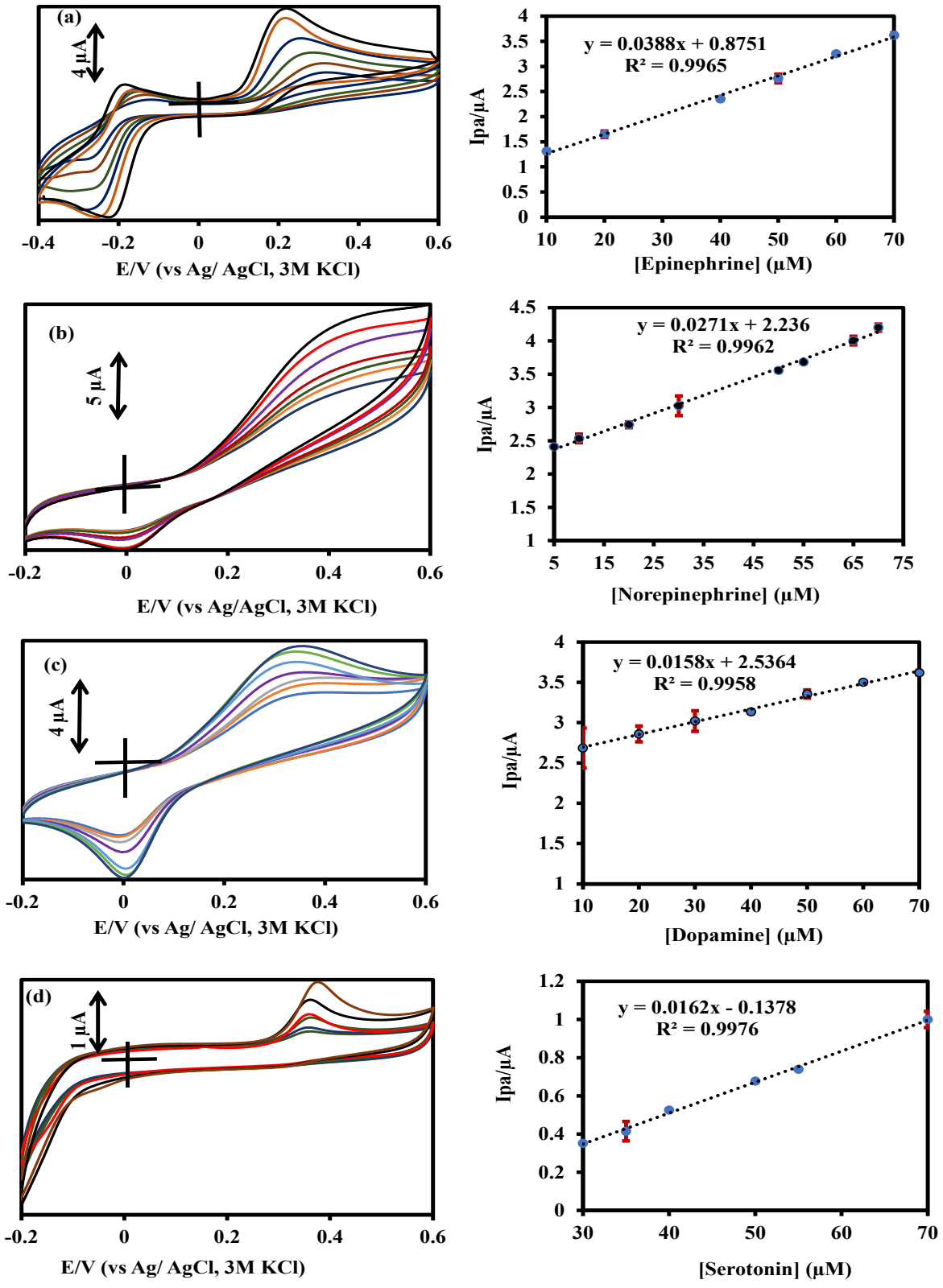

Figure 4.17: Cyclic voltammograms of **(a)** epinephrine, **(b)** norepinephrine, **(c)** dopamine, and **(d)** serotonin on Au-PA-Mn(OAc)OcPhOPc at increase concentration at the range of 3.0 – 70.0 µM.

4.7.6 DPV detection of neurotransmitters using Au-PA-Mn(OAc)OcPhOPc

Differential pulse voltammetry (DPV) was used for the electroanalysis of epinephrine, norepinephrine, dopamine and serotonin employing Au-PA-Mn(OAc)OcPhOPc sensors. At increase concentration from 3.0 – 70.0 μM, the current of the neurotransmitters increased. **Figure 4.18 (a)** shows the voltammograms of epinephrine with the oxidation peak at 253 mV. The DPV was used for the estimation of limit of detection, the limit of quantitation and the sensitivity. The LoD, LoQ and the sensitivity were calculated to be 3.91 ± 0.03 μM, 13.00 ± 0.03 μM and 1.07 mA. μM^{-1}. cm^{-2} respectively. **Figure 4.18 (b),** displayed an increase in peak current of norepinephrine. The LoD, LoQ and the sensitivity obtained to be 21.54 ± 0.007 μM, 71.79 ± 0.007 μM and 0.19 mA. μM^{-1}. cm^{-2} respectively. **Figure 4.18 (c)** shows increased in the peak current of dopamine. The LoD, LoQ and the sensitivity were calculated to be 13.50 ± 0.007 μM, 45.16 ± 0.007 μM and 0.31 mA. μM^{-1}. cm^{-2} respectively. **Figure 4.18 (d)** shows increased in the peak current of serotonin. The LoD, LoQ and the sensitivity were calculated to be 12.17 ± 0.003 μM, 40.57 ± 0.003 μM and 0.34 mA. μM^{-1} .cm^{-2} respectively. In **Figure 4.18,** the linear regression equations obtained for epinephrine, norepinephrine, dopamine and serotonin showed in **equations (4.24) to (4.27).**

$$Ipa\ (\mu A) = 0.022\ [Epinephrine] + 0.198,\ R^2 = 0.99 \quad (4.24)$$

$$Ipa\ (\mu A) = 0.004\ [Norepinephrine] + 0.636,\ R^2 = 0.99 \quad (4.25)$$

$$Ipa\ (\mu A) = 0.006\ [Dopamine] + 0.496,\ R^2 = 0.99 \quad (4.26)$$

$$Ipa\ (\mu A) = 0.007\ [Serotonin] + 0.261,\ R^2 = 0.99 \quad (4.27)$$

The results of the electroanalysis of Au-PA-FeOcPhOPc, Au-PA-CoOcPhOPc and Au-PA-Mn(OAc)OcPhOPc towards epinephrine, norepinephrine, and dopamine were summarized in **Table 4.3**

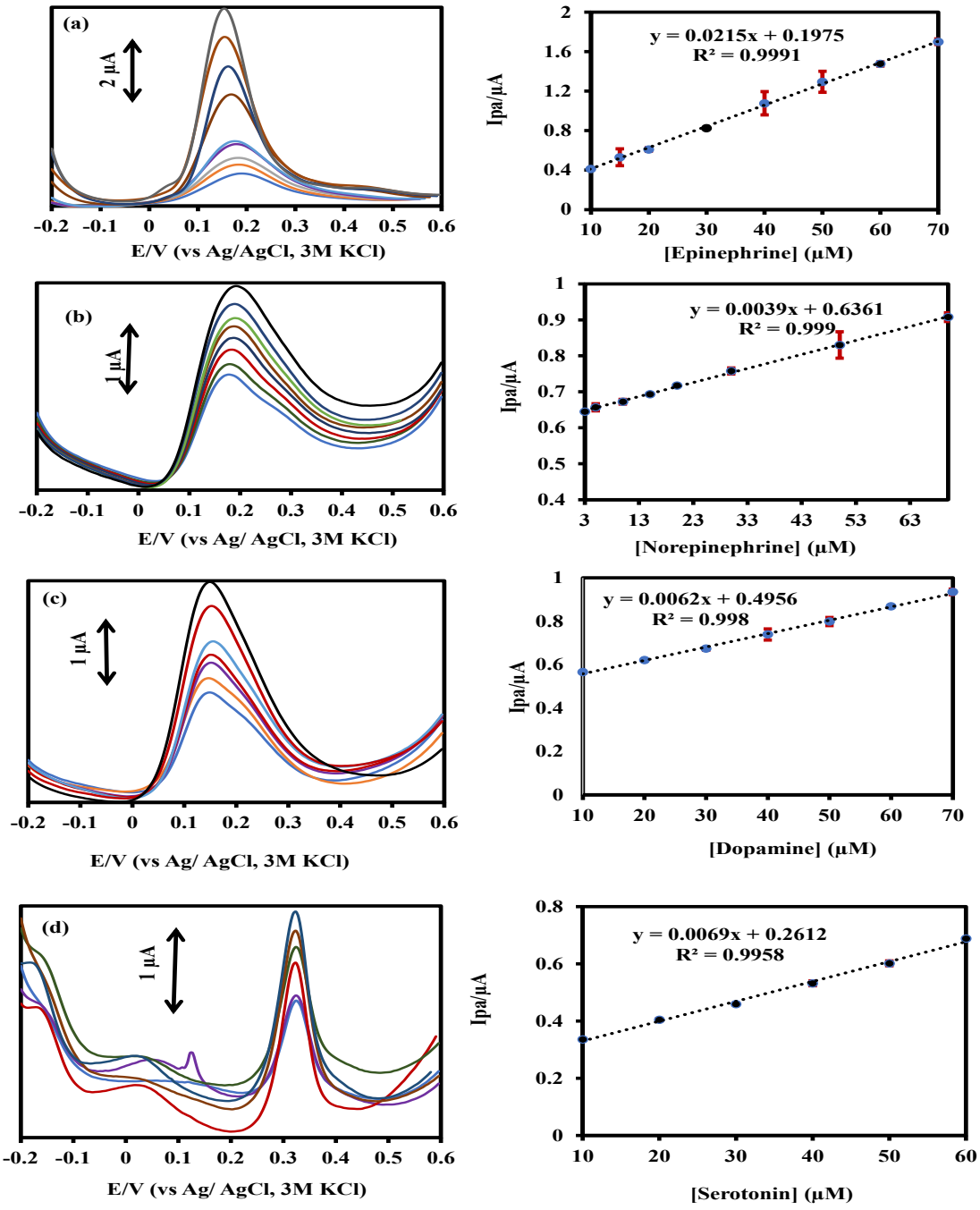

Figure 4.18: Differential pulse voltammograms of **(a)** epinephrine, **(b)** norepinephrine, **(c)** dopamine, and **(d)** serotonin at increase concentration at the range of 3.0 µM – 70.0 µM at the fixed potential at the scan rate of 50 $mV.s^{-1}$ at Au-PA-Mn(OAc)OcPhOPc sensor.

Table 4.4: Results of the electroanalysis of the neurotransmitters employing voltammetry methods

MPc Complex	Neurotransmitters	Voltammetry Method used	LoD (µM)	LoQ (µM)	Sensitivity ($mA.\mu M^{-1}.cm^{-2}$)	Correlation coefficient (R^2)
Au-PA-FeOcPhOPc	Epinephrine	CV	7.93 ± 0.05	26.44 ± 0.05	1.27	0.99
		DPV	1.44 ± 0.02	4.78 ± 0.02	1.15	0.99
	Norepinephrine	CV	8.64 ± 0.03	28.82 ± 0.03	1.16	0.99
		DPV	7.37 ± 0.01	24.56 ± 0.01	0.22	0.99
	Dopamine	CV	39.66 ± 0.01	132.20 ± 0.01	0.25	0.99
		DPV	19.50 ± 0.01	65.00 ± 0.01	0.08	0.99
	Serotonin	CV	6.30 ± 0.03	21.01 ± 0.03	1.60	0.99
		DPV	2.01 ± 0.01	6.70 ± 0.01	0.82	0.99
Au-PA-CoOcPhOPc	Epinephrine	CV	0.32 ± 0.03	1.06 ± 0.03	1.00	0.99
		DPV	1.01 ± 0.04	3.35 ± 0.04	1.03	0.99
	Norepinephrine	CV	0.22 ± 0.04	0.75 ± 0.04	1.41	0.99
		DPV	0.99 ± 0.06	3.31 ± 0.06	1.04	0.99
	Dopamine	CV	0.73 ± 0.01	2.44 ± 0.01	0.43	0.99
		DPV	0.25 ± 0.08	0.83 ± 0.08	4.16	0.98
	Serotonin	CV	0.56 ± 0.00	1.86 ± 0.00	0.57	0.99
		DPV	1.12 ± 0.05	3.74 ± 0.05	0.92	0.99

MPc Complex	Neurotransmitters	Voltammetry Method used	LoD (µM)	LoQ (µM)	Sensitivity ($mA.\mu M^{-1}.cm^{-2}$)	Correlation coefficient (R^2)
Au-PA-Mn(OAc)OcPhOPc	Epinephrine	CV	0.70 ± 0.03	2.32 ± 0.03	1.93	0.99
		DPV	3.91 ± 0.03	13.00 ± 0.03	1.07	0.99
	Norepinephrine	CV	1.00 ± 0.04	3.32 ± 0.04	1.35	0.99
		DPV	2.15 ± 0.01	7.18 ± 0.01	0.19	0.99
	Dopamine	CV	1.71 ± 0.08	5.70 ± 0.08	0.79	0.99
		DPV	13.50 ± 0.01	45.16 ± 0.01	0.31	0.99
	Serotonin	CV	1.67 ± 0.01	5.56 ± 0.01	0.81	0.99
		DPV	1.22 ± 0.00	4.06 ± 0.00	0.34	0.99

The results obtained from the electroanalysis with the Au-PA-CoOcPhPc sensor, gave lowest LoD and LoQ on norepinephrine. The result confirmed the sensor to be better for the detection of norepinephrine in terms of LoD, LoQ than Au-PA-Mn(OAc)OcPhOPc and Au-PA-FeOcPhOPc sensors when employing CV technique. On DPV results, the Au-PA-CoOcPhOPc was preferred on dopamine than on other neurotransmitters in terms of LoD, LoQ. The Au-PA-CoOcPhPc has higher sensitivity on dopamine and serotonin compare to norepinephrine and epinephrine. Electroanalysis on Au-PA-FeOcPhOPc sensor is best on serotonin in terms of LoD, LoQ and sensitivity than on dopamine, epinephrine and norepinephrine with CV technique. The DPV analysis at Au-PA-FeOcPhPc, gave best and lowest LoD, LoQ and sensitivity on epinephrine than serotonin, dopamine and norepinephrine. Therefore, the DPV technique can be recommended for the epinephrine detection and CV method for the serotonin detection when using the Au-PA-FeOcPhPc sensor. The Au-PA-Mn(OAc)OcPhPc sensor displayed best in terms of LoD, LoQ and sensitivity on epinephrine, than on norepinephrine, dopamine and serotonin with CV analysis. The DPV analysis with Au-PA-Mn(OAc)OcPhPc gave lowest LoD and LoD towards epinephrine, than serotonin, norepinephrine and dopamine. The sensitivity of Au-PA-Mn(OAc)OcPhPc is highest towards epinephrine detection with CV and DPV methods of analysis. The results obtained are within the reported values for the neurotransmitters LoD, LoQ and sensitivity **[17, 18]**. Most of the results obtained is better than the reported values, in terms of lower LoD, LoQ and sensitivity **[48-58]**. Findings from this study revealed that both the CV and DPV techniques can be employed for the neurotransmitter's detection, even though the techniques differ in operations. The DPV signals resulted from two signals (signal before and after the pulse) while CV measure the response of an active solution to current in a cycled potential sweep within several values. The DPV also shows difference in the speed of decay of the faradaic and the non-faradaic currents, while CV is useful for the verification of the redox behaviour of analytes **[70].** The two techniques, employed with

the same Au-PA-MOcPhPc sensors, detected the neurotransmitters. The effecacy of CoOcPhOPc, FeOcPhOPc and Mn(OAc)OcPhOPc complexes in the detection were highly noted in the results. The Au-PA-CoOcPhOPc, Au-PA-FeOcPhOPc and Au-PA- Mn(OAc)OcPhPc sensors are reliable tools towards the neurotransmitter's detection, screening off the interference, and therefore could be highly recommended.

4.8 The interference studies

Figure 4.19 shows the voltammograms of **(i)** Ascorbic acid (0.10 mM) **(ii)** epinephrine (0.10 mM) and **(iii)** increase concentration of dopamine (3.0 – 70.0 μM). The concentration of epinephrine was fixed while increasing the concentration of dopamine at Au-PA-CoOcPhOPc sensor. Epinephrine fixed peak was observed at around -0.122.98 V as shown in **Figure 4.19 (ii).** The increased peak current of dopamine was observed at 0.149 V as shown in **Figure 4.19 (iii)**. In **Figure 4.19 (i),** the AuPA-CoOcPhOPc sensor showed no response towards ascorbic acid, displayed no peak, confirming the repulsion of AA at Au-PA-CoOcPhOPc electrode. **Figure 4.19 (b)** shows the linear plot of the increasing concentration of dopamine. **Figure 4.19** confirmed that the modified Au-PA-CoOcPhOPc electrode could detected neurotransmitters in the presence of ascorbic acid.

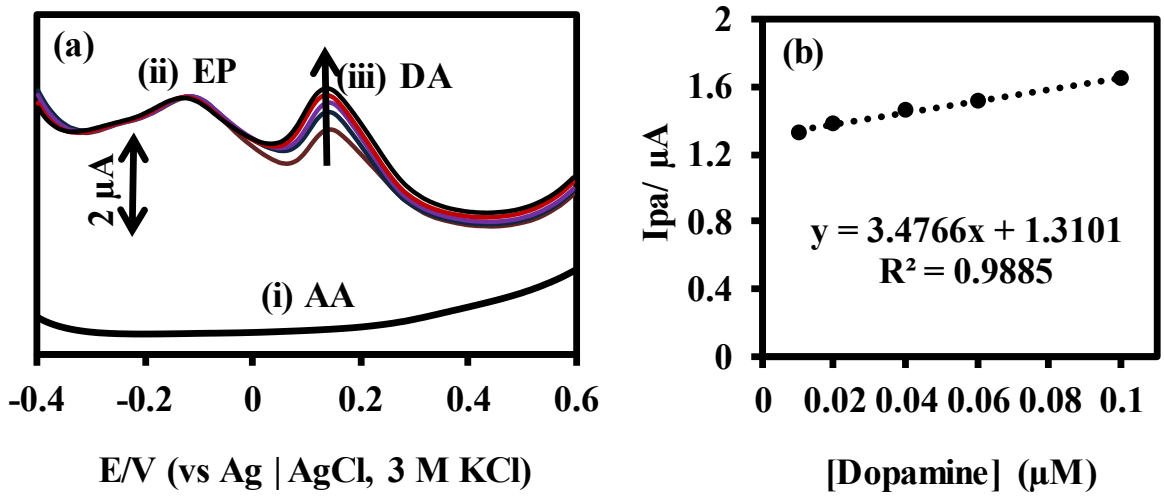

Figure 4.19: Differential pulse voltammograms of **(a) (i)** ascorbic acid (0.10 mM **(ii)** the fixed concentrations of epinephrine (0.10 mM) and **(iii)** increased concentration of dopamine (3.0 – 70.0 µM) at Au-PA-CoOcPhOPc

In **Figure 4.19 (b)**, the graphs show the increase in current with the increasing concentration of dopamine with the **Equation (4.28):**

$$Ipa\ (\mu A) = 0.027\ [Dopamine] + 1.437, R^2 = 0.99 \qquad \textbf{(4.28)}$$

Au-PA-CoOcPhOPc has high response towards neurotransmitters (epinephrine and dopamine) and repelled the Ascorbic acid (showing no peak) as shown in **Figure 4.19**.

4.9 Investigation of the reproducibility, repeatability, and stability of Au-PA-MOcPhPc

Figure 4.20 shows the CV of Au-PA-MOcPhOPc sensor in 0.10 mM of the neurotransmitters at repeated cyclic scans. An insignificant change in the peak current at repeated cyclic scans was

observed, confirming the stability of the sensor. The steady peak current at 15 to 20 cyclic scans established the stability of the film at the electrode surface. Fixed concentration of 0.10 mM epinephrine, norepinephrine, dopamine and serotonin was used at a fixed potential range of - 200 to 600 mV. The RSD values obtained for epinephrine, norepinephrine, dopamine and serotonin are 2.50 %, 3.00 %, 4.00 % and 3.50 % respectively.

The low RSD percentage obtained, confirmed the stability of the complexes used at the electrode surfaces. The low standard error obtained from series of electroanalysis results in **Table 4.3**, also confirmed the reproducibility of the Au-PA-MOcPhPc results. The electrode was regenerated in the buffer solution at 5 to 10 scans, which can be reused for analysis after several days, through which similar results could be obtained, confirming the repeatability of the Au-PA-MOcPhPc results. The results confirmed the stability, reproducibility, reusability and repeatability of the modified electrodes (Au-PA-MOcPhPc) used.

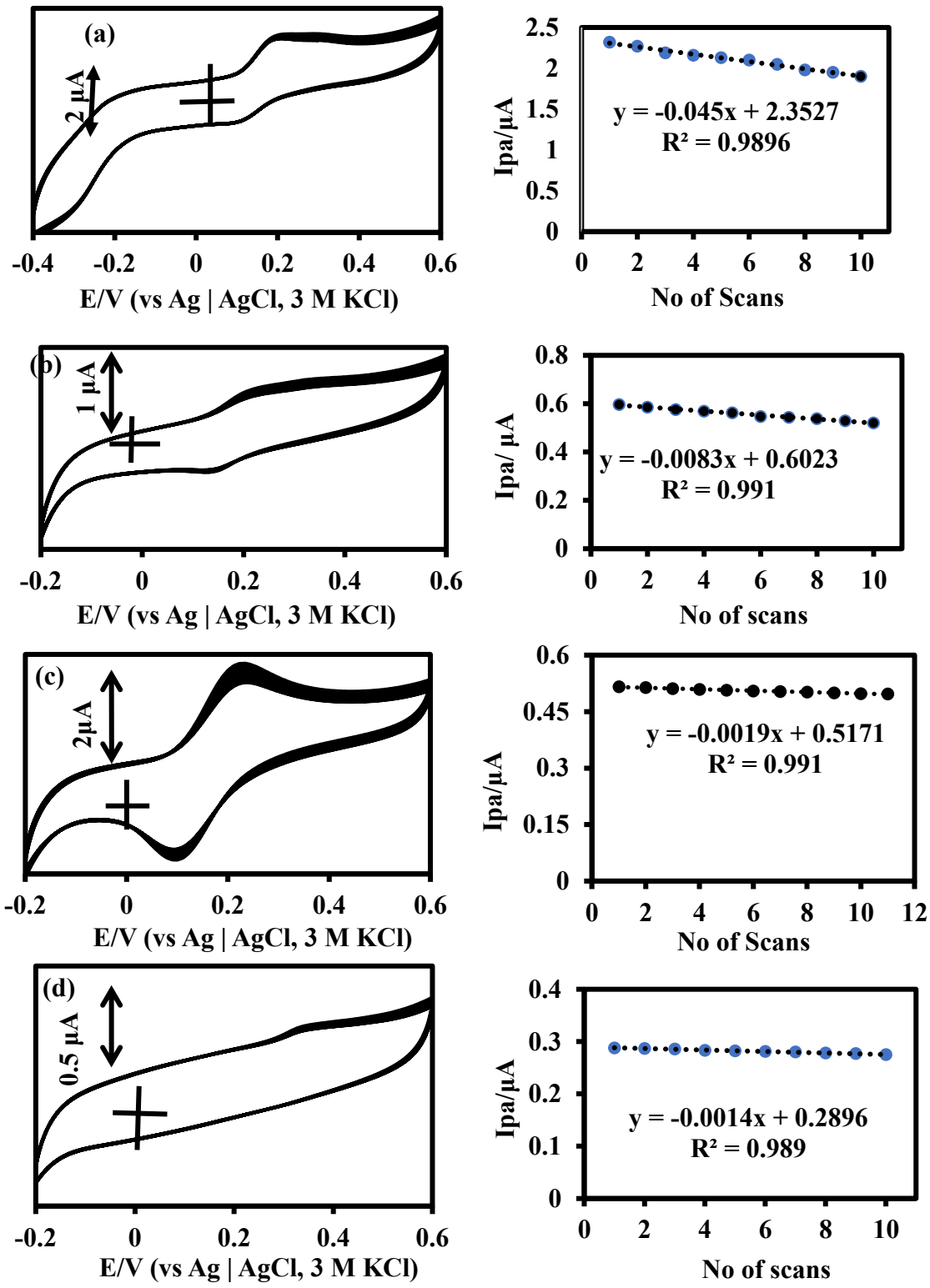

Figure 4.20: Repeated cyclic scans of 0.10 mM of (a) epinephrine, (b) norepinephrine, (c) dopamine and (d) serotonin using Au-PA-CoOcPhOPc sensor. Scan rate = 100 $mV.s^{-1}$.

5 CHAPTER FIVE: DISCUSSION

5.1 The comparative analytical performance of Au-PA-MOcPhOPc

5.1.1 Dopamine

The analytical performance of the Au-PA-MOcPhOPc towards the detection of the neurotransmitter was compared with other reported metallophthalocyanines modified electrochemical sensors for the detection of neurotransmitters. The LoDs results of the various Au-PA-MOcPhOPc modified electrode for determination of dopamine was summarized in **Table 5.1**. The LoD obtained with CV and DPV techniques at Au-PA-CoOcPhOPc sensor (0.74 μM and 0.25 μM respectively) are lower and better than the LoD obtained using Copper tetrasulphonated phthalocyanines (CuTsPc) sensor (10.00 μM). The LoD obtained with Au-PA-Mn(OAc)OcPhOPc sensor (1.71 μM) using CV technique for the detection of dopamine was lower and better than the LoD obtained using Copper tetrasulphonated phthalocyanines (CuTsPc) sensor (10.00 μM) **[56]**. At Au-PA-CoOcPhOPc sensor, the LoD obtained employing DPV techniques (0.25 μM), was found lower and better for the detection of dopamine when compared with the LoD of the AzoBridged tetracarboxylic metallophthalocyanines (0.33 μM) **[53]**, and LoD for Cobalt teratsulphonated phthalocyanines (CoTsPc) modified electrodes (0.87 μM) **[55]**. The LoD obtained from the detection of dopamine at Au-PA-CoOcPhOPc sensor, confirmed that the sensor using DPV (0.25 μM), could be recommended for clinical applications. The Diagnostic reference value for dopamine was found to be 0.20 μM **[17].** The results confirmed that the Au-PA-MOcPhPc modified gold electrode could detect dopamine without the problem of interference. Suggesting its practical applicability for dopamine detection. The lower LoD was due to the catalytic effect of the complexes resulting in electrostatic attraction between the negatively charged Au-PA-MOcPhOPc

and dopamine at pH 7.4, resulting in higher dopamine concentration effect and hence higher current signal output.

Table 5.1: Comparative analytical performance of phthalocyanines modified electrode for detection of dopamine.

Neurotransmitters	**Sensor**	**LoD (µM)**	**Ref.**
Dopamine (DA)	Diagnostic reference value	0.196	**[17]**
	Azo-Bridged tetracarboxylic metallophthalocyanines [Ni, Co and Cu]	0.33	**[53]**
	Cobalt tetra-sulphonated phthalocyanines (CoTsPc)	0.87	**[55]**
	Copper tetra-sulphonated phthalocyanines (CuTsPc)	10.0	**[56]**
	Au-PA-CoOcPhOPc (CV)	0.73	TW
	Au-PA-CoOcPhOPc (DPV)	0.25	TW
	Au-PA-FeOcPhOPc (CV)	39.6	TW
	Au-PA-FeOcPhOPc (DPV)	19.5	TW
	Au-PA-Mn(OAc)OcPhOPc (CV)	1.71	TW
	Au-PA-Mn(OAc)OcPhOPc (DPV)	13.50	TW

TW (This work)

5.1.2 Epinephrine

The results obtained from this research work were compared with the diagnostic reference values and other reported metallophthalocyanines modified electrochemical sensors for the detection of neurotransmitters. The LoD, LoQ, and the sensitivity of the Au-PA-MOcPhOPc modified electrodes for the determination of epinephrine were summarized in **Table 5.2**. The LoDs obtained using cyclic voltammetry technique at Au-PA-CoOcPhOPc sensor (0.32 μM) was lower and far better than the LoD obtained with cobalt tetraamino phthalocyanines sensor (0.50 μM) **[59]** and that of iron phthalocyanines sensors (0.50 μM) **[60].** The LoD obtained using the Au-PA-Mn(OAc)OcPhOPc (0.70 μM) employing CV technique was found lower and better than the diagnostic reference value (0.763 μM) for the human body **[17].** This confirmed that the sensor could be recommended for clinical use. Cyclic voltammetry technique could be recommended for the detection of epinephrine employing either Au-PA-CoOcPhOPc or Au-PA-Mn(OAc)OcPhOPc sensors. The lower LoD was due to the effect of the electrostatic attraction between the negatively charged Au-PA-MOcPhOPc electrodes and epinephrine at pH 7.4, resulting in overconcentration of epinephrine at the Au-PA-MOcPhOPc electrodes and hence higher current signal output.

Table 5.2: Comparative analytical performance of phthalocyanines modified electrode for detection of epinephrine

Neurotransmitters	Sensor	LOD (μM)	Ref.
Epinephrine (EP)	Diagnostic reference value	0.763	**[17]**
	Cobalt tetraamino phthalocyanines	0.50	**[59]**
	Iron Phthalocyanines	0.50	**[60]**
	Au-PA-CoOcPhOPc (CV)	0.32	**TW**
	Au-PA-CoOcPhOPc (DPV)	1.01	**TW**
	Au-PA-FeOcPhOPc (CV)	7.93	**TW**
	Au-PA-FeOcPhOPc (DPV)	1.44	**TW**
	Au-PA-Mn(OAc)OcPhOPc (CV)	0.70	**TW**
	Au-PA-Mn(OAc)OcPhOPc (DPV)	3.91	**TW**

TW (This work)

5.1.3 Norepinephrine

The results obtained using both CV (0.22 μM) and DPV (0.99 μM) at Au-PA-CoOcPhOPc sensors were lower and better in terms of the LoD and LoQ than the results obtained from MWCNT/ZnO/29H,31H-Pc sensor (1.70 μM) **[61].** The CV analysis with Au-PA-Mn(OAc)OcPhOPc sensor has lower LoD result (1.00 μM) for norepinephrine detection than MWCNT/ZnO/29H,31H-Pc sensor (1.70 μM). Generally, all the LoD results obtained from the detection of the norepinephrine at Au-PA-FeOcPhOPc, Au-PA-CoOcPhOPc and Au-PA-Mn(OAc)OcPhOPc sensors are within the diagnostic reference range of norepinephrine

concentration in normal human blood (0.464 – 10.049 μM) **[17]**. The LoDs of the Au-PA-MOcPhPc modified electrodes for determination of norepinephrine was summarized in **Table 5.3**. The electroanalysis LoD result with Au-PA-CoOcPhOPc sensors are lower and better in terms of the LoD (0.22 μM) than the diagnostic range. This confirmed that all the modified electrode used in this research work could be recommended for norepinephrine detection.

Table 5.3: Comparative analytical performance of phthalocyanines modified electrode for detection of norepinephrine.

Neurotransmitters	Sensor	LOD (μM)	Ref.
Norepinephrine (NEP)	Normal concentration in blood	0.464 – 10.049	**[17]**
	MWCNT/ZnO/29H,31H-Pc	1.70	**[61]**
	Au-PA-CoOcPhOPc (CV)	0.22	**TW**
	Au-PA-CoOcPhOPc (DPV)	0.99	**TW**
	Au-PA-FeOcPhOPc (CV)	8.64	**TW**
	Au-PA-FeOcPhOPc (DPV)	7.37	**TW**
	Au-PA-Mn(OAc)OcPhOPc (CV)	1.00	**TW**
	Au-PA-Mn(OAc)OcPhOPc (DPV)	2.15	**TW**

TW (this work)

5.1.4 Serotonin

The LoDs of various Au-PA-MOcPhOPc modified electrode for determination of serotonin and the reported LoD value were summarized in **Table 5.4**. The Au-PA-CoOcPhOPc sensor employing CV displayed low LoD (0.56 μM), which is lower and better when compared with

the reported result obtained using Cobalt (II) phthalocyanine and tyrosinase sensor (0.84 µM) **[62].** The diagnostic reference concentrations of serotonin ranges between 0.227 – 0.636 µM **[18].** The results obtained using CV at Au-PA-CoOcPhOPc (0.56 µM) is within the diagnostic reference concentrations of serotonin range. The cyclic voltammetry technique with Au-PA-CoOcPhOPc also gave the lowest LoD of 0.56 µM compare to other sensors used for the electroanalysis. The results confirmed that Au-PA-CoOcPhOPc sensor could be recommended for the serotonin detection, employing cyclic voltammetry technique. The Au-PA-CoOcPhOPc sensor is also suitable for the clinical diagnosis of serotonin.

Table 5.4: Comparative analytical performance of phthalocyanines modified electrode for detection of serotonin

Neurotransmitters	Sensor	LOD (µM)	Ref.
Serotonin (SER)	Normal concentration in blood	0.227 – 0.636	**[18]**
	Cobalt (II) phthalocyanine and tyrosinase	0.84	**[62]**
	Au-PA-CoOcPhOPc (CV)	0.56	**TW**
	Au-PA-CoOcPhOPc (DPV)	1.12	**TW**
	Au-PA-FeOcPhOPc (CV)	6.20	**TW**
	Au-PA-FeOcPhOPc (DPV)	2.01	**TW**
	Au-PA-Mn(OAc)OcPhOPc (CV)	1.67	**TW**
	Au-PA-Mn(OAc)OcPhOPc (DPV)	1.22	**TW**

TW (This work)

6 CONCLUSIONS

The investigations described in this thesis demonstrated the electrocatalysis of 2,3,9, 10, 16, 17, 23, 24-octacarboxyphenoxy metallophthalocyanines covalently immobilized on gold electrode and the application for the invitro detection of neurotransmitters. First, the 2, 3, 9, 10, 16, 17, 23, 24-octacarboxyphenoxy metallophthalocyanines with different central metals (Fe, Mn, and Co) were synthesized and covalently immobilised onto gold electrodes. The electrodes were pre-modified through electrochemical grafting of 4-nitrobenzene tetrafluoroborate diazonium salt to form phenylnitro radical surface (Au-PNO_2). The Au-PNO_2 was electrochemically reduced in methanol:water (1:10 by v:v) to form phenylamine gold electrode surface (Au-PA). The metallophthalocyanines complex was immobilized on the Au-PA via amide coupling forming Au-PA-MOcPhOPc. Secondly, fundamental studies were performed to evaluate the electrocatalysis of neurotransmitter at the Au-PA-MOcPhOPc electrode. The Au-PA-MOcPhOPc modified electrode had advantages in the amplification of the neurotransmitter's voltammetry signals, which was attributed to the overconcentration of the neurotransmitter at the Au-PA-MOcPhOPc surface. The overconcentration effect was due to the electrostatic attraction of the negatively charged Au-PA-MOcPhOPc surface and the positively charged neurotransmitters at pH 7.4. By taking advantages of the electronegativity of the Au-PA-MOcPhOPc surfaces resulting from the octa-carboxyl group (COO^-), the Au-PA-MOcPhOPc could screened off interfering cations such as ascorbic acid, which coexist with neurotransmitters in body fluids. The Au-PA-MOcPhOPc sensors could suppress the ascorbic acid voltammetry signal making the Au-PA-MOcPhOPc highly selective towards the detection of the neurotransmitters. The result from these studies demonstrated and achieved the accurate detection of the neurotransmitters without interference from ascorbic acid. The detection limit (LoD), the quantitation limit (LoQ) and the sensitivity were evaluated from the results obtained through the cyclic and differential pulse voltammetry methods. Most of the results obtained were within the range of the diagnostic reference values for the neurotransmitters in blood. The

Au-PA-MOcPhOPc sensor showed higher sensitivity for detection of neurotransmitter when compared to other reported sensors in literature. The Au-PA-MOcPhOPc sensor shows high stability and reproducibility due to the covalent immobilization of the MOcPhOPc onto the Au electrode surface.

7 REFERENCES

1. S. Amor, L.A.N. Peferoen, D.Y.S. Vogel, M. Breur, P. van der Valk, D. Baker, J.M. van Noort, Inflammation in neurodegenerative diseases - an update, *Immunology* 2014 (**2**) 151–166.
2. F. Patel and P. Mandal, Neurodegenerative diseases and their therapeutic approaches, *Neurons - dendrites and axons,* Chapter 1, Intech Open 2019, 1-20.
3. A. Dias, C. Ferri, N. Graham, B. Ineichen, M. Prince, R. Uwakwe, Neurological disorders a public health approach, *World Health Organization,* Epidemiology and Burden, Dementia, 2006 (**44**) Chapter 3.
4. R.L. Hewer, The World Health Organization, The economic impact of neurological illness on the health and wealth of the nation and of individuals, *Journal of Neurology, Neurosurgery and Psychiatry*, (Suppl.1) 1997 (**63**) S19–S23.
5. C. S. Paulose, A. Krishnakumar and A. Joseph, Neurotransmitters Functional Balance in Neurodegenerative disease management: *Recent Advances, Science and Sociology*, 5**(1)** 2007, 23-30.
6. P.M. Campeau, G. Bernard, P.T. Clayton, Neurotransmitter diseases and related conditions, *IEM digest / Molecular Genetics and Metabolism,* 2007 (**92**) 189– 197.
7. L.C. Andreae and J. Burrone, The role of spontaneous neurotransmission in synapse and circuit development, *Journal of Neuroscience Resources.,* 2018, 96 (**3**) 354–359.
8. V. Vorobyov, N. Bobkova, Intracerebral interplay and neurotransmitter systems involvement in animal models of neurodegenerative disorders: EEG approach expectations. *Neural Regeneration Research,* 2017, 12 (**1**) 66–67.

9. C.S. Stanford, and D.J. Heal, Catecholamine: Knowledge and understanding in the 1960s, now, and in the future, *Brain and Neuroscience Advances*, 2019**.**

10. C. Marecos, J. Ng, M.A. Kurian, What is new for monoamine neurotransmitter disorders, *Journal of Inherited Metabolic Disease* (JIMD), 2014, 37 (**4**) 619-626.

11. M. Bortolato, K.Chen, J. C. Shih, Monoamine oxidase inactivation: from pathophysiology to therapeutics, *Advance Drug Delivery Reviews,* 2008, 60 (**13-14**) 1527–1533.

12. K. Bera, A.K. Das, A. Rakshit, B. Sarkar, A. Rawat, B.K. Maity, S. Maiti, Fluorogenic detection of monoamine neurotransmitters in live cells, *American Chemical Society (ACS) Chemical Neuroscience.* 2018, 9 **(3)** 469-474.

13. J. Drozak , J. Bryła, Dopamine: Not just a neurotransmitter, *Postepy Higieny Medycyny Doswiadczalnej,* 2005 (**59**) 405-420.

14. C. Cassata, What Is Norepinephrine? Everyday health, medically reviewed by Robert Jasmer, 2015.

15. D. M. Fouad and W. A. El-Said, Selective Electrochemical detection of epinephrine using gold nanoporous film, *Journal of Nanomaterials,* Volume 2016.

16. J. Lv and F. Liu, The role of serotonin beyond the central nervous system during embryogenesis, *Front Cell Neuroscience.* 13 March 2017.

17. D. C. Dugdale and D. Zieve, Catecholamine blood test, Milton S. Hershey Medical center, Penn State Hershey Services, Reviewed 2019.

18. A. Scaccia, Serotonin: What you need to know, Healthline, medically reviewed by Debra Rose Wilson, 2017.

19. P. Muñoz, S. Huenchuguala, I. Paris, and J. Segura-Aguilar, Dopamine oxidation and autophagy, *Parkinson's disease,* Volume 2012.

20. G. Huether, I. Fettkötter, G. Keilhoff, and G. Wolf, Serotonin acts as a radical scavenger and is oxidized to a dimer during the respiratory burst of activated Microglia, *Journal of Neurochemistry,* 1997, 69 (**5**) 2096-2101.

21. S. Senapati, S.P. Das, A.K. Patnaik, Kinetics and mechanism of oxidation of L- ascorbic acid by Pt (IV) (aq) in aqueous hydrochloric acid medium, *Advances in Physical Chemistry,* 2015, Volume 2012.

22. J. J. Ruiz, A. Aldaz, and M. Dominguez, Mechanism of L-ascorbic acid oxidation and dehydro-L-ascorbic acid reduction on a mercury electrode in acid medium, *Canadian Journal of Chemistry,* 1977 (**55**) 2799-2806.

23. V. I. Chefer, A. C. Thompson, A. Zapata, and T. S. Shippenberg, Overview of brain microdialysis, *Curriculum Protoc Neuroscience*; Chapter: Unit 7, 2009 **(1)** 1-35.

24. A. Zinellu, S. Sotgia, E. Pisanu, B. Scanu, M. Sanna, M. F. Usai, R. Chessa, L. Deiana, C. Carru, Quantification of neurotransmitter amino acids by capillary electrophoresis laser-induced fluorescence detection in biological fluids, *Analytical and Bioanalytical* 2010, 398 (**4**)1973–1978.

25. B. J. Venton, Q. Cao, Fundamentals of Fast-Scan cyclic voltammetry for dopamine detection, Analyst, Critical review, *The Royal Society of Chemistry* 2020, 145 **(4)**1158-1168.

26. N. Nakatsuka, A. M. Andrews, Neurochips enable nanoscale devices for high resolution in vivo neurotransmitter sensing, *Neuropsychopharmacology Reviews* 2016, 41 (**1**) 378–379.

27. L. Nan-Sen, W. Li, W. Mi-Xia, X. Sheng-Wei, Y. Wei-Dong, C. Xin-Xia, A wearable wireless electrochemical instrument used for In-vivo neurotransmitter detection, *China Journal Analytical Chemistry*, 2015, 43 (**1**) 93–97.

28. A. G. Zestos, Carbon nanoelectrodes for the electrochemical detection of neurotransmitters, *International Journal of Electrochemistry,* 2018, Volume 2018.

29. T. H. Holm, T. J. Isaksen, and K. Lykke-Hartmann, HPLC neurotransmitter analysis, chapter 29, M. Bublitz (ed.), P-Type ATPases: methods and protocols, *Methods in Molecular Biology,* 2016 (**1377**) 333-340.

30. T. Kim, J. Choi, H. Kim, and H. Kim, Quantification of neurotransmitters in mouse brain tissue by using liquid chromatography coupled electrospray tandem mass spectrometry, *Journal of Analytical Methods in Chemistry*, 2014, Volume 2014.

31. S. Parrot, V. Sauvinet, V. Riban, A. Depaulis, B. Renaud and L. Denoroy, High temporal resolution for in vivo monitoring of neurotransmitters in awake epileptic rats using brain microdialysis and capillary electrophoresis with laser induced fluorescence detection, *Journal of Neuroscience Methods,* 2004, 140, (**1-2**) 29–38.

32. Y. Ou, A. M. Buchanan, C. E. Witt and P. Hashemi, Frontiers in electrochemical sensors for neurotransmitters detection: towards measuring neurotransmitters as chemical diagnostics for brain disorders, *Analytical Methods,* 2019 (**21**) 2738-2755.

33. R.A. Durst, A.J. Baumner, R. W. Murray, R.P. Buck, P. Andrieux**,** chemically modified electrodes: recommended terminology and definitions, *International Union of Pure and Applied Chemistry,* 69, **(6),** 1317-1997.

34. T. Li., O. Kasian, S. Cherevko, S. Zhang, S. Geiger, C. Scheu, P. Felfer, D. Raabe, B. Gault, and K. J. J. Mayrhofer, Atomic-scale insights into surface species of electrocatalysts in three dimensions, *Nature Catalysis,* 2018, 1 (4), 1-6.

35. M. D. Brown, M. H. Schoenfisch, Catalytic selectivity of metallophthalocyanines for electrochemical nitric oxide sensing, *Electrochim Acta,* 2018 (**273**) 98–104.

36. M. Grobosch, C. Schmidt, R. Kraus, M. Knupfer, Electronic properties of transition metal phthalocyanines: The impart of the central metal atom (d^5-d^{10}), *Organic Electronics* 2010, 11, (**9**) 1483–1488.

37. T. Koczorowski, W. Szczolko and T. Goslinski, Physicochemical properties and catalytic applications of iron porphyrazines and phthalocyanines, *Recent progress in organometallic chemistry*, 2017 (**5**) 101-121.

38. C. G. Claessens, U. Hahn, T. Torres, Phthalocyanines: From outstanding electronic properties to emerging applications, *The Chemical Record,* 2008 (**8**) 75–97.

39. S. H. Kim, J. W. Namgoong, S. B. Yuk, J. Y. Kim, W. Lee, C. Yoon, J. P. Kim, Synthesis and characteristics of metal-phthalocyanines tetrasubstituted at non-peripheral (a) or peripheral (b) positions, and their applications in LCD color filters, *Journal of Inclusion Phenomena Macrocyclic Chemistry* 2015 (**82**) 195–202.

40. R. Li, X. Zhang, P. Zhu, D. K. P. Ng, N. Kobayashi, and J. Jiang, Electron-donating or withdrawing nature of substituents revealed by the electrochemistry of metal-free phthalocyanines, *Inorganic Chemistry,* 2006 (**45**) 2327−2334.

41. M. G. Waltera, A. B. Rudineb and C. C. Wamser, Porphyrins and phthalocyanines in solar photovoltaic cells, *Journal of Porphyrins and Phthalocyanines,* 2010 (**14**) 759–792.

42. R. Burkitt, T. R. Whiffen, E. H. Yu, Iron phthalocyanines and MnOx composite catalysts for microbial fuel cell applications, *Applied Catalysis B: Environmental* 2016 (**181**) 279-288.

43. D. D. Eley, Phthalocyanines as semiconductors, *Nature* 1948 (**4125**) 819.

44. P. Vasudevan, N. Phougat and A. K. Shukla, Metal phthalocyanines as electrocatalysts for redox reactions, review, *Applied Organometallic Chemistry,* 1996, 10 (**8**) 591-604.

45. S. Baba, A. Suzuki, and T. Oku, Electronic structures and magnetic/ optical properties of metal phthalocyanine complexes, *AIP Conference Proceedings* 2016 (**1709**) 020012.

46. S. Yanagisawa, T. Yasuda, K. Inagaki, Y. Morikawa, K. Manseki, and S. Yanagida, Intermolecular interaction as the origin of red shifts in absorption spectra of zinc-phthalocyanine from first-principles, *Journal of Physical Chemistry A*, 2013, 117 **(44)** 11246-11253.

47. D. Mukherjee, R. Manjunatha, S. Sampath and A. K. Ray, Phthalocyanines as sensitive materials for chemical sensors, Springer International Publishing AG 2017 (**8**) 165-226.

48. M.T. Shreenivas, B.E. K. Swamy, U. Chandra, B. S. Sherigara, Cyclic voltametric investigation of dopamine at polt-(Gabapentin) modified carbon paste electrode, International Journal of Electrochemistry, 2011, volume 2011.

49. M. Pari, N. Mounesh, K. Venugopala, Synthesis, Spectral and electrochemical investigation of azo-bridged metallophthalocyanines polymer*, Analytical Bioanalytical Electrochemistry*, 2019, 11(**4**) 460-483.

50. M. F. Zampa, I. S. Araujo, J. R. S. Junior, V. Zucolotto, J. Robertode S. A. Leite, and C. Eiras, Development of a novel biosensor using cationic antimicrobial peptide and nickel phthalocyanine ultrathin films for electrochemical detection of dopamine, *International Journal of Analytical Chemistry,* 2011, Volume 2012.

51. N. Diaba, D. M. Moralesa, C. Andronescua, M. Masoud, W. Schuhmann, A sensitive and selective graphene/cobalt tetrasulfonated phthalocyanine sensor for detection of dopamine, *Sensors & Actuators: B. Chemical,* 2019 (**285**) 17–23.

52. S. L. de Moura, C. M. M. Jevenois, M. I. Pividori, J. A. V. dos Santos, V. Zucolotto, I. N. G. Passos, J. R. dos Santos Júnior, Influence of natural polysaccharides on the redox processes of CuTsPc thin films and dopamine sensing, *International Journal of Materials Science and Applications* 2013 **(2)**146-156.

53. B. O. Agboola and K. I. Ozoemena, Efficient Electrocatalytic Detection of epinephrine at gold electrodes modified with self-assembled metallo-octacarboxy phthalocyanine complexes, *Electroanalysis* 20, 2008 (**15**) 1696–1707.

54. A. Sivanesan, S. A. John, Selective electrochemical epinephrine sensor using self-assembled monomolecular film of 1,8,15,22-tetraamino phthalocyanatonickel (II) on gold electrode, *Electroanalysis* 20, 2008 (**21**) 2340–234.

55. B. O. Agboola, A. Mocheko, J. Pillay and K. I. Ozoemena, Nanostructured cobalt phthalocyanines single walled car bon nanotube platform: electron transport and electrocatalytic activity on epinephrine, *Journal of Porphyrins Phthalocyanines* 2008 **(12**) 1289-1299.

56. S. Shahrokhian, M. Ghalkhani, M. K. Amini, Application of carbon-paste electrode modified with iron phthalocyanine for voltammetric determination of epinephrine in the presence of ascorbic acid and uric acid, *Sensors and Actuators B,* 2009 (**137**) 669–675.

57. N. G. Mphuthi, A. S. Adekunle and E. E. Ebenso, Electrocatalytic oxidation of Epinephrine and Norepinephrine at metal oxide doped phthalocyanines/MWCNT composite sensor. *Scientific Reports,* 2016 (**6**) 1-20.

58. I. M. Apetrei, C. Apetrei, Amperometric tyrosinase based biosensors for serotonin detection, *Romanian Biotechnological Letters*, 2013 (**18**) 8253-8262.

59. T. Ndlovu, O. A. Arotiba, S. Sampath, R. W. Krause and B. B. Mamba, An exfoliated graphite-based bisphenol an electrochemical sensor, *Sensors* 2012 (**12**) 11601-11611.

60. B. O. Agboola and K. I. Ozoemena, Self-assembly and heterogeneous electron transfer properties of metallo-octacarboxyphthalocyanine complexes on gold electrode, *Physical Chemistry Chemical Physics*, 2008 (**10**) 2399–2408.

61. L. Koefoed, Steen, U. Pedersen, and K. Daasbjerg, Covalent modification of glassy carbon surfaces by electrochemical grafting of aryl iodides, *Langmuir* 2017 (**33**)

3217−3222.

62. S. Boland, F. Barrière and D. Leech, Designing stable redox-active surfaces: chemical attachment of an osmium complex to glassy carbon electrodes prefunctionalized by electrochemical reduction of an in-situ-generated aryldiazonium, *Langmuir* 2008, 24 **(12**) 6351-6358.

63. L. Cheng, X. Ge and L. Huang, Direct amidation of non-activated phenyl acetic acid and benzylamine derivatives catalysed by $NiCl_2$, *Royal Society Open Science,* 2018 **(5)** 171870.

64. J. R. Dunetz, J. Magano and G. A. Weisenburger, Large-scale applications of amide coupling reagents for the synthesis of pharmaceuticals, *Organic Process Research Development,* 2016 20 **(2)** 140-177.

65. S. E. Maree and T. Nyokong, Syntheses and photochemical properties of octasubstituted phthalocyaninato zinc complexes, *Journal of Porphyrins Phthalocyanines* 2001 **(5)** 782–792.

66. S. R. Nxele, P. Mashazi and T. Nyokong, Electrode modification using alkynyl substituted Fe (II) phthalocyanines via electrografting and click chemistry for electrocatalysis, *Electroanalysis*, 2015, 27 **(10)** 2468-2478.

67. P. J. Stephens, Theory of magnetic circular dichroism. *The Journal of Chemical Physics,* 1970 52 **(7)** 3489.

68. P. N. Mashazi, P. Westbroek, K. I. Ozoemena, T. Nyokong, Surface chemistry and electrocatalytic behaviour of tetra-carboxysubstituted iron, cobalt and manganese phthalocyanines self-assembled monolayers on gold electrode. *Electrochimica Acta* 2007 **(53)** 1858-1869.

69. M. A. Rauf, S. Hisaindee, J.P. Graham, M. Nawaz, Solvent effects on the absorption and fluorescence spectra of Cu (ii) phthalocyanines and DFT calculations, *Journal of Molecular Liquids* 2012 **(168)** 102-109.

70. E. Marsili, J. B. Rolletson, D. B. Baron, R. M. Hozalski, D. R. Bond, Microbial biofilm voltammetry: direct electrochemical character of catalytic electrode, National Library of medicine, *Applied and environmental microbiology*, 2008, 74 **(23),** 7329-7337.